**CHARACTERIZATION OF THE REACTION CYCLE OF MJ0796:
A MODEL ARCHAEAL ADENOSINE TRIPHOSPHATE-
BINDING CASSETTE TRANSPORTER
NUCLEOTIDE BINDING DOMAIN**

APPROVED BY SUPERVISORY COMMITTEE

_____
Philip J. Thomas, Ph. D.

_____
Margaret Phillips, Ph. D.

_____
Joseph Albanesi, Ph. D.

_____
Elizabeth Goldsmith, Ph. D.

To my parents, Dean and Martha Moody,
and in loving memory of Margaret Antoinette Townsend.

CHARACTERIZATION OF THE REACTION CYCLE OF MJ0796: A MODEL ARCHAEAL ADENOSINE TRIPHOSPHATE-BINDING CASSETTE TRANSPORTER NUCLEOTIDE BINDING DOMAIN

by

JONATHAN EDWARD MOODY

DISSERTATION
Presented to the Faculty of the Graduate School of Biomedical Sciences
The University of Texas Southwestern Medical Center at Dallas
In Partial Fulfillment of the Requirements
For the Degree of

DOCTOR OF PHILOSOPHY
The University of Texas Southwestern Medical Center at Dallas

Dallas, Texas

December, 2006

Acknowledgements

The work described herein would not have been possible without the contributions made by numerous individuals. I would first like to thank my mentor and friend, Phil Thomas. You have been a wonderful person to learn from and work for. I truly appreciate your professional guidance, endless encouragement, and your infectious enthusiasm for science. The members of the Thomas lab that you have assembled mirror the qualities that you model for us so well.

Concerning the Thomas lab, I must first thank Linda Millen for her unceasing efforts to single-handedly ensure that things go smoothly in the lab, whether ordering materials, getting our pipetman calibrated, or patiently enduring the newest lab members' impatient questioning! Special recognition also goes to Anita Contreras for serving so well as our departmental administrative assistant. In addition to the laboratory administration, my fellow graduate students have made the past five years an extremely enjoyable experience. Patrick Thibodeau, Michael Dorwart, Rhesa Stidham, Karen Lewis, and Michael Brinkman, thank you for countless helping hands and stimulating discussions along the way. Current and former post-doctoral researchers Chris Wigley, Michael Corboy, Changwei Liu, Li Zhu, Balajee Somalinga, and John Richardson, thank you for

insightful comments in lab meetings and for being so easy to learn from and work with. Finally, Pritam Kambuj, John Pruit, Jarod Watson, and Elizabeth Barney have been invaluable lab staff, without whom daily operations would not have been possible. Special thanks to Derk Binns for analytical ultracentrifuge training.

I would also like to thank my committee, Margaret Philips, Joseph Albanesi, and Elizabeth Goldsmith for their heartfelt interest in and support of my thesis project. I will always regret underutilizing each of your amazing intellects during the course of my graduate research. It has been a pleasure working with you during committee meetings, journal clubs, and retreats.

The Molecular Biophysics graduate program and the Division of Basic Sciences have been wonderfully run operations, and I must thank Steve Sprang, Kevin Gardner, Phil Perlman, and Melanie Cobb for their excellent leadership. I would also like to thank Nancy McKinney for everything she does for the graduate school, and for administering the DCMB NIH training grant.

I must also thank our collaborators, John Hunt's group at Columbia, for their crystallographic efforts and manuscript comments. Special thanks go to Hajime Tokuda's group in Japan for their kind gift of plasmid pNASCDE. Funding for this work has been provided by a Welch Foundation grant to Philip Thomas and direct support from a position on the NIH predoctoral training grant, Division of Cell & Molecular Biology Training Program.

CHARACTERIZATION OF THE REACTION CYCLE OF MJ0796: A MODEL ARCHAEAL ADENOSINE TRIPHOSPHATE-BINDING CASSETTE TRANSPORTER NUCLEOTIDE BINDING DOMAIN

Jonathan Edward Moody, Ph. D.

The University of Texas Southwestern Medical Center at Dallas, December, 2006

Supervising Professor: Philip J. Thomas, Ph. D.

Adenosine-triphosphate binding cassette (ABC) transporters couple nucleotide hydrolysis to vectorial transport of solutes across lipid bilayers. These proteins, found in all kingdoms of life, have been implicated in a variety of human

genetic disorders and engender drug resistance in cancer cells and infectious prokaryotes. Despite the widely varying solutes transported by these protein machines, a conserved functional mechanism is suggested by the high degree of amino acid conservation found in the nucleotide binding domains of all ABC transporters.

Using two model archaeal ABC transporter nucleotide binding domains, MJ0796 and MJ1267, from *Methanocaldococcus jannaschii* the highly conserved Walker A, Walker B, and LSGGQ motifs were probed using site-directed mutagenesis. Catalytic carboxylate mutants, MJ0796-E171Q and MJ1267-E179Q, exhibited nucleotide-dependent dimerization upon analytical gel filtration and equilibrium centrifugation experiments. This self-association was negatively affected by changes in the electrostatic environment, as shown using alanine substitutions at these loci as well as altering the ionic conditions of the experiments. The MJ0796-E171Q protein was crystallized, and its structure solved to 1.9 angstrom resolution. The structure reveals an ATP sandwich dimer with two nucleotides bound at the dimeric interface, with each binding site composed of Walker A and B residues from one monomer and LSGGQ residues from the opposing monomer.

A proposed reaction cycle based upon the MJ0796-E171Q dimer structure was probed using Walker A, Walker B, and LSGGQ point mutants. Mixtures of the Walker A mutant MJ0796-K44A with LSGGQ mutant MJ0796-S147F, both

hydrolytically deficient in isolation, did not exhibit activity. In stark contrast, mixtures of MJ0796-S147F and MJ0796-E171Q did exhibit 25% wild type activity, suggesting a mechanism whereby two nucleotide binding events and a single hydrolysis event complete the minimal reaction cycle. This also suggests that during wild type hydrolysis, two nucleotides are hydrolyzed per cycle. These heterodimeric mutant mixtures were further analyzed using tryptophan fluorescence emission and anisotropy. Mixing experiments were performed using a full transporter system, the lipoprotein release machinery from *Escherichia coli*. A modified ABC transporter reaction cycle is presented.

Table of Contents

Prior Publications

Moody, J. E., Millen, L., Binns, D., Hunt, J. F. and Thomas, P. J. (2002) Cooperative, ATP-Dependent Association of the Nucleotide Binding Cassettes During the Catalytic Cycle of ATP-Binding Cassette Transporters. *J. Biol. Chem.* **277**, 21111-21114.

Smith, P. C., Karpowich, N., Millen, L., Moody, J. E., Rosen, J., Thomas, P. J., and Hunt, J. F. (2002) ATP Binding to the Motor Domain from an ABC Transporter Drives Formation of a Nucleotide Sandwich Dimer. *Mol. Cell* **10**, 139-149.

Moody, J. E. and Thomas, P. J. (2005) Nucleotide Binding Domain Interactions During the Mechanochemical Reaction Cycle of ATP-Binding Cassette Transporters. *J. Bioenerg. Biomem.* **37**, 475-479.

Moody, J. E. and Thomas, P. J. Probing the Reaction Cycle of a Model Archaeal ABC Transporter Nucleotide Binding Domain. *In preparation.*

List of Figures

List of Tables

List of Abbreviations

ABC	ATP-binding cassette
ADP	adenosine 5’-diphosphate
AMP-PNP	adenosine 5′-(β,γ-imido)triphosphate
ATP	adenosine 5’-triphosphate
ATP-γ-S	adenosine 5'-(3-thiotriphosphate)
CFTR	cystic fibrosis transmembrane conductance regulator
DTT	dithiothreitol
EDTA	ethylenediaminetetraacetic acid
hNBD1	*Homo sapiens* CFTR N-Terminal NBD
IPTG	isopropyl β-D-1-thiogalactopyranoside
mNBD1	*Mus musculus* CFTR N-Terminal NBD
NBD	nucleotide binding domain
OD	optical density
PMSF	phenylmethanesulfonyl fluoride
RPM	revolutions per minute
TMD	transmembrane domain

Chapter I

Introduction

Adenosine triphosphate (ATP)-Binding-Cassette (ABC) transporters couple nucleotide binding and hydrolysis to the transport of a wide variety of solutes across biological membranes. Over one third (18 of the 48) of the human ABC transporters have been linked to genetic disorders (Dean, 2005), the most common of them being cystic fibrosis in which the *ABCC7* gene product (cystic fibrosis transmembrane conductance regulator, or CFTR) exhibits a severely reduced, or lack of, chloride channel function (Riordan *et al*., 1989; Anderson *et al*., 1991a). In addition to causing a variety of human diseases, ABC transporters engender multiple drug resistance in both prokaryotic and eukaryotic cells, a significant hurdle faced in the battles against microbial infection and cancer (Juliano and Ling, 1976; Cole *et al*., 1992; van Veen *et al*., 1996). The manner in which these proteins harness the energy of ATP binding and hydrolysis to the translocation of solutes across lipid bilayers has thus garnered great interest.

ABC transporters share a common domain organization of two transmembrane domains (TMDs) and two soluble nucleotide binding domains (NBDs). The TMDs are highly divergent, as it is these domains which likely contain the binding sites for each transporter's specific solutes. In stark contrast,

NBD sequences from all levels of life are highly conserved. The high degree of similarity between NBDs of all ABC transporters suggests that the mechanism of energy utilization by these systems is likewise conserved. Due to the high number of human genetic disorders linked to ABC transporters, as well as complications arising from prokaryotic and cancer cell drug resistance conferred by ABC transporters, structural and biochemical characterization of the NBDs has become paramount to the eventual discovery and development of reagents to help address these terrible diseases.

The experimental studies summarized herein address the mechanochemical reaction cycle of ABC transporter NBDs. Chapter II provides a literature review of the historical genetic and biochemical studies of bacterial NBD proteins. In addition, Chapter II relates the initial structural characterizations of these conserved domains and the conundrums these crystallization studies presented. Chapter III details the utilization of a catalytic carboxylate mutant form of an archaeal nucleotide binding domain to help settle the aforementioned conundrums, while Chapter IV describes the continued dissection of the ABC transporter nucleotide binding domain reaction cycle and its necessary components. Finally, Chapter V outlines the major questions remaining to be answered and predicts future advances and new directions taken by the ABC transporter research community.

Chapter II

Literature Review

Introduction

Beginning with the discovery of periplasmic components of bacterial osmotic shock-sensitive permeases (Pardee *et al*., 1966), extensive characterization of bacterial uptake systems of then unknown composition was underway. By studying the histidine permease, the first genetically characterized system, the transport machinery was shown to be comprised of multiple components (Ames and Lever, 1970; Ames and Lever, 1972). Evidence for interaction between the periplasmic substrate binding protein, HisJ, with the membrane-bound component(s) of this system was provided soon thereafter (Kustu and Ames, 1974; Ames and Spudich, 1976). While work continued on the highly soluble, more easily purified substrate binding proteins such as HisJ, the maltose binding protein (MalE), and the first periplasmic binding protein crystallized, AraF (Phillips, *et al*., 1976; Quiocho *et al*., 1977), less was known about the two highly hydrophobic components and one "not recognizably hydrophobic" membrane-associated component (Ames, 1986). By demonstrating the inclusion of MalK in the soluble protein fraction in mutant *Escherichia coli* strains defective in *malG*, one of the highly hydrophobic components of the

maltose transporter, researchers were able to illustrate that these "not recognizably hydrophobic" components were peripheral membrane proteins (Shuman and Silhavy, 1981) rather than membrane-anchored as was long thought of HisP of the histidine permease (Ames and Nikaido, 1978; Hung *et al*., 1998). It became immediately apparent that HisP and MalK were homologous to each other as DNA sequences of permease components were published (Higgins *et al*., 1982; Gilson *et al*., 1982a; Gilson *et al*., 1982b). The regions of highest conservation were noted to share homology with several proteins known to have ATP-binding sites (Walker *et al*., 1982; Higgins *et al*., 1985) soon after nucleotide binding to HisP and MalK was demonstrated (Hobson *et al*., 1984). As additional DNA sequences of periplasmic permease components became available, the "conserved component" was postulated to bind nucleotide in all such transporters as an energy-coupling mechanism. The following functional mechanism for periplasmic permeases was proposed: the solute-binding protein binds its substrate in the periplasm and subsequently docks with the transport machinery (two "highly hydrophobic" components plus the "conserved" component) located in the inner membrane. Active transport of the solute into the cytoplasm then occurs in a nucleotide dependent manner using the three membrane-associated components.

The term "ATP-Binding Cassette (ABC) Transporter" was coined in 1990 by Higgins and colleagues (Hyde *et al*., 1990), although "traffic ATPase" was put

forth by Ames and coworkers as an alternative (Ames *et al*., 1990) to describe the proteins. The ABC transporter gene superfamily is prevalent throughout the three domains of life, accounting for, on average, 3% and 5% respectively of each archaebacterial and eubacterial genome sequenced to date (Ren *et al*., 2004), while eukaryotic ABC transporters range in number from the 31 found in *Saccharomyces cerevisiae* to 48 human transporters to over 100 found in *Arabidopsis* and *Oryza* (Bauer *et al*., 1999; Dean *et al*., 2001; Garcia *et al*., 2004). The solutes transported by these protein machines range from ions (Human Cl^- channel CFTR) (Riordan *et al*., 1989), amino acids and sugars (*Salmonella typhimurium* histidine permease His $JQMP_2$ and *Escherichia coli* maltose transporter $MalEFGK_2$) (Higgins *et al*., 1982; Gilson *et al*., 1982; Duplay *et al*., 1984; Froshauer and Beckwith, 1984; Dassa and Hofnung, 1985) to large (~50kDa) proteases (*Erwinia chrysanthemi* metalloprotease secretion machinery PrtDEF) (Letoffe *et al*., 1990), even larger (~80kDa) protein toxins (*E. coli* α-haemolysin secretion machinery HlyBD-TolC) (Goebel and Hedgpeth, 1982) to gigantic (~900kDa) biofilm components (*Pseudomonas fluorescens* LapBCE) (Hinsa *et al*., 2003).

ABC transporters can act as importers, as in the case of the bacterial periplasmic binding protein dependent systems responsible for the uptake of amino acids, metal ions and sugars. It is only these particular importers that possess the solute binding proteins. Alternatively, ABC transporters can export

cytoplasmic solutes outside of the cell (bacterial multidrug transporter LmrA) (van Veen *et al*., 1996) or, in the case of eukaryotic transporters, into an intracellular compartment such as the endoplasmic reticulum or mitochondria (TAP and Atm1p respectively) (Trowsdale *et al*., 1990; Leighton and Schatz, 1995). Additionally, ABC transporters can be responsible for Type I secretion involving the TolC protein channel that spans the periplasmic space of gram-negative bacteria. Most eukaryotic ABC transporters function as exporters, while this protein superfamily contains both importers and exporters in prokaryotes.

ABC Transporter Domain Organization

The minimal functional unit of ABC transporters is thought to be two transmembrane domains (TMDs), homologous to the aforementioned "highly hydrophobic" components of periplasmic permeases, and two nucleotide binding domains (NBDs), homologous to the bacterial "not recognizably hydrophobic" but "conserved" component (Ames, 1986). This proposed domain architecture was based upon protein sequence data (Hyde *et al*., 1990) and reconstitution of the *Salmonella typhimurium* histidine permease and *Escherichia coli* maltose transporter (Kerppola *et al*., 1991; Davidson and Nikaido, 1991). These four domains can be coded for in a variety of ways, as summarized in Figure 2.1. For instance, most bacterial transporters are encoded by separate genes specific for each TMD and NBD (Figure 2.1a-c) arranged in an operon, while alternative

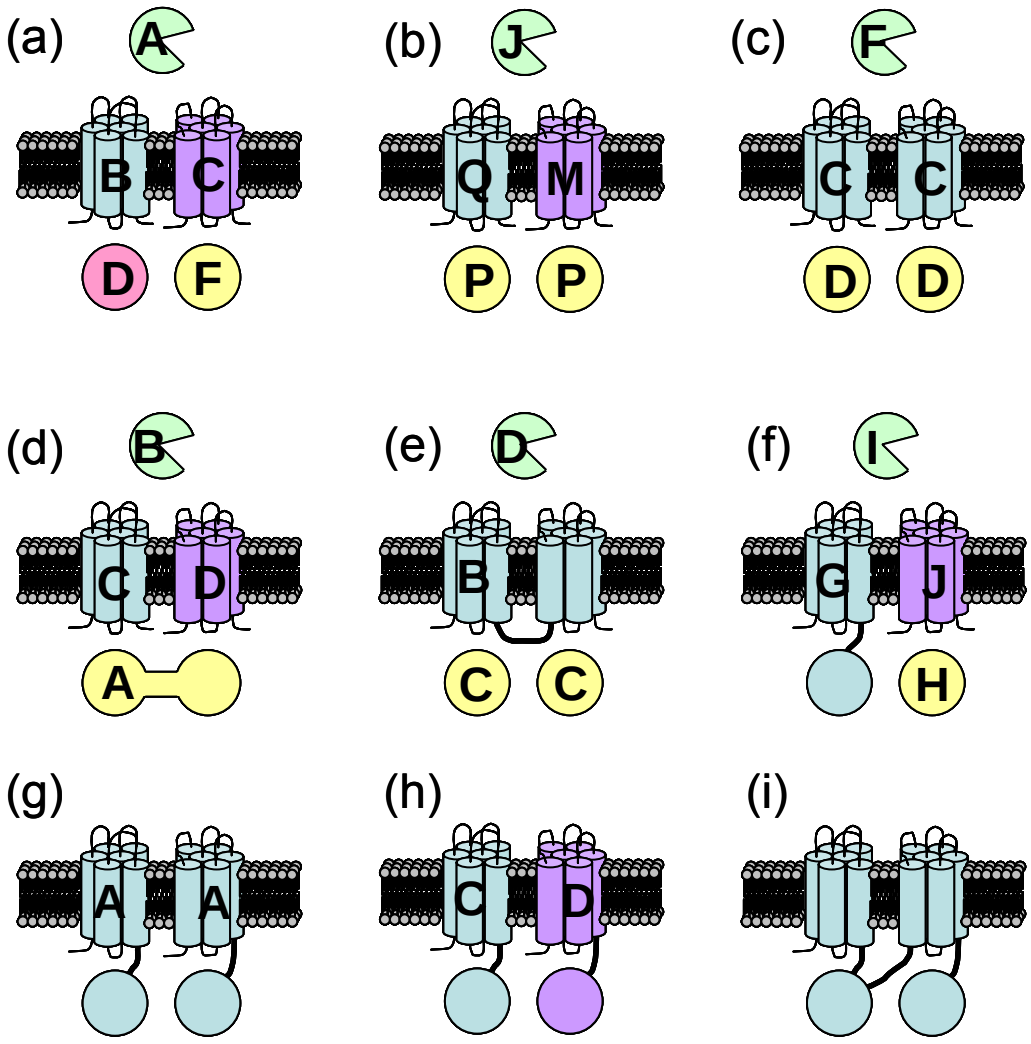

Figure 2.1 Domain Organization of ABC Transporters – Periplasmic binding proteins in (a) – (f) shown in *light green*. Transmembrane domains illustrated by groups of *six cylinders*. Nucleotide binding domains shown by *circles*. (a) Oligopeptide transporter OppABCDF with five different proteins. (b) Histidine permease $HisJQMP_2$ with four different subunits. (c) Vitamin B_{12} transporter $BtuFD_2C_2$ with three different subunits. (d) Ribose transporter RbsBCDA with fused NBDs. (e) Ferrichrome transporter $FhuDBC_2$ with fused TMDs. (f) Transporter YhiIGJH with only one half transporter (TMD-NBD). (g) Lipid transporter $MsbA_2$ with two identical half transporters. (h) Cytochrome b transporter CydCD with two different half transporters. (i) Example of a typical eukaryotic ABC transporter with all four domains on a single polypeptide (TMD1-NBD1-TMD2-NBD2 i.e., CFTR, ABCR, PGP, etc.). Eukaryotic ABC transporters also adopt the domain organizations shown in (g) and (h). Reviewed in Higgins, 1992.

arrangements with two domains fused together are possible but less prevalent (Figure 2.1d-h). On the other hand, eukaryotic ABC transporters exist either as "half" transporters with two domains on each polypeptide (Figure 2.1g-h) or full transporters, which contain all four domains (Figure 2.1i) on a single polypeptide. 17 human ABC transporters are half transporters, while 27 of the 48 human ABC transporters are full transporters. Of the remaining four human ABC transporters, subfamilies ABCE and ABCF contain genes that possess two NBDs on a single polypeptide, akin to bacterial NBD RbsA (*yellow* subunit in Figure 2.1d), but no clearly associated TMDs. As such they are not ABC transporters *per se* despite containing the highly conserved NBDs, and have not been linked to any membrane transport functions (Bisbal *et al*., 1995; Richard *et al*., 1998).

ABC Transporter NBD Conservation & Function of Conserved Residues

The aforementioned wide variance of solutes, their vectorial transport, and domain organization is reflected in the limited sequence conservation between TMDs of ABC transporters, in which the solute binding sites are thought to reside. On the other hand, the primary sequence of ABC transporter NBDs is highly conserved across all kingdoms of life, originally noted by Ames and Nikaido (Gilson *et al*., 1982b). The NBDs invariably contain three major highly conserved amino acid sequences: the Walker A (GxxGxGKS/T, where x can be various amino acids) and Walker B (ΦΦΦΦD, where Φ is a hydrophobic residue)

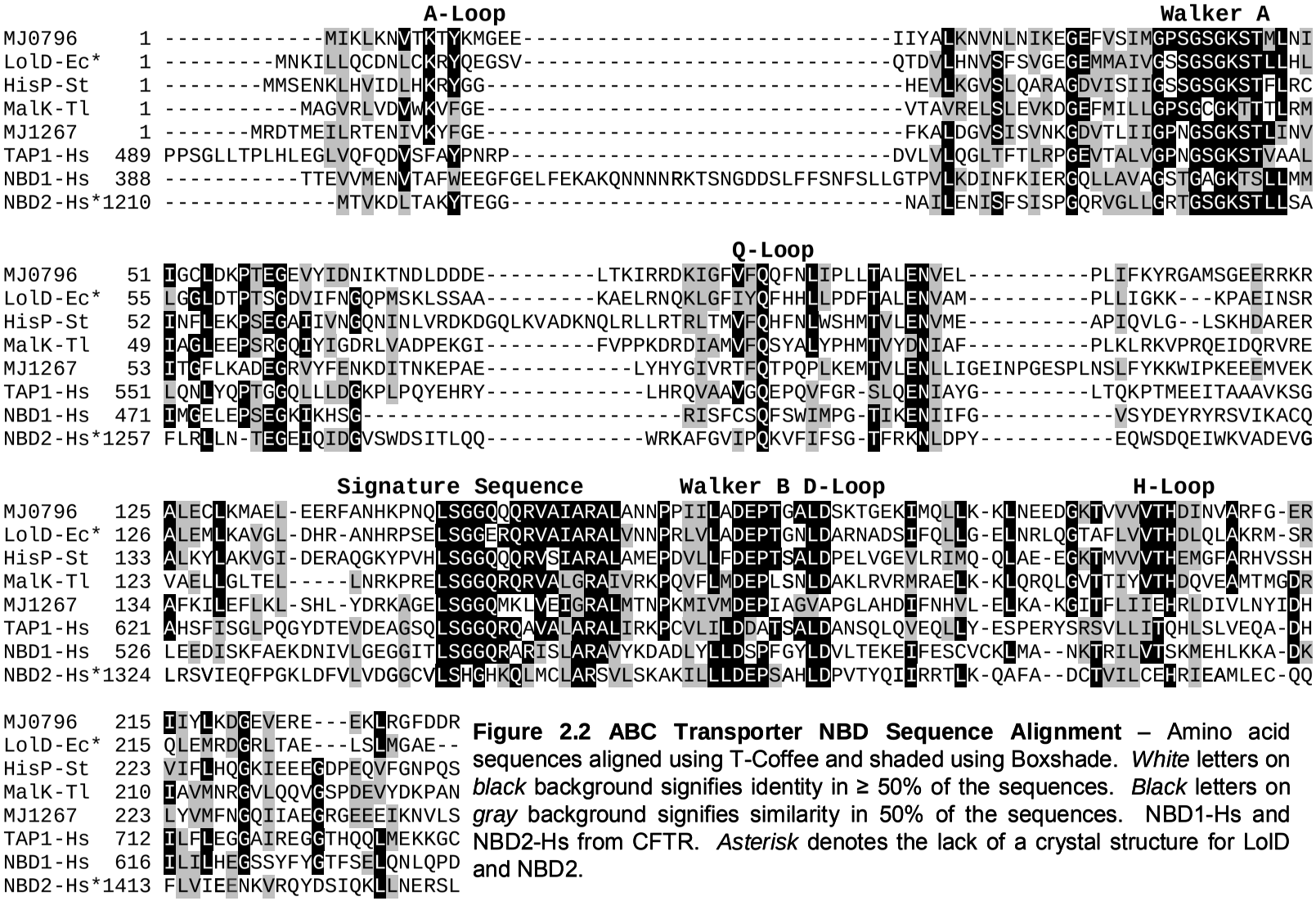

Figure 2.2 ABC Transporter NBD Sequence Alignment – Amino acid sequences aligned using T-Coffee and shaded using Boxshade. *White* letters on *black* background signifies identity in ≥ 50% of the sequences. *Black* letters on *gray* background signifies similarity in 50% of the sequences. NBD1-Hs and NBD2-Hs from CFTR. *Asterisk* denotes the lack of a crystal structure for LolD and NBD2.

nucleotide binding motifs (Walker *et al*., 1982) in addition to the ABC "signature" sequence, or "linker peptide" of LSGGQ (Ames *et al*., 1990). A multiple sequence alignment of selected structurally characterized ABC transporter NBDs is presented in Figure 2.2. In addition to the major three conserved regions, the aptly named A-, Q-, D-, and H- loops have been added to the list of areas of NBD similarity (Hung *et al*., 1998) as they each contain a near-invariant aromatic, glutamine, aspartate, and histidine residue respectively.

These highly conserved regions have been probed using mutational screens and site-directed mutagenesis in a number of ABC transporter NBDs. The Walker A motif, based upon the crystal structures of adenylate kinase, recA, and F_1-ATPase (Fry *et al*., 1986; Story and Steitz, 1992; Abrahams *et al*., 1994), was initially predicted to be crucial for nucleotide binding. Although most mutations in this motif, especially substitutions of the invariant lysine residue, do severely impair or knock out transport activity as expected (Shyamala *et al*., 1991; Delepelaire, 1994; Schneider *et al*., 1994; Kashiwagi *et al*., 1995; Koronakis *et al*., 1995; Loo and Clarke, 1995; Aparicio *et al*., 1996), some conservative mutations in this motif retain nucleotide binding capability (Azzaria *et al*., 1989; Delepelaire, 1994; Schneider *et al*., 1994). These findings suggest that the Walker A residues, while extremely important for nucleotide binding and hydrolysis, are able to accommodate mild perturbations without sacrificing transport activity.

The highly conserved aspartate residue in the Walker B motif has also been shown to be crucial for ATP binding and transport activity in a number of ABC transporter NBDs, as mutation of this residue severely impair function (Azzaria *et al*., 1989; Shyamala *et al*., 1991; Panagiotidis *et al*., 1993; Koronakis *et al*., 1995; Loo and Clarke, 1995). Immediately C-terminal of the Walker B aspartate is a highly conserved glutamate residue. This residue, when mutated to a glycine or aspartate in the polysialic acid transporter NBD KpsT from *Escherichia coli*, exhibited a dominant negative effect on wild type KpsT without affecting nucleotide binding (Bliss *et al*., 1996). In addition, mutation of the analogous glutamate in HisP resulted in slight impairment of nucleotide binding but a drastic reduction in histidine transport (Shyamala *et al*., 1991). Similar results were later obtained with mouse Mdr3, a p-glycoprotein homolog (Urbatsch *et al*., 2000).

In addition to the highly conserved Walker A and Walker B motifs, ABC transporter nucleotide binding domains contain the aforementioned signature sequence of LSGGQ (Ames *et al*., 1990; Higgins, 1992). As opposed to the Walker motifs, this signature motif is unique to ABC transporter NBDs. Because of this, and the fact that natural mutations in human CFTR that cause cystic fibrosis (G551D, G551S) have been located in this region (Welsh and Smith, 1993), the LSGGQ motif has been studied intensely. Most mutations isolated or created in this region abolish transport activity without significantly affecting

nucleotide binding (Panagiotidis *et al*., 1993; Hoof *et al*., 1994; Carson *et al*., 1995; Koronakis *et al*., 1995; Bliss *et al*., 1996; Browne *et al*., 1996; Li *et al*., 1996; Wilkinson *et al*., 1996; Bakos *et al*., 1997). Interestingly, mutation of the serine residue of the LSGGQ motif to phenylalanine in *E. coli* KpsT acts as a *cis* suppressing mutation to the E150G-KpsT dominant negative mutant discussed above.

Two highly conserved residues in the ABC transporter NBDs, in addition to the Walker A, Walker B, and signature motifs, have been shown to affect transport activity without changing nucleotide binding characteristics. A conserved glutamine residue in the amino acid stretch between the Walker A motif and the LSGGQ sequence, aptly named the Q-loop, has been shown to inhibit / diminish transport when mutated in the histidine permease and maltose transporter (Shyamala *et al*., 1991; Walter *et al*., 1992). In addition, a highly conserved histidine residue, C-terminal to the Walker B motif in the region named the H-loop, when mutated, abolishes transport in the histidine permease, maltose transporter, and polysialic acid transporter without altering nucleotide binding (Shyamala *et al*., 1991; Walter *et al*., 1992; Bliss *et al*., 1996).

ABC Transporter ATPase Activity: Cooperativity, Stoichiometry of ATP Hydrolysis and Transport, and Necessity of Two NBDs

The isolated NBDs of the histidine permease and maltose transporters, HisP and MalK respectively, have been shown to hydrolyze ATP in a cooperative fashion, with a Hill coefficient of near 2 for each (Davidson *et al*., 1996; Liu *et al*., 1997). In addition, Ames and colleagues elegantly illustrated that a dimer most likely is the oligomeric species responsible for ATPase activity exhibited in the soluble NBDs by measuring ATP hydrolysis as a function of HisP concentration (Nikaido *et al*., 1997.) Although wild type NBD dimers had not yet been stably isolated, additional evidence for NBD dimerization was provided for MalK (Kennedy and Traxler, 1999), whose C-terminal regulatory domain engenders small amounts of dimerization. Initial attempts to measure the stoichiometry of ATP hydrolysis and transport in reconstituted transport systems gave mixed results (Ames *et al*., 1989; Bishop *et al*., 1989; Davidson and Nikaido, 1990), measurements of *in vivo* stoichiometry suggested that two ATP molecules were hydrolyzed for each maltose molecule imported (Mimmack *et al*., 1989). Ambudkar and colleagues proposed that ATP hydrolysis is required at two distinct steps during the reaction cycle of p-glycoprotein based upon nucleotide trapping experiments (Sauna and Ambudkar, 1999; Sauna and Ambudkar, 2000).

As evidence for ABC transporter NBD dimers began accumulating, the question of whether both NBDs are necessary in the functional unit was probed.

Results from the maltose transporter, as well as from studies of human p-glycoprotein and the yeast **a**-factor exporter STE6, suggested that both NBDs are strictly required, as mutation of a single active site resulted in the loss of activity (Azzaria *et al.*, 1989; Berkower and Michaelis, 1991; Loo and Clarke, 1995; Davidson and Sharma, 1997). Alternatively, a study of HisP suggested that only one intact ATP hydrolysis site was sufficient for transport activity (Nikaido and Ames, 1999). The authors mixed wild type subunits with hydrolytically-deficient H211R-HisP (mutation of the highly conserved H-loop histidine residue discussed above) and measured transport activity of the heterodimers. Although the mutant-wild type heterodimers exhibited histidine transport, the maximal transport activity as well as ATPase activity was half that of a wild type dimer, correlating with the number of intact active sites in each (normally two per $HisP_2$, only one in the wild type-H211R heterodimer). The authors present an explanation of this 50% activity of the mixed dimers with a model incorporating a shortened reaction cycle with one hydrolysis event coupled to a single transport event. In this model, the normal reaction cycle of the histidine permease would utilize two ATP molecules to power the transport of two histidine molecules in the same time that the mixed dimers perform half of each (see Figure 6 in Nikaido and Ames, 1999). Interestingly, hydrolytically-deficient H211D-HisP was unable to form such half-productive heterodimers with wild type (Nikaido and Ames, 1999), suggesting that whatever function this highly conserved residue performs requires a basic

sidechain, and that other basic sidechains near the active site are unable to fulfill this activity. Mutation of the corresponding H-loop histidine residue in MalK, H192, to arginine resulted in abolition of transport activity when mixed with wild type MalK (Davidson and Sharma, 1997). The discrepancy between the results of the HisP study and the preceding work on STE6 and p-glycoprotein may result from the fact that the HisP utilized reconstituted transport systems (Nikaido and Ames, 1999), while the eukaryotic transport studies were conducted *in vivo* (Berkower and Michaelis, 1991; Loo and Clarke, 1995). This suggests that two intact subunits are needed to engender functional transport at a sufficient level *in vivo*, while slower transport turnover (i.e., the half-productive mutant-wild type HisP heterodimers from Nikaido and Ames, 1999) results in measurable activity in reconstituted systems but is simply not enough to sustain *in vivo* turnover requirements.

Structural Characterization of ABC Transporter NBDs

Recent structural studies of ABC transporter NBDs have provided a glimpse at the atomic level of the specific residues involved in ATP binding and hydrolysis in addition to the overall secondary structure organization of the highly conserved domain, nicely complementing the thirty years of genetic and biochemical data summarized above. The crystal structure of *Salmonella thyphimurium* HisP in complex with ATP (Hung *et al*., 1998) for the first time

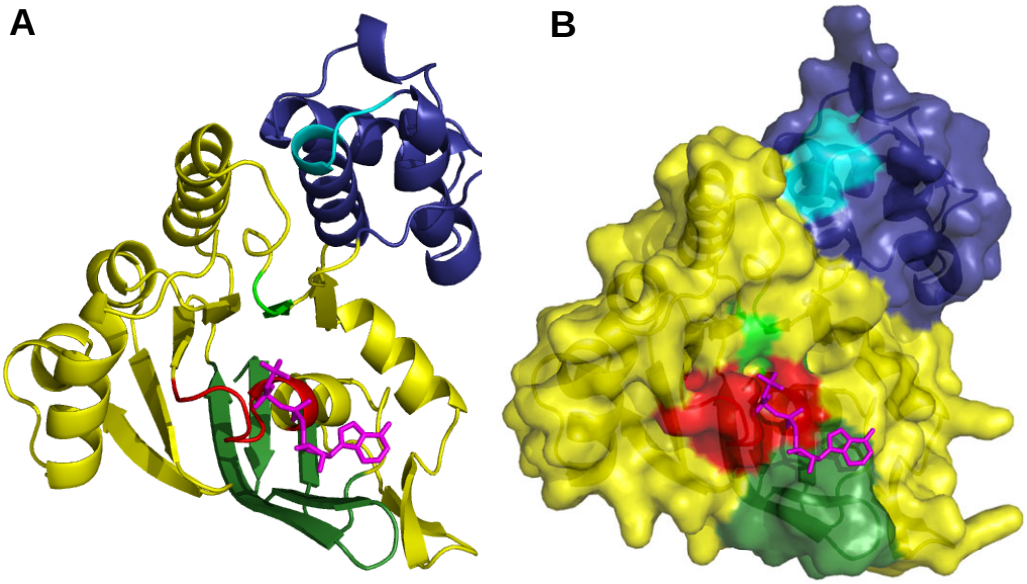

Figure 2.3 Crystal Structure of *Salmonella typhimurium* HisP – (A) Cartoon of HisP structure (pdb:1BOU). F_1-type α/β core subdomain shown in *yellow*. Anti-parallel β subdomain shown in *forest green*. α-helical subdomain shown in *dark blue*. Walker A motif highlighted in *red*. Walker B motif highlighted in *bright green*. LSGGQ signature sequence highlighted in *cyan*. ATP shown in *magenta*. (B) Surface representation of HisP with colors identical to (A).

illustrated the soluble domain's organization into a RecA-like / F_1-type mixed α/β nucleotide binding core subdomain (shown in *yellow* in Figure 2.3) containing the Walker A and Walker B motifs (highlighted in *red* and *bright green* respectively in Figure 2.3) in addition to an anti-parallel β-sheet subdomain (shown in *green* in Figure 2.3) and an α-helical subdomain (shown in *dark blue* in Figure 2.3) containing the LSGGQ signature motif (shown in *cyan* in Figure 2.3). The ATP molecule is coordinated by Walker A and Walker B residues, as well as the highly conserved aromatic residue in the anti-parallel β subdomain, the glutamine in the Q-loop, and the histidine of the H-loop (Figure 2.4).

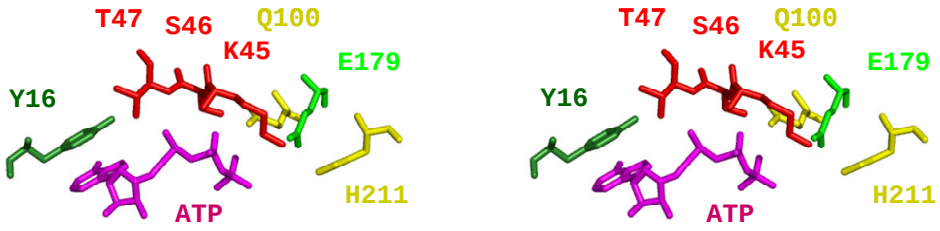

Figure 2.4 ATP Binding Site of HisP – Stereo view (cross-eyed) of nucleotide binding in HisP. ATP shown in *magenta*. Y16 shown in *forest green*. K45, S46 and T47 shown in *red*. Q100 and H211 shown in *yellow*. E179 shown in *bright green*.

A breakthrough in the field, this initial ABC transporter NBD structure also begged three important questions. First of all, why were the signature sequence residues, so highly conserved throughout evolution (Figure 2.2) and implicated in ATP binding and hydrolysis by mutational studies (summarized above), located over 20 Å away from the observed nucleotide binding site (Figure 2.3)? In addition, why was the bound nucleotide so unexpectedly solvent exposed (Figure 2.3B)? Finally, how could the dimeric arrangement of HisP molecules in the crystal explain the positive cooperativity measured in ATP hydrolysis (Davidson *et al*., 1996; Liu *et al*., 1997)?

Within a few years of the publication of the HisP structure, four additional ABC transporter NBD crystal structures were reported. The first five ABC transporter NBD crystal structures, along with the structure of the distantly related ABC ATPase Rad50 (Figure 2.5), presented six distinct crystallographic dimers (Hung *et al*., 1998; Hopfner *et al*., 2000; Diederichs *et al*., 2000; Karpowich *et al*., 2001; Yuan *et al*., 2001; Gaudet and Wiley, 2001; Figure 2.6). As mentioned

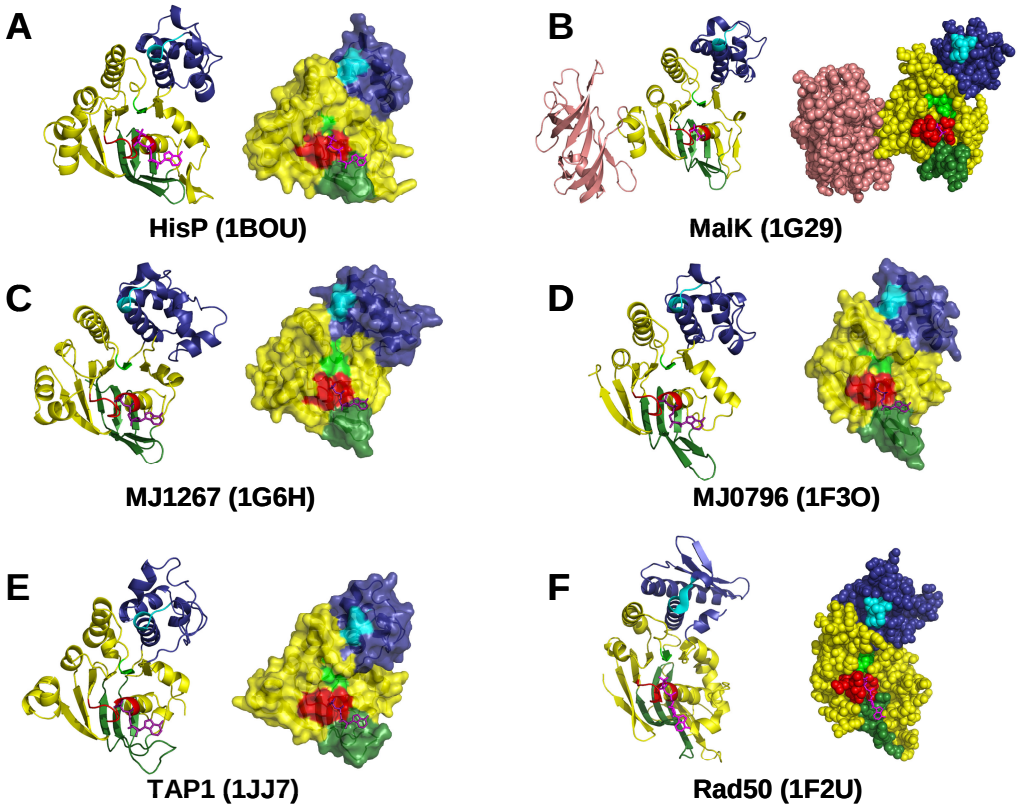

Figure 2.5 ABC Transporter NBD Crystal Structures – Cartoon and surface representations. F_1-type α/β core subdomains shown in *yellow*. Anti-parallel β subdomains shown in *forest green*. α-helical subdomain shown in *dark blue.* MalK C-terminal domain shown in *salmon*. Walker A motif highlighted in *red*. Walker B motif highlighted in *bright green*. LSGGQ signature sequence highlighted in *cyan*. ATP shown in *magenta*. ADP shown in *purple*. Surface representations of MalK (B) and Rad50 (F) shown with *spheres* since crystallographic dimers interfered with the normal surface representation.

above, the HisP dimer structure places the nearest signature sequence residues over 20 Å away from the ATP molecules at the binding site, and the dimeric interface involves β-strands from the anti-parallel β-sheet subdomain (Hung *et al*., 1998; Figure 2.6A). The second ABC transporter NBD structure published, that

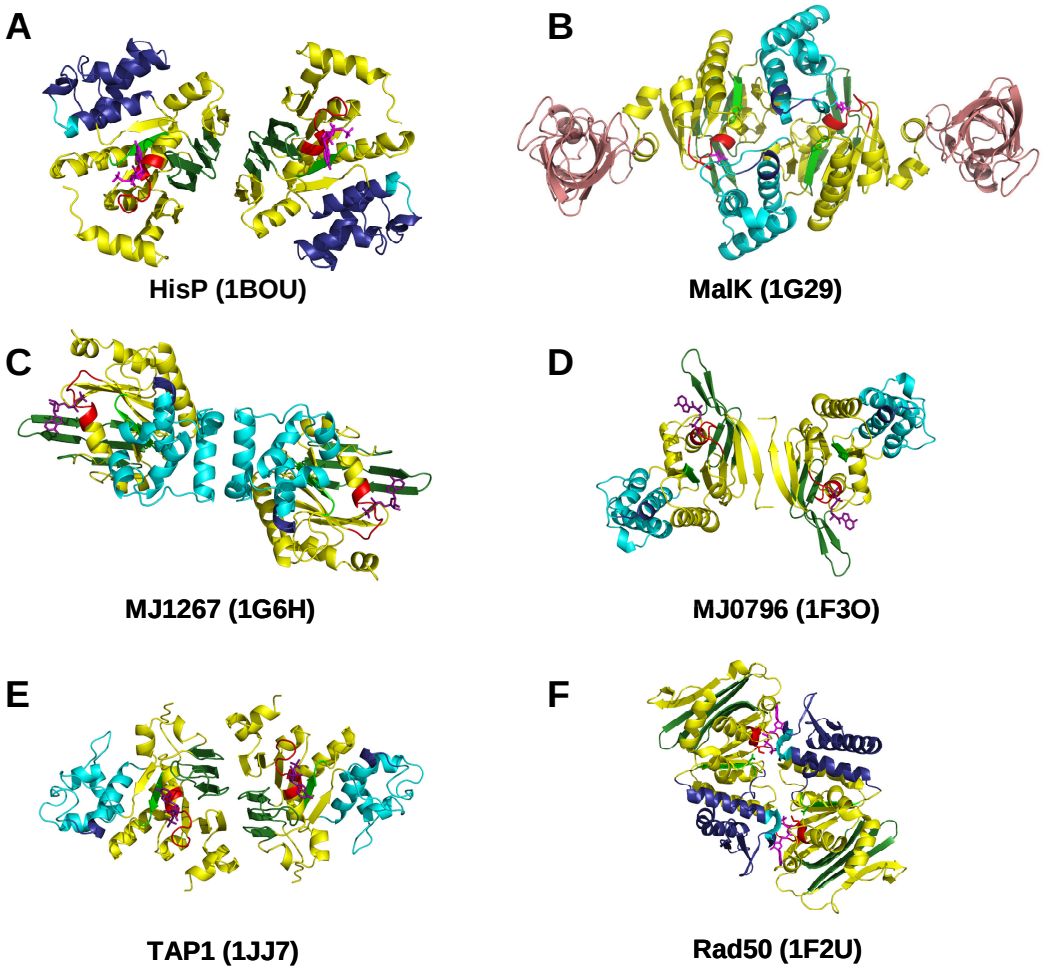

Figure 2.6 Crystallographic ABC Transporter NBD Dimers – Cartoon representations. F_1-type α/β core subdomains shown in *yellow*. Anti-parallel β subdomains shown in *forest green*. α-helical subdomain shown in *dark blue* (A,F) or *cyan* (B-E). MalK C-terminal domain shown in *salmon*. Walker A motif highlighted in *red*. Walker B motif highlighted in *bright green*. LSGGQ signature sequence highlighted in *dark blue* (A,F) or *cyan* (B-E). ATP shown in *magenta*. ADP shown in *purple*.

of MalK from *Thermococcus litoralis* (Figure 2.5B), exhibited a different dimeric interface involving all three subdomains, although the nearest signature sequence residues remained 20 Å distant from the pyrophosphate moieties (the electron density was not clear for the adenosine groups of ADP). In addition, MalK

possesses a C-terminal regulatory domain which is visible in the crystal structure (Diederichs *et al*., 2000; Figure 2.6B). Two NBDs from the hyperthermophilic archaeon *Methanocaldococcus jannaschii*, MJ1267 and MJ0796, were crystallized (Karpowich *et al*., 2001; Yuan *et al*., 2001). Although the crystallographic dimers observed in the MJ1267 and MJ0796 structures appeared unlikely to be physiologically relevant (Figure 2.6D-E), the overall fold of the NBD was remarkably similar to HisP and MalK (Figure 2.5). The first eukaryotic ABC transporter NBD crystallized, human TAP1 (transporter associated with antigen presentation) (Trowsdale *et al*., 1990) exhibited a crystallographic dimer involving the anti-parallel β subdomain (Figure 2.6F) (Gaudet and Wiley, 2001). The crystal structure of *Pyrococcus furiosus* Rad50, a structural maintenance of chromosomes (SMC) family member bearing distant sequence similarity to ABC transporter NBDs (Hopfner *et al*., 2000) ultimately pointed the field in the right direction regarding the disputed dimeric interface.

Rad50, a double strand break repair (DSBR) protein comprised of an N-terminal fragment containing a Walker A motif and a C-terminal fragment containing both the Walker B motif and a pseudo-signature sequence, was crystallized in monomeric form in the absence of nucleotide as well as an AMP-PNP bound dimeric form (Hopfner *et al*., 2000; Figure 2.5F; Figure 2.6E). The dimeric structure possesses two nucleotide binding sites, located at the monomer-monomer interface, comprised of residues from the Walker A and Walker B

motifs from one Rad50 monomer and residues from the pseudo-signature sequence of the opposing Rad50 monomer (Figure 2.7), while the anti-parallel β-sheet subdomains, structurally divergent from the anti-parallel β-subdomains from ABC transporter NBDS, exist on the periphery. This preliminarily addressed the three major concerns stemming from the crystallographic HisP and MalK dimers: (1) The highly conserved signature sequence residues contribute to the nucleotide binding site, accommodating the mutational data on the LSGGQ motif. (2) The ATP molecule is almost completely buried, a much more likely scenario physiologically than the exposed nucleotide of the HisP structure (Figure 2.3B, Figure 2.5). (3) Two nucleotides bind at the dimer interface, accommodating ATPase cooperativity results.

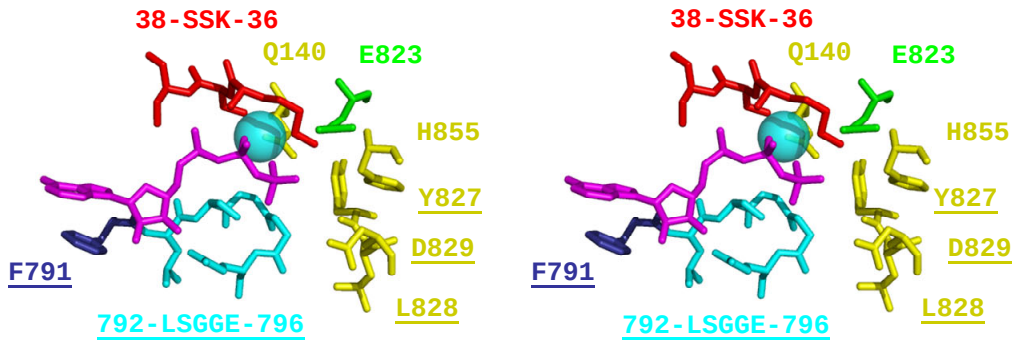

Figure 2.7 ATP Binding in Rad50 – Stereo view (cross-eyed). ATP shown in *magenta*. K36, S37 and S38 shown in *red*. Q140 and H855 shown in *yellow*. E823 shown in *bright green*. *Underlined* residues are from the opposing monomer in the Rad50 dimer. F791 shown in *dark blue*. LSGGE sequence shown in *cyan*. Y827, L828 and D829 shown in *yellow*. Magnesium ion shown in *cyan sphere*.

Several hypotheses for the physiological ABC transporter dimer had been proposed based on crystallographic dimers of HisP, Rad50, and MalK (Hung *et*

al., 1998; Hopfner *et al*., 2000; Diederichs *et al*., 2000). Studies of MJ1267 and MJ0796 (Karpowich *et al*., 2001; Yuan *et al*., 2001), homologs of *E. coli* LivG and LolD respectively (Rahamanian *et al*. 1973; Oxender *et al*., 1980; Yakushi *et al*. 2000), presented evidence that strongly supported the Rad50 model of dimerization based on the mapping of previously described mutations affecting transport in the maltose transport system and sequence conservation data onto the MJ0796 dimer model (Thomas and Hunt, 2001; Yuan *et al*., 2001). In addition, the MJ1267 structural study, the first to illustrate both ADP-bound and nucleotide-free forms of the same NBD, detailed the 15º rigid body rotation of the α-helical subdomain with respect to the F_1-type α/β core and anti-parallel β-sheet subdomains in the absence of the γ-phosphate of ATP (Karpowich *et al*., 2001; denoted by *cyan* in Figure 2.5C). This rotation, also exhibited by the ADP-bound structure of MJ0796 (denoted by *cyan* in Figure 2.5D), was proposed to serve a role in the coupling of nucleotide binding and hydrolysis to transport (Yuan *et al*., 2001). Hopfner and colleagues suggested a unified molecular mechanism for ABC transporters and SMC proteins (Hopfner *et* al., 2000) although the Rad50 dimeric arrangement remained to be seen in an ABC transporter. They proposed that ATP-driven cooperativity and allosteric control of dimerization are essential for both Rad50 DSBR and ABC-ATPase activity in general. While an attractive model, additional biochemical and structural work on ABC transporter NBDs was necessary to validate their claims.

Chapter III

Biochemical and Structural Characterization of Catalytic Carboxylate Mutant Archaeal ATP-Binding Cassette Transporter Nucleotide Binding Domains

Introduction

The crystal structures of a homodimeric half-ABC transporter (one TM domain and one NBD in each monomer), MsbA (Chang and Roth, 2001), and isolated NBDs (Hung *et al*., 1998; Diederichs *et al*., 2000; Karpowich *et al*, 2001; Yuan *et al*., 2001; Gaudet and Wiley, 2001) had not resolved the oligomeric organization of ABC transporter nucleotide binding domains. The first four ABC transporter NBDs crystallized exhibited four different dimeric interfaces (Yuan *et* al., 2001). The authors compare the buried solvent-accessible surface area, surface complementarity, and number of van der Waals contacts and hydrogen bonds in an attempt to determine which, if any, of the first four NBD dimeric interfaces witnessed represent the physiologically relevant conformation (see Figure 4 in Yuan *et al*., 2001; Figure 2.6). These initial NBD structures exhibit unusually solvent-exposed nucleotide binding sites (Figure 2.3, Figure 2.5), while the LSGGQ signature sequence is nearly 20Å away from the bound nucleotide,

although mutations in this motif have been shown to affect ATP hydrolysis (Panagiotidis *et al*., 1993; Hoof *et al*., 1994; Carson *et al*., 1995; Koronakis *et al*., 1995; Bliss *et al*., 1996; Browne *et al*., 1996; Li *et al*., 1996; Wilkinson *et al*., 1996; Bakos *et al*., 1997). The crystal structure of the distantly related DNA repair protein Rad50 (Hopfner *et al*., 2000) suggests a resolution of this conundrum and provides a potential mechanism for the power stroke of ABC transporters.

In the Rad50 structure, two opposing nucleotide binding domains bind the non-hydrolyzable ATP analogue AMP-PNP with the Walker A and B motifs of one monomer and an LSGGQ-like sequence of the other monomer completing the two binding pockets in a dimer that sandwiches the two nucleotides at the interface (Hopfner *et al*., 2000; Figure 2.6F, Figure 2.7). This arrangement, predicted a year earlier (Jones and George, 1999), forms a much more occluded active site and is consistent with the effect of LSGGQ signature sequence mutations on ATP hydrolysis summarized in Chapter II. In the absence of AMP-PNP Rad50 is monomeric, suggesting a model for the mechanism of ABC-type ATPases wherein ATP-driven dimerization of the NBDs couples ATP binding and hydrolysis to useful thermodynamic output (Hopfner *et al*., 2000; Figure 2.8). In ABC transporters, the formation of such an ATP-dependent dimer and/or dissociation of the dimer driven by ATP hydrolysis could mediate rearrangements of the TM domains that support solute transport across the membrane.

However, there are four observations that have caused the Rad50 model for the mechanochemistry of ABC transporters to remain controversial. First, isolated wild type NBDs from ABC transporters have not been observed to stably dimerize upon binding either ATP or non-hydrolyzable analogues (Liu *et al*., 1997; Kennedy and Traxler, 1999). Second, no such nucleotide sandwich complex (i.e., ATP-bridged dimer) has been observed in any of the crystal structures of isolated NBDs that have been reported in various nucleotide-bound states (Hung *et al*., 1998; Diederichs *et al*., 2000; Karpowich *et al*, 2001; Yuan *et al*., 2001; Gaudet and Wiley, 2001; Figure 2.6). Third, the only dimer observed in the low-resolution crystal structure of the MsbA integral membrane protein positions the NBDs in a geometry where they are incapable of forming such a complex (Chang and Roth, 2001). Finally, although Rad50 shares an F_1-type α/β core subdomain with ABC transporter NBDs, its structure has diverged quite considerably in the anti-parallel β subdomain and the α-helical subdomain. While Rad50 does possess an LSGGQ-like signature motif, its position is altered relative to that observed in ABC transporter NBDs by a 5 residue expansion in the α helix that it caps. Furthermore, the other elements contacting the nucleotide in the symmetry-related subunit in the Rad50 dimer are derived from the regions where its structure diverges from that of ABC transporter NBDs, i.e., the anti-parallel β subdomain and the subdomain that replaces the α-helical subdomain. Considering these structural differences in combination with the failure to observe

such a dimer in an ABC transporter NBD, the Rad50 model for the structural mechanics of ABC transporters has remained controversial.

This model, although disputed, suggests that an NBD mutant that binds but is unable to hydrolyze ATP might form a stable ATP sandwich dimer like that witnessed in the Rad50 crystal structure. To test this hypothesis and gain insight into the mechanism of ABC transporters, we mutated the catalytic base of two archaeal NBDs, characterized their ability to form nucleotide dependent dimers, and determined the first crystal structure of a stable ATP sandwich dimer of NBDs from an ABC transporter.

Materials and Methods

Protein Expression and Purification (for biochemical assays) - Wild type and mutant MJ0796 proteins were expressed for 4-5 hours in BL21 Codon + *E. coli* cells in the presence of kanamycin after induction with 1mM IPTG at OD_{600nm} between 0.4 and 0.8. Cells were pelleted, frozen at -80°C, and lysed in 50mM Tris pH 7.6, 50mM NaCl, 1mM EDTA, 4mM DTT, and 1mM PMSF. Lysed cells were sonicated on ice at 50% duty cycle using a micro tip at power setting 5 – 6 for 30 seconds every minute for ten minutes. Sonicated cells were then spun for 15 minutes in JA25.5 rotor at 12,000 g at 4°C. Supernatant was collected and heated at 65 - 70°C for 10 minutes, then spun for 10 minutes in JA25.5 rotor at 75,000 g at 4°C. Supernatant was filtered using 0.45μM syringe filter and injected onto a DEAE column at 4°C using an Akta Prime. A gradient of 100% buffer A1 to 100% buffer B1 was run. Buffer A1: 50mM Tris pH 7.6, 1mM EDTA, and 1mM DTT. Buffer B1: 50mM Tris pH 7.6, 1M NaCl, 1mM EDTA, and 1mM DTT. Fractions containing MJ0796 were pooled, $(NH_4)_2SO_4$ added to 1M, and injected onto a butyl sepharose column at 4°C using an Akta Prime. A gradient of 100% buffer A1 to 100% buffer B1 was run. Buffer A1: 25mM Tris, 25mM Bis-Tris Propane pH 7.5, 600mM $(NH_4)_2SO_4$, 1mM EDTA, and 1mM DTT. Buffer B1: 25mM Tris, 25mM Bis-Tris Propane pH 7.5, 1mM EDTA, and 1mM DTT. Fractions containing MJ0796 were pooled and concentrated to 5mL using Amicon Ultra concentration devices at 3750 RPM at 4°C. 0.45μM filtered

concentrate injected onto an S-200 column at 4°C using an Akta Prime. Buffer A1: 50mM Tris pH 7.5, 200mM NaCl, 10% glycerol, 1mM EDTA, and 1mM DTT. Fractions containing MJ0796 were pooled and concentrated to >1 mg/mL (as determined using Bio-Rad protein concentration determination kit) using Amicon Ultra concentration devices at 3750 RPM at 4°C. Aliquots of protein were frozen in liquid N_2 and stored at -80°C.

Protein Expression and Purification (for crystallization) – Following cell harvesting and lysis as described above, the supernatant from a 30 minute centrifugation at 4°C in an SA600 rotor was heat-shocked at 65°C for 10 minutes. Streptomycin sulfate was added to the resulting suspension to a final concentration of 4% (w/v), and this mixture was incubated for 30 minutes at 4°C prior to centrifugation in the SA600 rotor for 30 minutes at 4°C. The resulting supernatant was purified on QEAE and butyl Sepharose-FF columns as described above. The pooled fractions from the hydrophobic interaction column containing 50-100 mM $(NH_4)_2SO_4$ was concentrated to ~1mg/mL in a Centriprep-10 which resulted in the appearance of a protein precipitate. The protein was resolubilized by diluting the suspension 1:1 with 1M arginine-HCl pH 7.5 prior to adding Na-ATP and Na-EDTA to final concentrations of 20mM and 1mM respectively. Although the resulting solution appeared clear, it was filtered through a 0.45μm ceullose acetate filter after 30 minute incubation at 4°C. The filtrate was concentrated to 3mg/mL using a Centriprep-10 prior to exchange into a buffer

containing 20mM Na-ATP, 1mM EDTA, 10% glycerol, 4mM DTT, and 10mM Tris pH 8.0 using a HiPrep 26/10 desalting column. After concentration of the protein to about 5 mg/mL in this buffer, single-use aliquots were frozen in liquid N_2 and stored at -80°C.

Crystallization – Crystals were grown by hanging drop vapor diffusion, mixing the purified protein 1:1 with a well solution containing 18% (w/v) PEG 4000, 10% isopropanol, 100mM Na-HEPES pH 7.0. Crystals generally grew to full size (~100μm^3) within 12 hours. They were cryo-protected for 30 seconds in a solution containing 25% PEG 4000, 10% isopropanol, 100mM Na-HEPES pH 7.0 prior to freezing in liquid propane.

Structure Determination and Refinement – Molecular replacement and model building was performed as described in Smith *et al*., 2002.

ATPase Activity Measurement - ADP production was assessed by monitoring NADH depletion using the lactate dehyrogenase / pyruvate kinase coupled assay described previously (Rosing *et al*., 1976). Mutant and wild type MJ0796 concentration was 0.5-1.0 μM. Assays were conducted using a UV/VIS spectrophotometer while measuring the decrease in absorbance at 340nm. Data was fit using SigmaPlot.

HPLC Gel Filtration - Samples were run at 1mL/min on Beckman System Gold using TOSOH GFC-200 column at room temperature in mobile phase of 50mM Tris pH 7.6, 200mM NaCl and detected at 220nm.

Analytical Ultracentrifugation – Mutant and wild type MJ0796 samples at 20μM were spun in a Beckman XLI centrifuge using the An60Ti rotor. Sample buffer was 50mM Tris-HCl, pH 7.6, 200mM NaCl, and 1mM EDTA. Molecular weights of the various monomers were determined using ProtParam, and buffer densities were determined using Sednterp. Data were collected at 17,000 and 24,000 RPM at 4°C using interference optics at 675nm and was fit using SigmaPlot to the following equations- single-species fit: Fringe Data = $e^{(\ln(c) + H*M(r*r-r0*r0)}$ + offset, where c = concentration, M = single species mass in Daltons, $H = (1-\bar{\upsilon}\rho)\omega^2/2RT$, $\bar{\upsilon}$ = protein density, ρ = solvent density, $\omega = 2\pi RPM/60$, r = radius in cm, and r0 = innermost radius. Monomer – dimer equilibrium: Fringe Data = $e^{(\ln(c) + H*M(r*r-r0*r0)}$ + $e^{(2\ln(c) + \ln(Ka) + 2H*M(r*r-r0*r0)}$ + offset, where c = concentration, M = monomeric mass in Daltons, $H = (1-\bar{\upsilon}\rho)\omega^2/2RT$, $\bar{\upsilon}$ = protein density, ρ = solvent density, $\omega = 2\pi RPM/60$, r = radius in cm, r0 = innermost radius, and Ka = association constant with regard to fringe data. To determine the association constant with regard to protein concentration, the following conversion was used: $K_{a,\ concentration} = (K_{a,\ fringe} * 3.31) / (2 * M)$ where M = monomeric molecular mass.

Results and Discussion

Mutational studies of the bacterial NBDs HisP (Shyamala *et al*., 1991) and KpsT (Bliss *et al*., 1996) in addition to mouse Mdr3 (Urbatsch *et al*., 2000) indicate that a highly conserved glutamate residue, found at the C terminus of the Walker B aspartate residue in the sequence ΦΦΦΦD**E**PTSALD, (where Φ is a hydrophobic residue), is critical for ATPase and transport activity. This glutamate residue is in position to activate a nearby water molecule in the HisP structure and was thus predicted to serve as the catalytic carboxylate (Hung *et al*., 1998; Yoshida and Amano, 1995). To further investigate the role of this glutamate residue, we generated either glutamate to glutamine or alanine

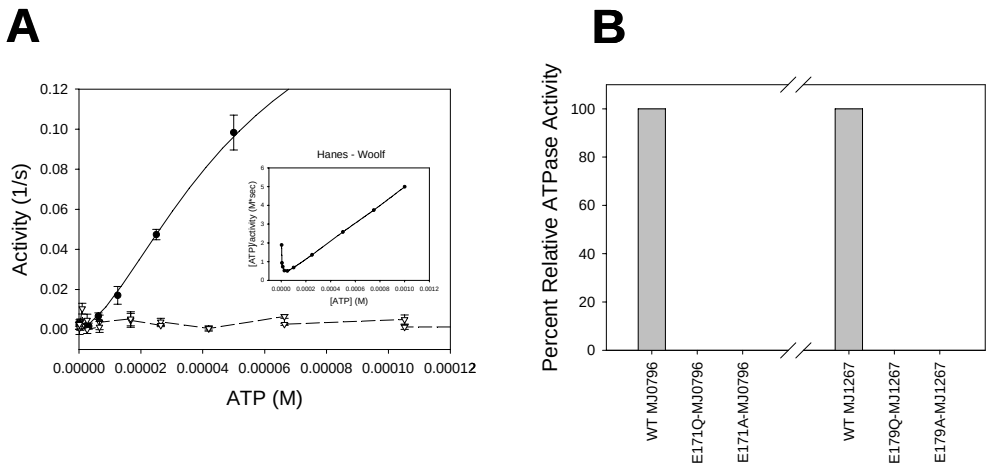

Figure 3.1 MJ0796 & MJ1267 ATPase Activity – 1μM protein samples were analyzed using a coupled assay. (A) Wild type MJ0796 (*solid circles* and *solid line*) and E171Q-MJ0796 (*open inverted triangles* and *dashed line*) data fit to the Hill equation using SigmaPlot. Inset shows Hanes – Woolf plot of wild type MJ0796 data. (B) Summary of ATPase activity for wild type, E171Q-, and E171A-MJ0796, as well as for wild type, E179Q-, and E179A-MJ1267 proteins.

mutations in MJ0796 and MJ1267, two well characterized archaeal ABC transporter NBDs.

Biochemical and Biophysical Characterization of MJ0796 and MJ1267

ATPase activity of the NBDs was determined using a coupled assay (Rosing *et al*., 1975). Wild type MJ0796 exhibited a V_{max} of 0.2 sec^{-1} with a K_m of 0.00005M ATP (Figure 3.1A). This turnover rate is presumably lower in the intact transporter, as reconstituted maltose and histidine transporters have been shown to hydrolyze nucleotide at rates approximately ten times lower than in the isolated NBDs (Nikaido *et al*., 1997). The Hanes-Woolf plot (Figure 3.1A, *inset*) presents a shape diagnostic of positively cooperative ATP binding/hydrolysis consistent with the Hill coefficient of 1.7 as fit to the equation $V = V_{max} * ([ATP]^H / (K_m{}^H + [ATP]^H))$. Positive, two-site cooperativity was previously observed for wild type bacterial MalK (Davidson *et al*., 1996) and HisP (Liu *et al*., 1997). On the other hand, the E171Q mutant of MJ0796 had undetectable ATPase activity (Figure 3.1A). The equivalent mutation in the MJ1267 NBD, E179Q, also eliminated measureable ATPase activity (Figure 3.1B). Alanine substitutions for these two glutamate residues (E171A and E179A in MJ0796 and MJ1267 respectively) also resulted in zero detectable ATPase activity (Figure 3.1B). These results show that the functional group of the conserved glutamate residue at the C terminus of the Walker B motif is required for ATP hydrolysis.

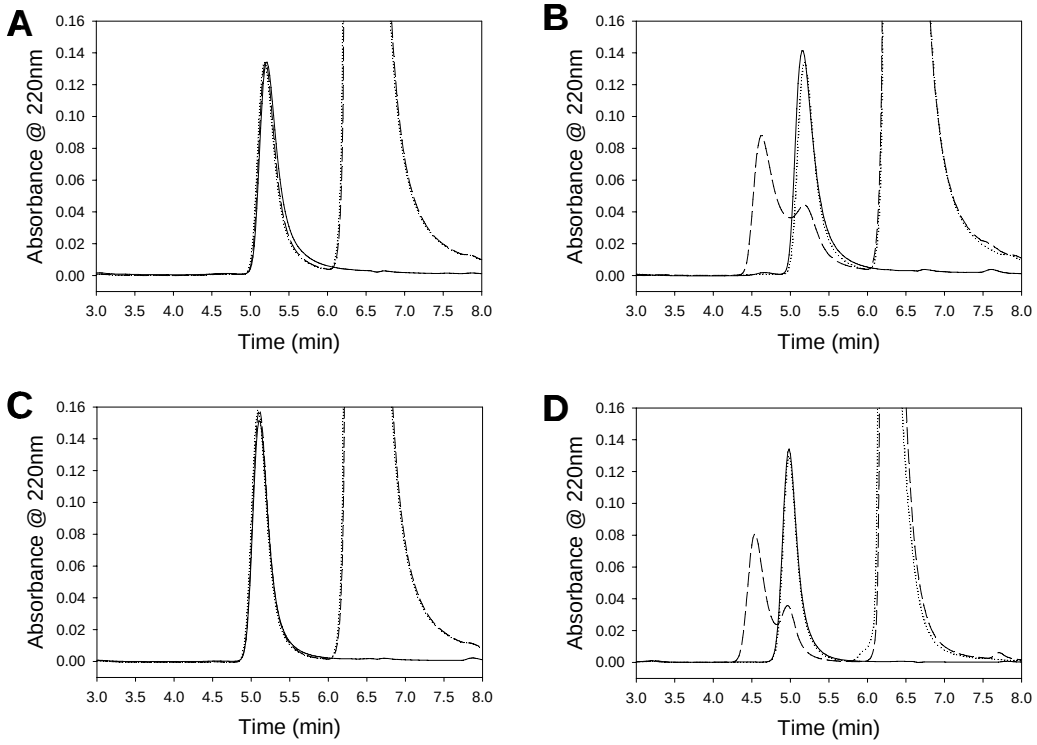

Figure 3.2 Analytical Gel Filtration – 30μM protein samples were run at 1mL/min. (A) Wild type MJ0796, (B) E171Q-MJ0796, (C) Wild type MJ1267, and (D) E179Q-MJ1267 in absence of nucleotide (*solid line*) or presence of 10mM ATP (*dashed line*) or 10mM ADP (*dotted line*).

Based on the Rad50 model for the transport cycle (Figure 2.8), the hydrolysis deficient glutamate to glutamine mutants of ABC transporter NBDs would be expected to form a similar ATP-bound homodimer provided their nucleotide binding ability is unaltered by the mutation. To assay the ability of mutant NBDs to form stable nucleotide-dependent dimers, we performed experiments wherein protein samples were mixed with ADP, ATP, or non-hydrolyzable ATP analogues, and then resolved on a size exclusion column. The data (Figures 3.2A-D) show that both wild type and mutant forms of MJ0796 and

MJ1267 migrated as monomers in the absence of ATP. However, the E171Q mutant of MJ0796 migrated largely as a homodimer in the presence of ATP (Figure 3.2B) while the E179Q mutant of MJ1267 behaved similarly (Figure 3.2D). Wild type MJ0796 and MJ1267 migrated as monomers regardless of the presence of ATP (Figures 3.2A, 3.2C). ADP did not support the formation of a stable dimer of either wild type (Figures 3.2A, 3.2C) or glutamate to glutamine mutants (Figures 3.2B, 3.2D). Moreover, the addition of ADP inhibited ATP-dependent dimer formation of the E179Q mutant of MJ1267, as appreciable dimerization only occurs when the millimolar ratio of ADP:ATP decreased to 2:8 and 0:10 (*cyan* and *gray* traces in Figure 3.3). The fact that the mutant ATP-containing dimer was stable during elution in the absence of nucleotide in the mobile phase indicates that the nucleotide sandwich dimers only slowly dissociate in the absence of ATP hydrolysis. Consistent with our findings, previous studies of wild type HisP (Liu *et al*., 1997) and MalK (Kennedy and Traxler, 1999) exhibit no more than a small degree of dimerization in the presence of nucleotide.

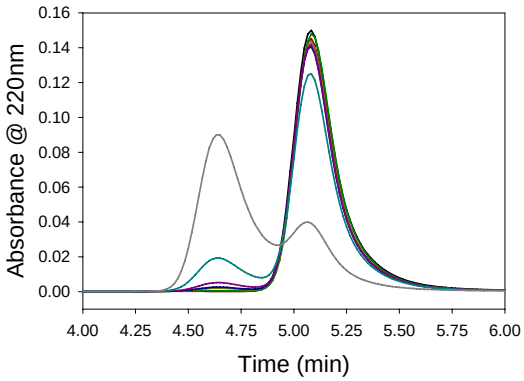

Figure 3.3 Effect of ADP on Dimerization – 30μM E179Q-MJ1267 run at 1mL/min in the absence of nucleotide (*black*), or in the presence of ADP:ATP millimolar ratios of 10:0 (*red*), 8:2 (*green*), 6:4 (*yellow*), 5:5 (*blue*), 4:6 (*pink*), 2:8 (*cyan*), and 0:10 (*gray*) added to sample.

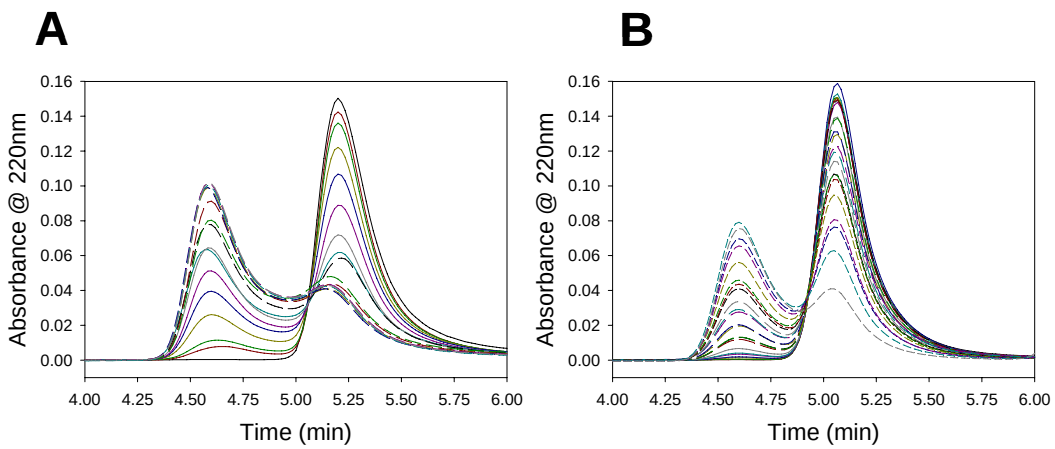

Figure 3.4 ATP-Dependent Dimerization of E171Q-MJ0796 & E179Q-MJ1267 – 30μM protein samples were run at 1mL/min. (A) E171Q-MJ0796 alone (*black solid*) or in presence of increasing amounts of ATP; *solid* lines: 10μM (*red*), 20μM (*green*), 30μM (*yellow*), 40μM (*blue*), 50μM (*pink*), 60μM (*cyan*), 70μM (*gray*), *dashed* lines: 80μM (*black*), 90μM (*red*), 100μM (*green*), 120μM (*yellow*), 150μM (*blue*), 200μM (*pink*), 300μM (*cyan*), 500μM (*gray*). (B) E179Q-MJ1267 alone (*black solid*) or in presence of increasing amounts of ATP; *solid* lines: 10μM (*red*), 20μM (*green*), 30μM (*yellow*), 40μM (*blue*), 50μM (*pink*), 60μM (*cyan*), 70μM (*gray*), *large dashed* lines: 80μM (*black*), 90μM (*red*), 100μM (*green*), 120μM (*yellow*), 150μM (*blue*), 200μM (*pink*), 250μM (*cyan*), 300μM (*gray*), *small dashed* lines: 400μM (*black*), 500μM (*red*), 1mM (*green*), 2mM (*yellow*), 5mM (*blue*), 10mM (*pink*), 20mM (*cyan*), 30mM (*gray*).

The dependence of the dimerization of the E171Q mutant of MJ0796 on ATP concentration is shown in Figure 3.4A. The midpoint of the titration was between 50 and 100 μM ATP, consistent with the K_m for ATP hydrolysis observed for wild type (Figure 3.1A). Analogous results demonstrating the ATP-dependent dimerization of the E179Q mutant of MJ1267 NBD are shown in Figure 3.4B. The midpoint of the titration occurred at a higher ATP concentration for this protein, approximately 300-400μM ATP, suggesting that the relative rate of E179Q-MJ1267 dimer dissociation is greater than the dissociation of E171Q-MJ0796 dimers.

To determine the energetics of the ATP-dependent homodimerization of E171Q-MJ0796 observed by analytical gel filtration, samples were analyzed at a protein concentration of 50μM by equilibrium analytical ultracentrifugation (data summarized in Table 3.1). In the absence of ATP, a K_D of 200mM was calculated for monomer-homodimer equilibrium, indicating that the protein was present primarily as a monomer under these conditions, consistent with gel filtration results upon purification. Again ADP did not support dimerization in the equilibrium analytical ultracentrifugation analysis. In contrast, the addition of 2mM ATP resulted in a reduction of the K_D to sub-micromolar levels, indicating that the protein was present primarily as a dimer under these conditions. The steep dependence seen in Table 3.1 of the K_D for monomer-homodimer equilibrium on ATP concentration is expected if dimerization is coupled to positively cooperative ATP binding in the symmetric sandwich dimer (Goldsmith, 1997).

Nucleotide	Salt (200mM)	Single Species Fit (Da)	K_D μM
0	NaCl	37,000	208
100μM ATP	NaCl	42,000	134
400μM ATP	NaCl	41,000	147
2mM ATP	NaCl	53,000	0.07
10mM ATP	NaCl	53,000	0.02
10mM ATP	KCl	52,000	0.60
10mM ADP	NaCl	39,000	208

Table 3.1 Analytical Ultracentrifugation Results – 56μM samples of E171Q-MJ0796 spun at 17,000 & 24,000 rpm. Data analyzed using SigmaPlot.

The non-hydrolyzable ATP analogues ATPγS and AMP-PNP failed to promote cassette dimerization in gel filtration experiments on wild type MJ0796

and MJ1267 and only poorly promoted dimerization of the mutant cassettes (Figure 3.5). These results suggest that these analogues, while useful in numerous other applications, are not always accurate mimetics of their natural counterparts. The subtle electrostatic and steric differences between conventional nucleotides and the non-hydrolyzable analogues apparently prevent stable NBD dimerization. This observation likely explains the difficulty experienced in isolating wild type NBD dimers in the presence of non-hydrolyzable analogues without the benefit of additional dimer-stabilizing interactions, such as the C-terminal domain in MalK (Kennedy and Traxler, 1999).

The addition of Mg^{2+} or the substitution of K^+ for Na^+ during analytical gel filtration and ultracentrifugation experiments inhibited the formation of the E171Q-MJ0796 dimer. Addition of 10mM $MgCl_2$ lowered the dimer level by ~25% in the presence of 10mM ATP. Likewise a decrease in dimerization was seen when KCl was substituted for NaCl (Figure 3.5). In KCl the K_D for dimerization increased slightly compared to that for NaCl (Table 3.1).

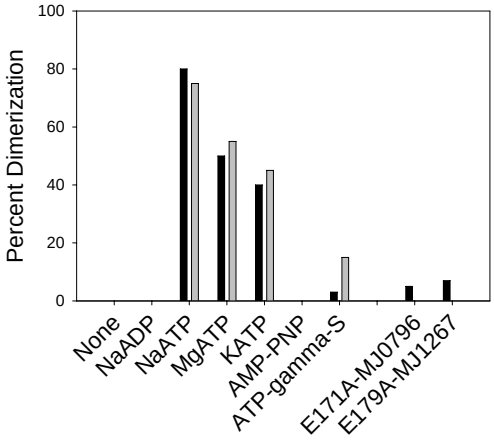

Figure 3.5 Analytical Gel Filtration Summary – 30μM protein samples run at 1mL/min. Various salt and nucleotide combinations at 10mM tested with E171Q-MJ0796 (black bars) and E179Q-MJ1267 (gray bars). Wild type MJ0796 and wild type MJ1267 did not dimerize under any conditions tested. The last two data columns show dimerization of E171Q-MJ0796 and E179A-MJ1267 in presence of 10mM NaATP.

Interestingly, mutating the catalytic glutamate in MJ0796 and MJ1267 to alanine (E171A and E179A respectively) diminished ATP-dependent dimerization to 5% and 10% of the level achieved with the E171Q and E179Q mutants respectively (Figure 3.5). The ability of these modifications of the ionic environment to alter the energetics of dimer formation reinforces the idea that carefully balanced electrostatic effects play a critical role in mediating the ATP-dependent dimerization of ABC transporter NBDs. Upon ATP hydrolysis, additional alterations in the electrostatics of the interface due to deprotonations and/or product release could effectively destabilize the sandwich dimer. The structure of E171Q-MJ0796 was solved by x-ray crystallography and details the specific nature of these interactions.

Crystal Structure of E171Q-MJ0796

The crystal structure of the ATP-bound E171Q-MJ0796 dimer was determined by molecular replacement at 1.9Å resolution (Smith *et al* 2002). The structure illustrates a symmetrical ATP sandwich complex similar to that observed in Rad50 (Figure 2.6E; Figure 3.6). The LSGGQ signature motif of one NBD completes the ATPase active site in the sandwich dimer by contacting the nucleotide triphosphate bound to the Walker A motif of the opposing NBD (Figure 3.6). A diagram illustrating the intermolecular contacts in a single active site is presented in Figure 3.7, adapted from Smith *et al*. The subunit-nucleotide

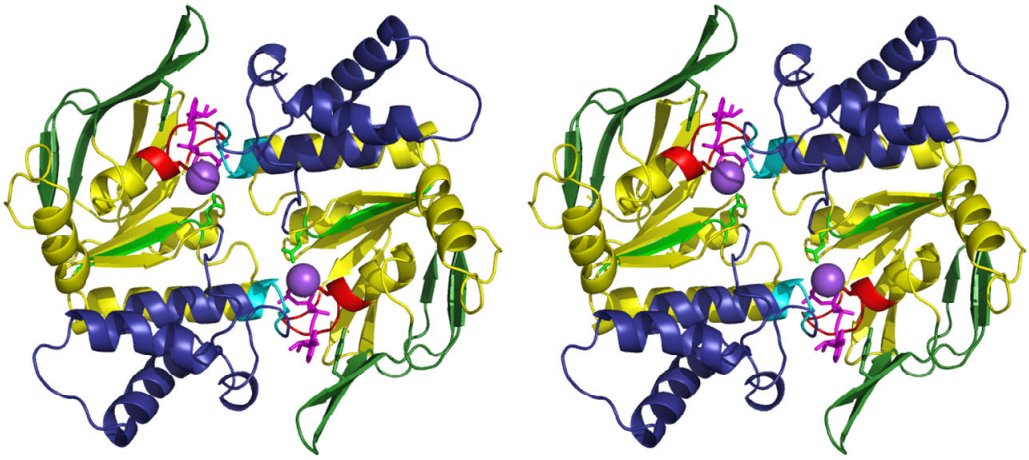

Figure 3.6 E171Q-MJ0796 Sandwich Dimer – pdb: 1L2T Stereo view (cross-eyed). Anti-parallel β subdomain shown in *forest green*. F_1-type α/β core subdomain shown in *yellow*. α-helical subdomain shown in *blue*. Walker A motif highlighted in *red*. Walker B motif highlighted in *bright green*. LSGGQ signature sequence highlighted in *cyan*. ATP shown in *magenta*. Na^+ ions shown by *purple spheres*. Y11, K44, S147 and Q171 shown in *ball and stick*.

contacts are highly similar between the two active sites in the dimeric structure.

Dimer formation buries 1100 $Å^2$ of solvent-accessible surface area per monomer, slightly less than the 1500 $Å^2$ buried in the Rad50 structure (Hopfner *et al*., 2000), although much of the buried surface in the Rad50 structure is derived from regions of the protein divergent from true ABC transporter NBDs. Nearly half of the buried surface in the E171Q-MJ0796 dimer sandwich is from the two nucleotides, assuming that they are bound to the Walker A motif before dimerization as was the case in the ADP-bound monomeric structure of MJ0796 (Yuan *et al*., 2001). The dimeric interaction involves seventy-two van der Waals contacts (≤ 3.6 Å) and twelve hydrogen bonds (≤ 3.3 Å). Thirty-eight of the van der Waals contacts and eight of the hydrogen bonds involve one of the

nucleotides, while six of the thirteen residues contacting residues in the opposing monomer also contact one of the nucleotides. While it is clear that the two ATP molecules make major contributions to the dimeric interactions, only eight van der Waals contacts and four hydrogen bonds in the dimer interface involve the γ-phosphates (see Figure 3.7), despite the fact that the gel filtration and analytical ultracentrifugation assays on MJ0796 and MJ1267 detailed above illustrate the importance of ATP for dimerization versus the inability of ADP and non-hydrolyzable ATP analogues to promote oligomerization.

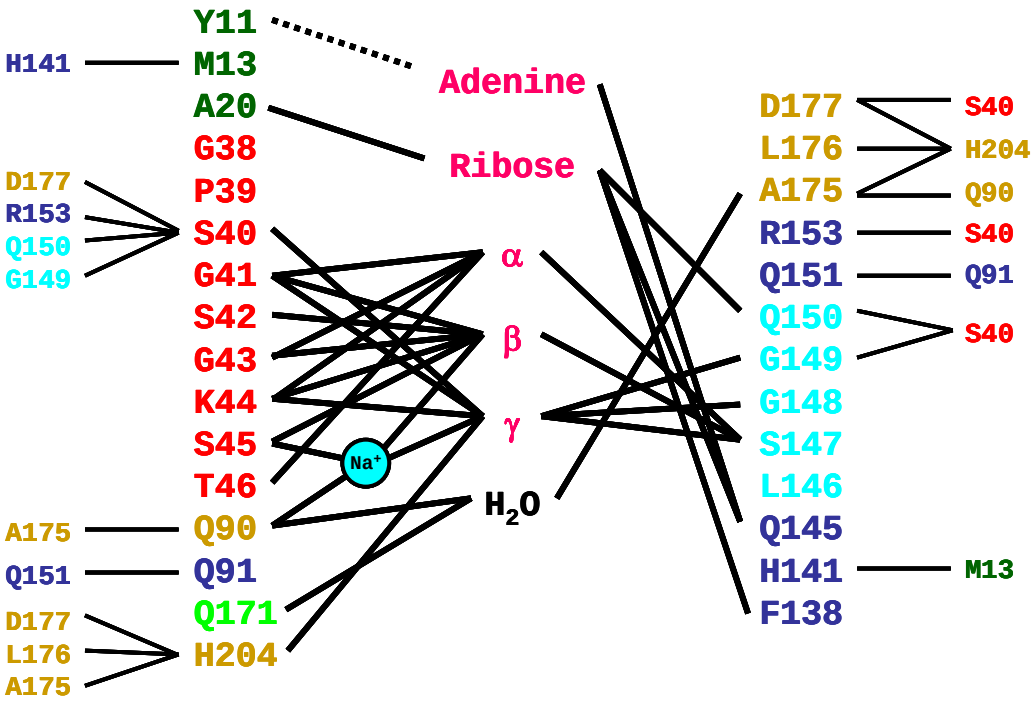

Figure 3.7 E171Q-MJ0796 Contact Diagram – *Solid lines* denote hydrogen bonds and van der Waals contacts. *Dotted line* denotes ring stacking. Residues in second column (Y11-H204) reside in one monomer, while residues in third column (D177-F138) reside in opposing monomer. Colors are as in Figure 3.6. Intersubunit contacts are listed in the first and fourth columns.

Comparison to Rad50 and ADP-Bound MJ0796

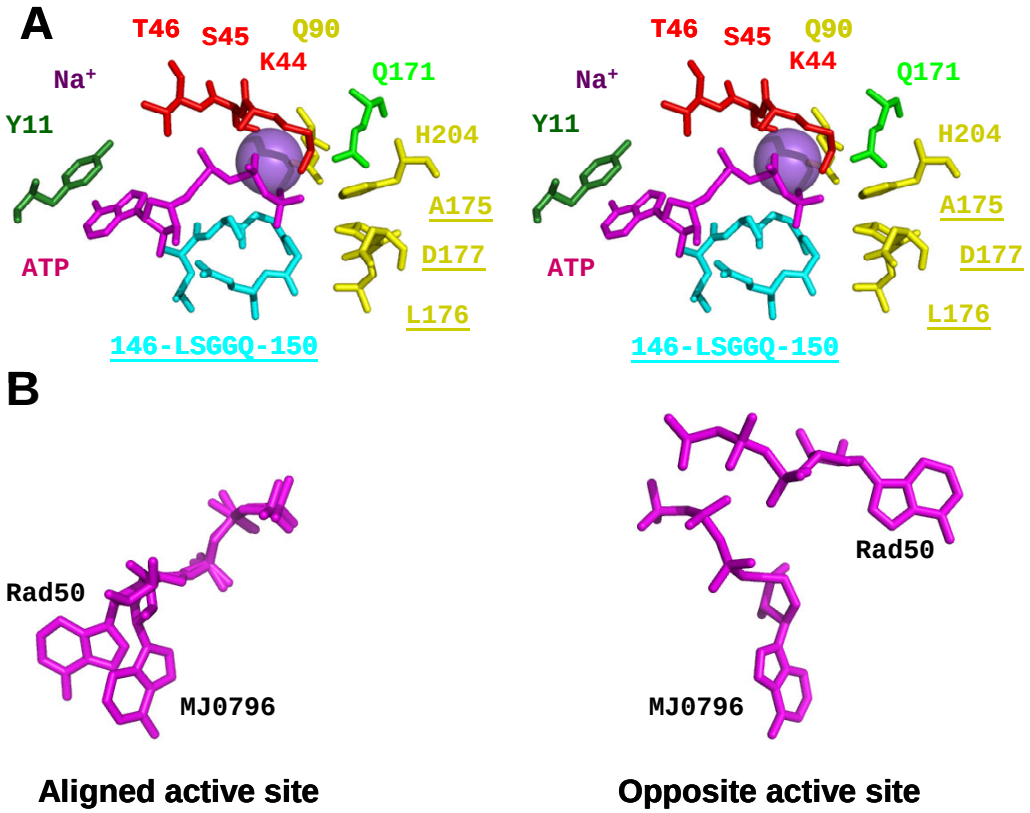

Figure 3.8 E171Q-MJ0796 Versus Rad50 – (A) Stereo view (cross-eyed). ATP shown in *magenta*. K44, S46 and T47 shown in *red*. Q90 and H204 shown in *yellow*. Q171 shown in *bright green*. *Underlined* residues are from the opposing monomer in the MJ0796 dimer. LSGGQ sequence shown in *cyan*. A175, L176 and D177 shown in *yellow*. Na^+ ion shown in *purple sphere*. (B) Aligned ATP molecules from a single active site in E171Q-MJ0796 and Rad50 on left side, resulting difference in opposite active site on right.

While several structural features of the Rad50 dimer (Hopfner *et al*., 2000) are similar in the E171Q-MJ0796 ATP sandwich dimer, the details of the dimeric interactions are different. Closely similar contacts are made to the ATP molecules at the dimeric interfaces in the two different structures. However, because of the structural divergence of the antiparallel β subdomain mentioned

above, the sugar and purine base of the nucleotide adopt a different conformation in Rad50 compared to E171Q-MJ0796 (Figure 2.7, Figure 3.8). Contacts to the ribose and adenine of ATP are made by homologous residues, the identity of the aromatic residue ring stacking with the adenine is different (Y11 in MJ0796 versus F791 in Rad50), the ultimate residue of the signature sequence contacting the ribose is different (Q150 in MJ0796 versus E796 in Rad50), and the additional contacts to these groups (the ribose and adenine moieties of ATP) are made by sidechains from divergent segments of the proteins (A20 from the antiparallel β subdomain and Q145 from the α-helical subdomain in MJ0796 versus E60, T62, and V64 from Lobe I in Rad50). In all of these three major differences of ATP coordination, residues fulfilling analogous roles (i.e., the aromatic residue ring stacking with the adenine base of ATP) are located in separate domains, and sometimes even in opposite subunits such as Y11 in MJ0796 versus F791 in Rad50. The ATP binding site composition is summarized in Figure 3.8A. The largest difference between the two dimer structures concerns the relative location of the active sites caused by differences in the distance between the Walker A motif and the LSGGQ signature sequence in the different proteins. If one aligns the active site in one of the subunits of the E171Q-MJ0796 dimer with a single active site of Rad50, the nucleotides in the other active sites are displaced by 5Å (Figure 3.8B).

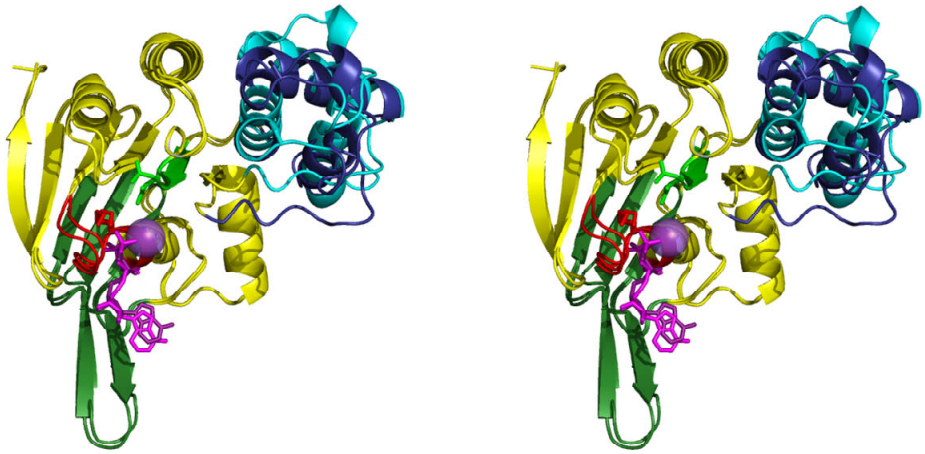

Figure 3.9 E171Q-MJ0796 Versus ADP-bound MJ0796 – pdb: 1L2T & 1F30. Stereo view (cross-eyed). Anti-parallel β subdomains shown in *forest green*. F_1-type α/β core subdomains shown in *yellow*. α-helical subdomains shown in *dark blue* and *cyan* respectively. Walker A motif highlighted in *red*. Walker B motif highlighted in *bright green*. LSGGQ signature sequence highlighted in *cyan* and *dark blue* respectively. ATP shown in *magenta*, while ADP shown in *purple*. Sodium ion shown in *purple sphere*. K44, S147 and E/Q171 shown in *ball and stick*.

The differences between the ADP-bound wild type MJ0796 monomer and ATP-bound E171Q-MJ0796 sandwich dimer (Figure 3.9) are highly similar to those based on Yuan *et al*'s comparison of the original MJ0796 structure to the HisP structure (Yuan *et al*., 2001; Hung *et al*., 1998). The γ-phosphate linker moves ~5Å to contact the Na^+ cofactor and hydrolytic water, leaving no room for a larger K^+ cofactor (Figures 3.7 and 3.9). The helix containing the LSGGQ signature motif moves ~7Å as part of a 17° rigid-body rotation of the α-helical subdomain. This reorientation in the ATP-bound dimer coincides with the strong interactions between the LSGGQ signature motif and the γ-phosphates of ATP, which is only possible when both α-helical subdomains adopt the ATP-bound

orientation illustrated with *dark blue* in Figure 3.9.

Functional Implications

This reorientation of the α-helical subdomain could be constrained by the TM domains, supported by the MsbA crystal structure in which the TM domain contacts the NBD in the analogous area illustrated in Figure 3.9 (Chang and Roth, 2001). In the full transporter, substrate binding to the TM domains could cause reorientation of the α-helical subdomain relative to the F1-like α/β core subdomain if conformational changes in the TM domains contacting the NBDs were to engender a reorientation like the one shown in Figure 3.9. Causing the NBD to adopt this conformation would likely enhance binding of nucleotide, as has been observed in many ABC transporters (Davidson, 2002), and also stabilize the nucleotide sandwich dimer. It remains to be seen what engenders this rigid-body rotation of the α-helical subdomain relative to the binding core, whether it is due to interactions between the invariant glutamine residue (Q90 in MJ0796) in the γ-phosphate linker and the nucleotide γ-phosphate as previously suggested (Karpowich *et al*., 2001) or due to allosteric interactions with the TM domains as hypothesized above.

The ATP binding site of the MJ0796 monomer is slightly acidic but becomes much more so when ATP binds (see Figures 5C and 5D in Smith *et al*). When the ATP-bound monomers dimerize, this negatively-charged surface binds to the LSGGQ signature motif of the opposing monomer, whose charge is neutral except for R153 (see Figure 3.7). The active site in the nucleotide sandwich dimer thus possesses a high concentration of negative charge in the absence of Mg^{2+}. Our experiments described above suggest that charge balance at the NBD active sites plays a vital role in the reaction cycle of ABC transporter NBDs. By removing a negative charge from the dimeric interface such as in the E171Q-MJ0796 and E179Q- MJ1267 mutants, a stable dimer is observed by analytical

A

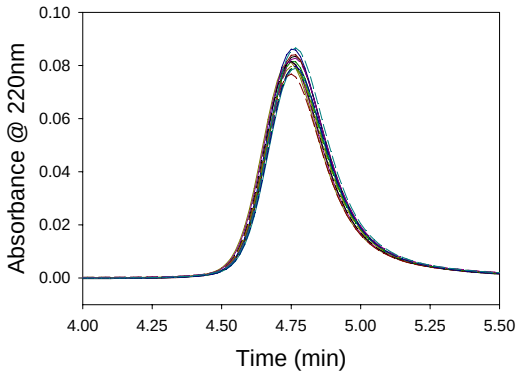

B

ATP μM	Single Species Fit (Da)	K_D μM
0	48,000	10
1	49,000	9
3	49,000	9
6	49,000	8
15	49,000	7
40	50,000	7
100	50,000	7
250	50,000	7
600	50,000	6

Figure 3.10 K44A/E171Q-MJ0796 Analytical Gel Filtration & Ultracentrifugation – (A) 30μM samples were run at 0.8mL/min. K44A/E171Q-MJ0796 alone (*black solid*) or in presence of increasing amounts of ATP; *solid* lines: 25μM (*red*), 50μM (*green*), 75μM (*yellow*), 100μM (*blue*), 150μM (*pink*), 200μM (*cyan*), *dashed* lines: 250μM (*black*), 500μM (*red*), 1mM (*green*), 2mM (*yellow*), 5mM (*blue*), 10mM (*pink*), 20mM (*cyan*). (B) Analytical ultracentrifugation results form 17,000 & 24,000 rpm spin. K44A/E171Q-MJ0796 at 30μM. Data fit using SigmaPlot.

gel filtration when the nucleotide is present with Na^+ as a cofactor instead of the usual Mg^{2+}, and the amount of dimerization seen in these two mutant proteins depends on the cation cofactor present as well as the mutated residue, whether glutamine or alanine (Figure 3.5). Secondly, the monomeric structure of ATP-bound HisP in the absence of Mg^{2+} (Hung *et al*., 1998) is consistent with our biochemical data showing that wild type MJ0796 and MJ1267 do not stably dimerize upon binding ATP in the absence of the divalent cation cofactor (Figures 3.2A and 3.2C). Finally, by removing both a negative and positive charge from the active site of MJ0796 in the double mutant K44A/E171Q, the electrostatic environment of the dimeric interface is altered such that only dimers of this double mutant can be isolated, presumably containing nucleotide that remains bound from bacterial expression during the entire purification protocol (analytical gel filtration and ultracentrifugation results for K44A/E171Q-MJ0796 summarized in Figure 3.10). Therefore, electrostatics at the dimeric interface play a vital role in dimerization, and an additional negative charge at each active site (as would be the case with Mg^{2+} in the active site of the E171Q-MJ0796 dimer) prevents formation of a stable sandwich dimer (Figure 3.5 & Table 3.1).

When ATP is hydrolyzed, a surplus negative charge could form due to deprotonation of the inorganic phosphate product or the sidechain of the proton-accepting catalytic base. Even without the aforementioned increase in charge, the accumulation of negative charge associated with nucleotide binding detailed

above is likely to cause strong repulsion of the inorganic phosphate product, which carries a net charge of at least -2 following hydrolysis assuming that H^+ can leave the active site. As illustrated by the effect of ADP upon NBD dimerization above (Figure 3.3), the contacts between the LSGGQ signature motif and the γ-phosphate of the nucleotide (Figure 3.7) must make up a large part of the stability of the dimeric interface in the E171Q-MJ0796 sandwich dimer. This raises the possibility that the γ-phosphate remains bound to the LSGGQ signature motif even after hydrolysis (Smith *et al*., 2002). Since the ADP product most likely remains bound to the Walker A residues as witnessed in the monomeric ADP-bound MJ0796 crystal structure (Yuan *et al*., 2001), repulsion of the negatively-charged inorganic phosphate product by the concentrated negative engendered by nucleotide binding could push the NBDs apart.

Combining the wealth of biochemical and structural information gained by studying the archaeal MJ0796 and MJ1267 NBDs, the reaction cycle illustrated by Figure 3.11 was hypothesized (Moody *et al*., 2002) . *Step 1* involves the binding of two ATP molecules (illustrated in *magenta*) to the nucleotide-free NBDs, causing the α-helical subdomain rotation illustrated by the color change from *cyan* to *dark blue*. Alternatively, if the TM domains allosterically control this subdomain reorientation as suggested above, the cycle could begin with *step 1'* prior to nucleotide binding, and following this potential conformational signal from the TM domains ATP would bind to the NBDs in *step 1''*. Dimerization of

the ATP-bound monomers, *step 2*, presumably occurs quite rapidly and stably in the E171Q-MJ0796 mutant as determined using the analytical gel filtration and ultracentrifugation results. Hydrolysis of ATP, the step at which the E171Q-MJ0796 mutant is blocked, proceeds in *step 3*. The ADP•P_i-bound dimer decays due to the electrostatic repulsion of the inorganic phosphate transiently bound to the LSGGQ signature motif of one monomer and the ADP (illustrated in *purple*) bound to the Walker A motif of the opposing monomer as outlined above, and the Pι is released upon monomerization in *step 4*. During this part of the cycle, the α-helical subdomains of the NBDs return to the original orientation following release of the phosphate, denoted by the color change from *dark blue* to *cyan*. ADP then dissociates from the binding pocket of each monomer in *step 5* to complete the cycle.

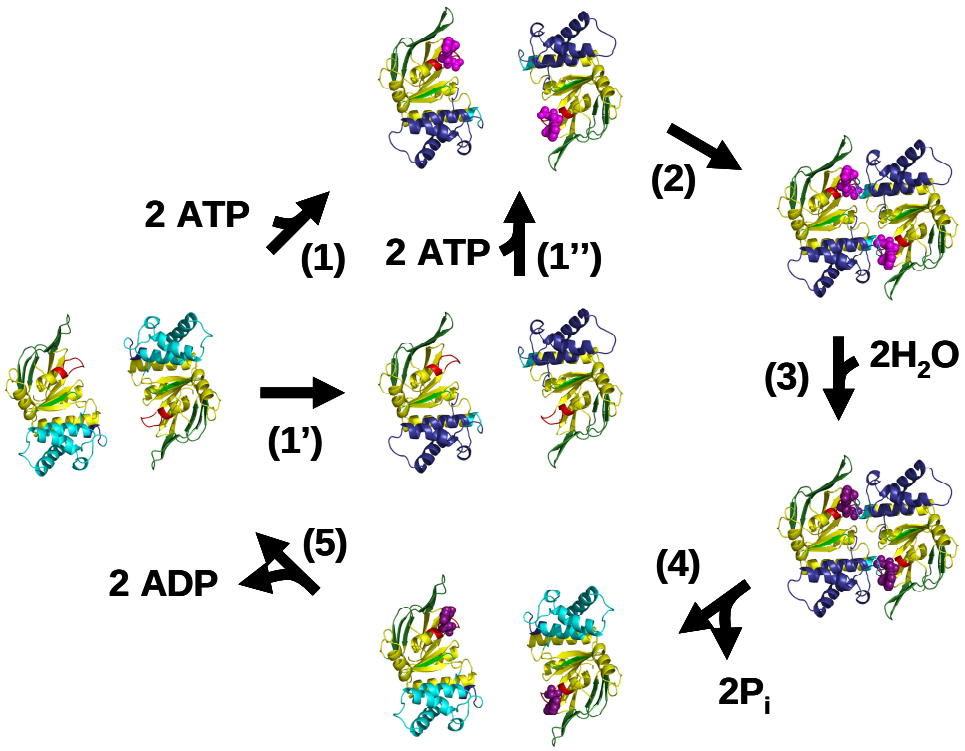

Figure 3.11 Mechanochemical Reaction Cycle for ABC Transporter NBDs – Anti-parallel β subdomain shown in *forest green*. F_1-type α/β core subdomain shown in *yellow*. α-helical subdomain shown in *cyan* versus *dark blue* in nucleotide-free and ADP-bound NBDs versus ATP-bound NBDs respectively. ATP shown in *magenta*, while ADP shown in *purple*. Walker A motif highlighted in *red*. Walker B motif highlighted in *bright green*. LSGGQ signature sequence highlighted in *dark blue* versus *cyan* in nucleotide-free and ADP-bound NBDs versus ATP-bound NBDs respectively.

Chapter IV

Probing the Mechanochemical Reaction Cycle of ATP-Binding Cassette Transporter Nucleotide Binding Domains

Introduction

Concomitant with the solution of the E171Q-MJ0796 sandwich dimer structure (Smith *et al*., 2002), a second full-length ABC transporter crystal structure was reported in the presence of a transition state analogue (Locher *et al*., 2002). BtuCD, a "half" transporter from *E. coli*, was crystallized in a nucleotide-free state (with tetra-vanadate in the active site) with two NBDs oriented in approximately the same fashion as those seen in the E171Q-MJ0796 dimer, although the buried solvent-accessible surface area was much less and the LSGGQ signature motif of each monomer was located almost 5Å further away from the opposing Walker A residues than in the E171Q-MJ0796 structure. As such, the BtuCD NBD dimer should be considered a semi-closed conformation.

In addition to this crystallographic support of the head to tail dimeric arrangement of E171Q-MJ0796, biochemical evidence was provided from Clarke and colleagues working on p-glycoprotein (Loo *et al*., 2002) as well as from

Davidson and coworkers studying MalK (Fetsch and Davidson, 2002) illustrating cross-linking of the LSGGQ signature motif to Walker A and B residues from opposing NBDs during the catalytic cycle. These studies nicely reinforce the biochemical and structural data of the initial publications concerning the archaeal NBDs MJ0796 and MJ1267 (Moody *et al*., 2002; Smith *et al*., 2002).

The simplified mechanism presented in Figure 3.11 illustrates two ATP molecules binding and subsequently being hydrolyzed in order to complete the nucleotide binding domain reaction cycle. Previous studies have been inconclusive and/or inconsistent in their determination of the stoichiometries of nucleotide binding and hydrolysis during ABC transporter functional cycles (Ames *et al*., 1989; Bishop *et al*., 1989; Davidson and Nikaido, 1990). The experiments summarized in this chapter aim to probe the dimeric interface exhibited by the E171Q-MJ0796 structure (Figure 3.6; Smith *et al*., 2002) and in subsequent structures of *Escherichia coli* MalK (Chen *et al*., 2003) and *Salmonella typhimurium* MsbA (Reyes and Chang, 2005), as well as to determine the number of binding and hydrolysis events necessary and sufficient to complete the NBD reaction cycle using isolated cassettes as well as a full transport system as experimental tools.

Materials and Methods

Plasmid construction and bacterial strains - Single and double mutants of MJ0796 were constructed by performing site-directed mutatgenesis using *pfu*Turbo DNA polymerase (Invitrogen) with pET28a vector (Novagen) containing wild type (or mutant where applicable) MJ0796 sequence as the template. All MJ0796 constructs were transformed into BL21 Codon Plus *E. coli* cells (Invitrogen) and selected for using kanamycin (50 μg/mL.) The zeocin resistance gene was amplified from pPicza (Invitrogen) and digested with XbaI. Fragment was ligated into the XbaI site of pNASCDE (Narita *et al*., 2002) to construct plasmid D1. Single mutants (D1-K48A, D1-S147F, and D1-E171Q) were constructed by performing site-directed mutagenesis using *pfu*Turbo DNA polymerase (Invitrogen). LolD gene was amplified from plasmids D1, D1-K48A, D1-S147F, and D1-E171Q and digested with PstI and BmrI. Fragments were ligated into plasmids D1, D1-K48A, D1-S147F, and D1-E171Q digested with PstI and BmrI to form D2 plasmids (D2-WT.KA, D2-WT.SF, D2-WT.EQ, D2-KA.WT, D2-KA.SF, D2-KA.EQ, D2-SF.WT, D2-SF.KA, D2-SF.EQ, D2-EQ.WT, D2-EQ.KA, and D2-EQ.SF). All four D1 plasmids and 12 D2 plasmids were transformed into *E. coli* strain CDE4 (harboring plasmids pMAN1015 and pMAN885EH) (Narita *et al*., 2002) and selected for using ampicillin, chloramphenicol, kanamycin, tetracycline, and zeocin at 50, 35, 50, 10, and 25μg/mL respectively.

Protein Expression and Purification - Wild type and mutant MJ0796 proteins were expressed for 4-5 hours in BL21 Codon + *E. coli* cells in the presence of kanamycin after induction with 1mM IPTG at OD_{600nm} between 0.4 and 0.8. Cells were pelleted, frozen at -80°C, and lysed in 50mM Tris pH 7.6, 50mM NaCl, 1mM EDTA, 4mM DTT, and 1mM PMSF. Lysed cells were sonicated on ice at 50% duty cycle using a micro tip at power setting 5 – 6 for 30 seconds every minute for ten minutes. Sonicated cells were then spun for 15 minutes in JA25.5 rotor at 12,000 g at 4°C. Supernatant from 12k x g spin was heated at 65 - 70°C for 10 minutes then spun for 10 minutes in JA25.5 rotor at 75,000 g at 4°C. Supernatant from 75k x g spin was filtered using 0.45μM syringe filter and injected onto Akta Prime using a DEAE column 4°C running a gradient from 100% A1 to 100% B1. Buffer A1: 50mM Tris pH 7.6, 1mM EDTA, and 1mM DTT. Buffer B1: 50mM Tris pH 7.6, 1M NaCl, 1mM EDTA, and 1mM DTT. Fractions containing MJ0796 were pooled, $(NH_4)_2SO_4$ added to 1M, and injected onto Akta Prime using a butyl sepharose column at 4°C running a gradient from 100% A1 to 100% B1. Buffer A1: 25mM Tris, 25mM Bis-Tris Propane pH 7.5, 600mM $(NH_4)_2SO_4$, 1mM EDTA, and 1mM DTT. Buffer B1: 25mM Tris, 25mM Bis-Tris Propane pH 7.5, 1mM EDTA, and 1mM DTT. Fractions containing MJ0796 were pooled and concentrated to 5mL using Amicon Ultra concentration devices at 3750 RPM at 4°C. 0.45μM filtered concentrate injected onto Akta Prime Program #10 using an S-200 column at 4°C. Buffer: 50mM Tris pH 7.5,

200mM NaCl, 10% glycerol, 1mM EDTA, and 1mM DTT. Fractions containing MJ0796 were pooled and concentrated to >1 mg/mL (as determined using Bio-Rad protein concentration determination kit) using Amicon Ultra concentration devices at 3750 RPM at 4°C. Aliquots of protein were frozen in liquid N_2 and stored at -80°C.

Growth Assays - Strain CDE4 harboring pMAN1015, pMAN885EH, and D1 or D2 plasmids were grown in LB media containing ampicillin, chloramphenicol, kanamycin, tetracycline, and zeocin at 37°C until OD at 600nm reached 0.4-0.8. At time = 0 cultures were diluted into LB media at 42°C. Turbidity at 600nm was monitored every 2-3 hours, and cultures in log phase were diluted into fresh media at 42°C. Growth was monitored for 18-32 hours following temperature shift. When used, arabinose was 0.1% (w/v).

ATPase Activity Measurement - ADP production was assessed by monitoring NADH depletion using the lactate dehyrogenase / pyruvate kinase coupled assay described previously (Rosing *et al*., 1976). Mutant and wild type MJ0796 concentration was 1.0 μM. Assays were conducted using a UV/VIS spectrophotometer while measuring the decrease in absorbance at 340nm or with a SpectraMax Gemini plate reader while measuring the decrease in fluorescence when exciting at 340nm and measuring emission at 450nm. Data was fit using SigmaPlot.

Analytical Ultracentrifugation - Mutant and wild type MJ0796 samples at 20μM were spun in a Beckman XLI centrifuge using the An60Ti rotor. Sample buffer was 50mM Tris-HCl, pH 7.6, 200mM NaCl, and 1mM EDTA. Molecular weights of the various monomers were determined using ProtParam, and buffer densities were determined using Sednterp. Data was collected at 17,000 and 24,000 RPM at 4°C using interference optics at 675nm and was fit using SigmaPlot.

HPLC Gel Filtration – Samples were run at 1mL/min on Beckman System Gold using TOSOH GFC-200 column at room temperature in mobile phase of 50mM Tris pH 7.6, 200mM NaCl and detected at 220nm.

Fluorescence Assays - Mutant MJ0796 samples at 1μM were analyzed using either a PTI fluorometer or SpectraMax Gemini plate reader, exciting at 295nm and measuring emission at 343nm at 20°C. Sample buffer was 50mM Tris-HCl, pH7.6, 200mM NaCl, 10% glycerol and 1mM EDTA except when noted otherwise. Anisotropy experiments were conducted using a T format setup and the anisotropy was determined using horizontally and vertically polarized light using the equation $r = (I_{\parallel}/I_{\perp} - 1) / (2 + I_{\parallel}/I_{\perp})$.

Results and Discussion

While nearly half of the 1100 $Å^2$ solvent-exposed surface area buried at the dimeric interface of E171Q-MJ0796 is contributed by the two ATP molecules, the Walker B motif and D-Loop (Figure 2.2) make a series of hydrogen bonds and van der Waals contacts (Figure 3.7) with a serine residue in the Walker A motif of the opposing monomer, the putative attacking water molecule, and a highly

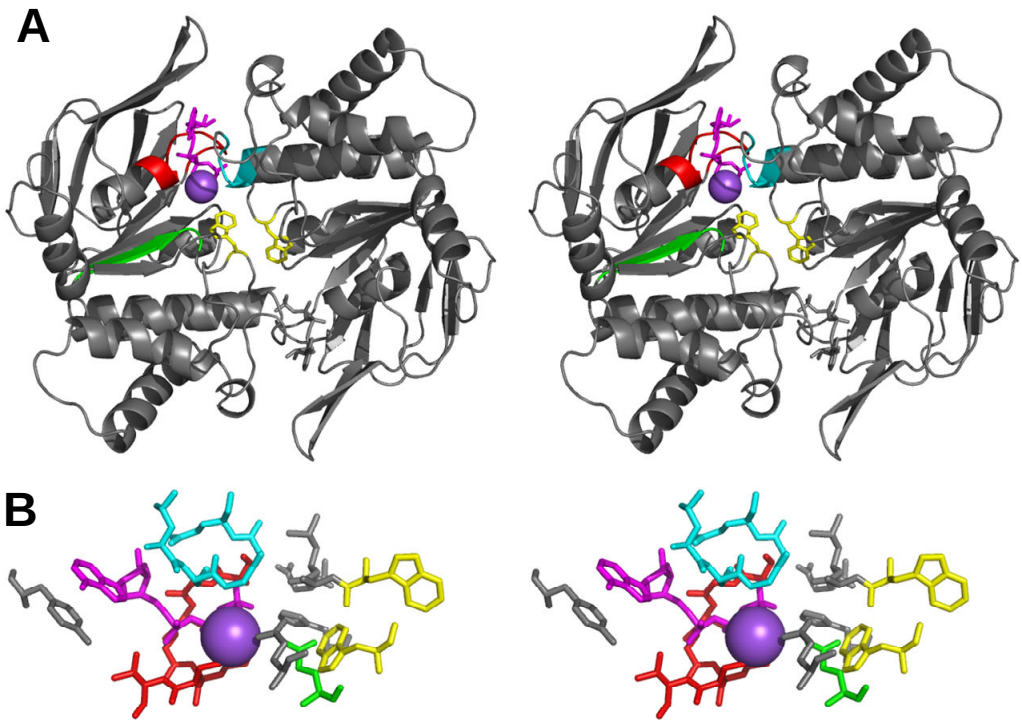

Figure 4.1 G174W Localization and Proximity to ATP Coordinating Residues - (A) Stereo view (cross-eyed) of MJ0796 cartoon. Walker A motif highlighted in *red*. Walker B motif highlighted in *bright green*. LSGGQ signature sequence highlighted in *cyan*. ATP shown in *magenta*. Na^+ ion shown by *purple sphere*. G174W shown in *yellow*. (B) Close-up stereo view (cross-eyed) of a single MJ0796 ATP binding site. Y11 (*gray*), 40-SGSGKST-48 (*red*), Q90 (*gray*), 146-LSGGQ-150 (*cyan*), Q171 (*green*), G174W (*yellow*), 175-ALD-177 (*gray*) and H204 (*gray*) shown in *ball and stick*.

conserved histidine residue (H204) in the aptly named H-Loop. In addition, the D-Loop, GALD in MJ0796, is in close apposition to the same sequence in the opposing monomer. In an attempt to affect the steric and hydrophobic nature of this region of the NBD sandwich dimer, the MJ0796 single mutant G174W was constructed. The location of this residue with respect to both the dimeric interface and ATP coordinating residues is illustrated in Figure 4.1. In addition to altering the dimeric interface, this mutation provides a fluorescent tag with which to monitor protein behavior, as wild type MJ0796 does not contain any tryptophan residues. Additional single mutants M13A, Q91E, and Q151E were constructed based on the subunit-subunit interactions detailed in Figure 3.7.

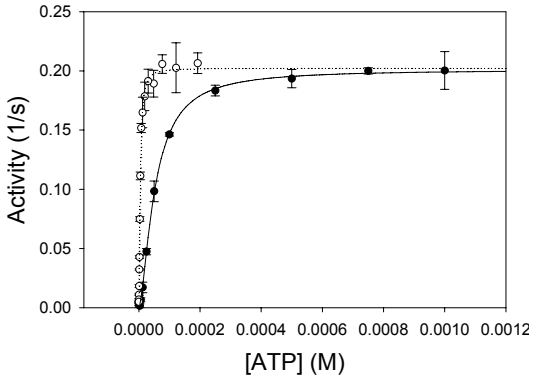

Figure 4.2 ATPase Characteristics - ATPase activity of wild type (*solid circles*) and G174W- (*open circles*) MJ0796 proteins plotted against ATP molar concentration. Data fit to the Hill equation for wild type (*solid line*) and G174W-MJ0796 (*dotted line*). Wild type MJ0796 fit produces a V_{max} of 0.2 sec^{-1}, K_m of 40μM, and a Hill coefficient of 1.6. G174W-MJ0796 fit displays a V_{max} of 0.2 sec^{-1}, K_m of 4μM, and a Hill coefficient of 1.7.

M13A-, Q91E-, Q151E-, and G174W-MJ0796 mutants purify to over 98% purity (data not shown) and exhibit ATPase activity as measured using a coupled assay (Figure 4.2 and Table 4.1). Interestingly, while the V_{max} of G174W-MJ0796 was identical to that of wild type MJ0796, 0.2 sec^{-1}, the K_m was reproducibly 10-fold lower (4μM ATP versus 40μM ATP for

G174W- and wild type MJ0796 respectively.) The Hill coefficient remains 1.6-1.7 for both G174W- and wild type MJ0796. By introducing this bulky hydrophobic residue near the NBD dimer interface, the enzyme actually becomes a better ATPase at lower nucleotide concentrations. This unexpected effect may be due to ring stacking of the inserted tryptophan residues, providing additional binding energy for the cassettes as they dimerize in response to ATP binding. The three other single mutants, M13A, Q91E, and Q151E, all exhibited ATPase characteristics indistinguishable from those of wild type MJ0796 (Table 4.1), illustrating the insignificance of these residues at the MJ0796 dimeric interface.

Protein	V_{max}	K_m	Hill
WT	$0.20s^{-1}$	50μM	1.6
M13A	$0.19s^{-1}$	48μM	1.7
Q91E	$0.21s^{-1}$	56μM	1.6
Q151E	$0.20s^{-1}$	44μM	1.5
G174W	$0.20s^{-1}$	4μM	1.7

Table 4.1 Summary of M13A-, Q91E-, Q151E-, and G174W-MJ0796 ATPase Characteristics - Coupled assays were conducted at 1μM protein at 30°C. Data fit to the Hill equation.

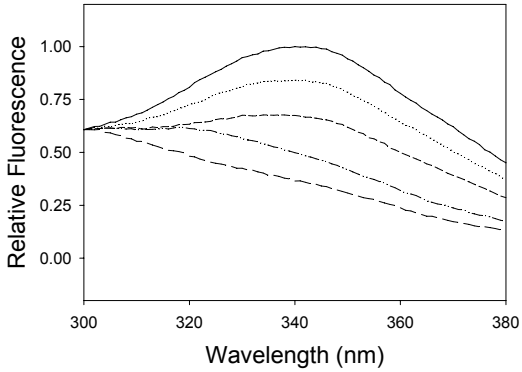

Figure 4.3 Fluorescence Emission Spectra of G174W-MJ0796 - Samples excited at 295nm and background subtracted. *Solid line* denotes 1μM G174W, *dotted line* represents 1μM plus 30μM ATP, *small dashed line* shows 1μM plus 60μM ATP, *dotted and dashed line* denotes 1μM plus 90μM ATP, and *large dashed line* illustrates 1μM plus 120μM ATP. All samples contain 10% glycerol and 1mM EDTA.

While G174W-MJ0796 possesses near-wild type V_{max}, its novel fluorescent tag allows one to monitor protein behavior. Figure 4.3 shows

the emission spectra of 1μM G174W-MJ0796 when excited at 295nm in the presence of increasing concentrations of ATP. Due to the single mutant's ATPase activity mentioned above, these experiments were performed in the presence of EDTA. As the ATP concentration increases from 0μM to 120μM, the emission peak at 343nm progressively disappears. Following this emission in a time-dependent manner, one witnesses the ATP-dependent fluorescence quench in the absence of divalent cations (from 30 to 90 seconds in Figure 4.4). When Mg^{2+} ions are added after 90 seconds, the fluorescence slowly and steadily returns to original levels in the presence of 120μM ATP, when corrected for dilution (*light gray trace* in Figure 4.4). In the presence of 12mM ATP and Mg^{2+} (*black trace* in Figure 4.4), the fluorescence remains quenched longer than the maximal time measured, 7200 seconds (data not shown). When the single mutant is entirely monomeric, as in the absence of nucleotide (*solid spectrum* in Figure 4.3 and initial 30 seconds of Figure 4.4) or after ATP hydrolysis (*light gray trace* after 900 seconds in Figure 4.4), the fluorescence emission is at a maximum. The addition of ADP to G174W-MJ0796 does not result in this fluorescence emission quench (data not shown), in agreement with the effect of ADP on E171Q-MJ0796 dimerization (Figure 3.3).

The aforementioned quench in fluorescence emission by G174W-MJ0796 in the presence of ATP could be due to either nucleotide binding or NBD dimerization. In order to correlate this nucleotide-dependent fluorescent behavior

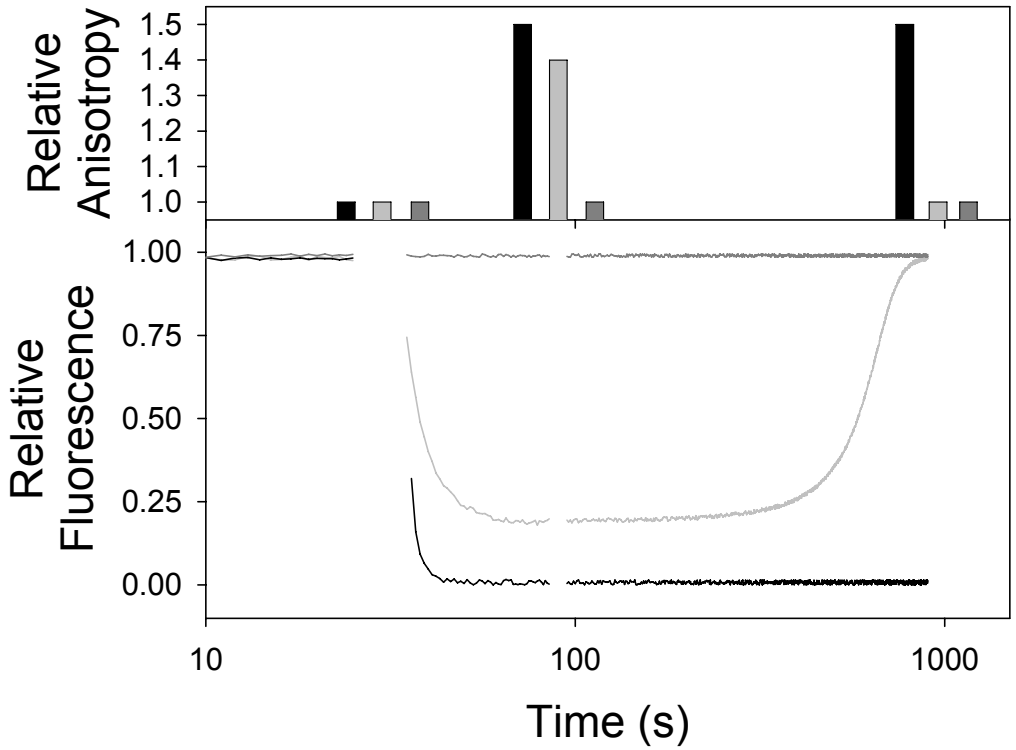

Figure 4.4 Fluorescence Time Course and Anisotropy of G174W-MJ0796 - Samples excited at 295nm and emission measured at 343nm. Fluorescence trace shown in lower panel, and relative anisotropy values in upper panel. At time = 0 sample of 1μM G174W plus 1mM EDTA was incubated for 30 seconds, upon which 1.2μM, 120μM, or 12mM ATP was added *(dark gray, light gray,* and *black traces* and *bars* respectively.) After 90 seconds, 10mM Mg^{2+} was added. Fluorescence values corrected for dilution at 30 and 90 seconds and background subtracted.

to its oligomeric state, relative anisotropy values were determined at equilibrium points along the time course of the experiment shown by Figure 4.4. The initial anisotropy in the absence of nucleotide was 0.08, and this value increased to 0.11 (1.4 in relative terms) after the addition of 120μM ATP (*black bars* in Figure 4.4). Addition of 12mM ATP resulted in an increase in relative anisotropy to 1.5, while the presence of 1.2mM ATP did not affect anisotropy (*light* and *dark gray bars*, respectively, in Figure 4.4). The anisotropy returned to original values after the

addition of Mg^{2+} to the 120μM ATP sample, while Mg^{2+} had no effect on the relative anisotropy of the 12mM and 1.2μM ATP samples as measured at 900 seconds. All of this evidence suggests that the emission at 343nm of G174W-MJ0796 monitors the oligomeric state of the mutated NBD.

This stable nucleotide-dependent fluorescence emission quench and relative anisotropy shift can be utilized to observe the behavior of other mutant MJ0796 proteins with the G174W background. In Figure 4.5, the relative fluorescence and anisotropy values of single mutant G174W-MJ0796 (*filled* and *open squares*) as a function of ATP concentration are compared to the double mutants E171Q/G174W-MJ0796 (*filled* and *open circles*) and K44A/G174W-MJ0796 (*filled* and *open diamonds*) in which the highly conserved extended Walker B glutamate and Walker A lysine residues have been mutated to glutamine and alanine respectively. In these experiments there was no Mg^{2+} present in solution, while EDTA was included to ensure the chelation of any additional divalent cations. Compared to the single mutant G174W-MJ0796, the double mutants undergo the fluorescence emission quench and correlative relative anisotropy increase at ATP concentrations roughly 100 times below (for E171Q/G174W-MJ0796) or above (for K44A/G174W-MJ0796) those of the single mutant. In all three cases, the increase in relative anisotropy values from 1 to 1.5 coincides with the increased emission quench as a function of nucleotide concentration.

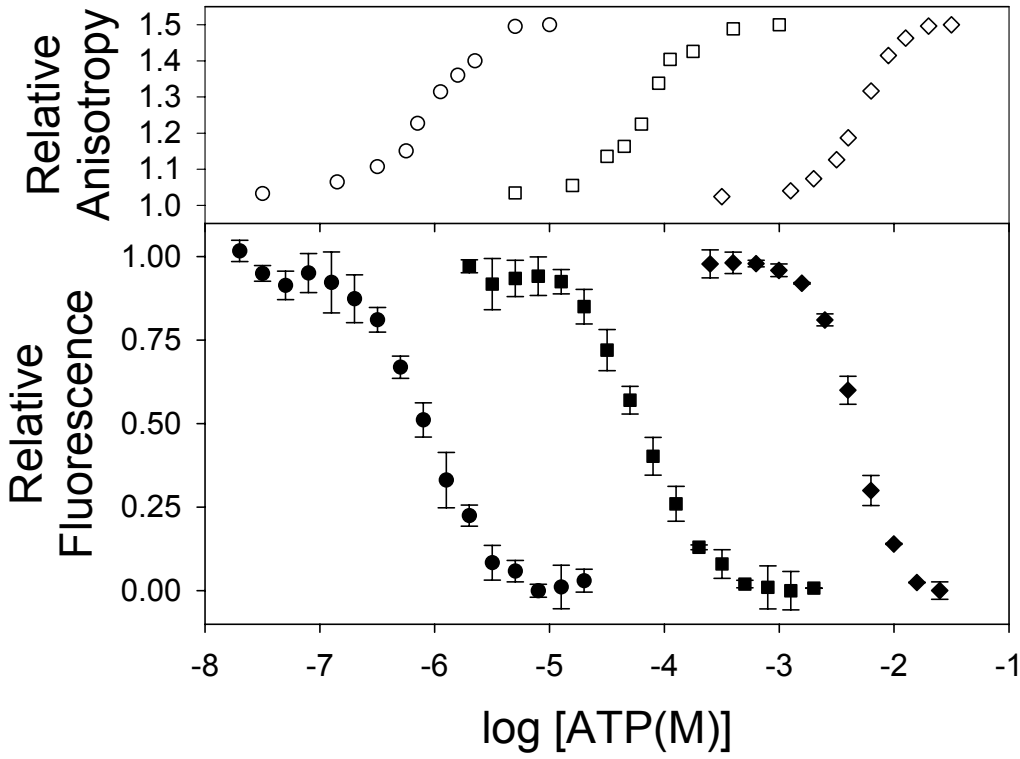

Figure 4.5 Relationship Between Fluorescence Emission Quenching and Anisotropy - Relative fluorescence (lower graph, *filled symbols*) and anisotropy (upper graph, *open symbols*) as a function of logarithmic ATP molar concentration. Emission was measured at 343nm while exciting at 295nm for all measurements. Proteins at 1μM plus 10mM EDTA present in all samples. Double mutant E171Q/G174W-MJ0796 shown by *circles*, single mutant G174W represented by *squares*, and double mutant K44A/G174W-MJ0796 illustrated by *diamonds*. Maximal fluorescence values at saturating ATP concentration set to 1.0 after background subtraction.

These results are not unexpected, as E171Q-MJ0796 was the mutation that first allowed the stable dimerization of an NBD for structural characterization, and it has been shown to tightly dimerize using analytical ultracentrifugation equilibrium experiments (Table 3.1). In addition, mutation of the invariant

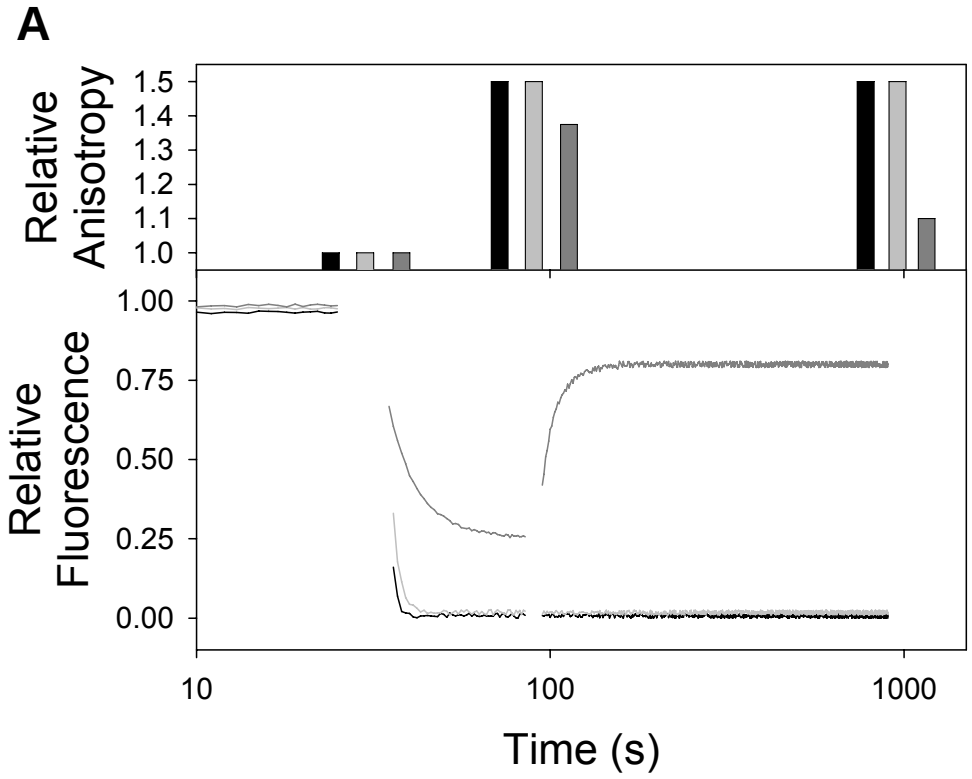

Figure 4.6 Fluorescent Behavior of E171Q/G174W- and K44A/G174W-MJ0796 - (A) Fluorescence time course and relative anisotropy values of E171Q/G174W-MJ0796, exciting at 295nm and measuring emission at 343nm. Relative fluorescence trace shown in lower graph by *solid lines*, and relative anisotropy values in upper graph by *vertical bars*. At time = 0 sample of 1μM E171Q/G174W-MJ0796 plus 1mM EDTA was incubated for 30 seconds, upon which ATP was added (*black trace* and *bars* show 12mM ATP, *light gray trace* and *bars* show 120μM ATP, and *dark gray trace* and *bars* show 1.2μM ATP). After 90 seconds, 10mM Mg^{2+} was added. Fluorescence values corrected for dilution at 30 and 90 seconds, background subtracted, and converted along with anisotropy values to relative amounts. (B – see next page) Same as in Fig. 4.6A except with K44A/G174W-MJ0796.

Walker A lysine has been used throughout the years as a "non-binder" of nucleotide (Shyamala *et al*., 1991; Delepelaire, 1994; Schneider *et al*., 1994; Kashiwagi *et al*., 1995; Koronakis *et al*., 1995; Loo and Clarke, 1995; Aparicio *et al*., 1996), while our experiments suggest that nucleotide binding leading to

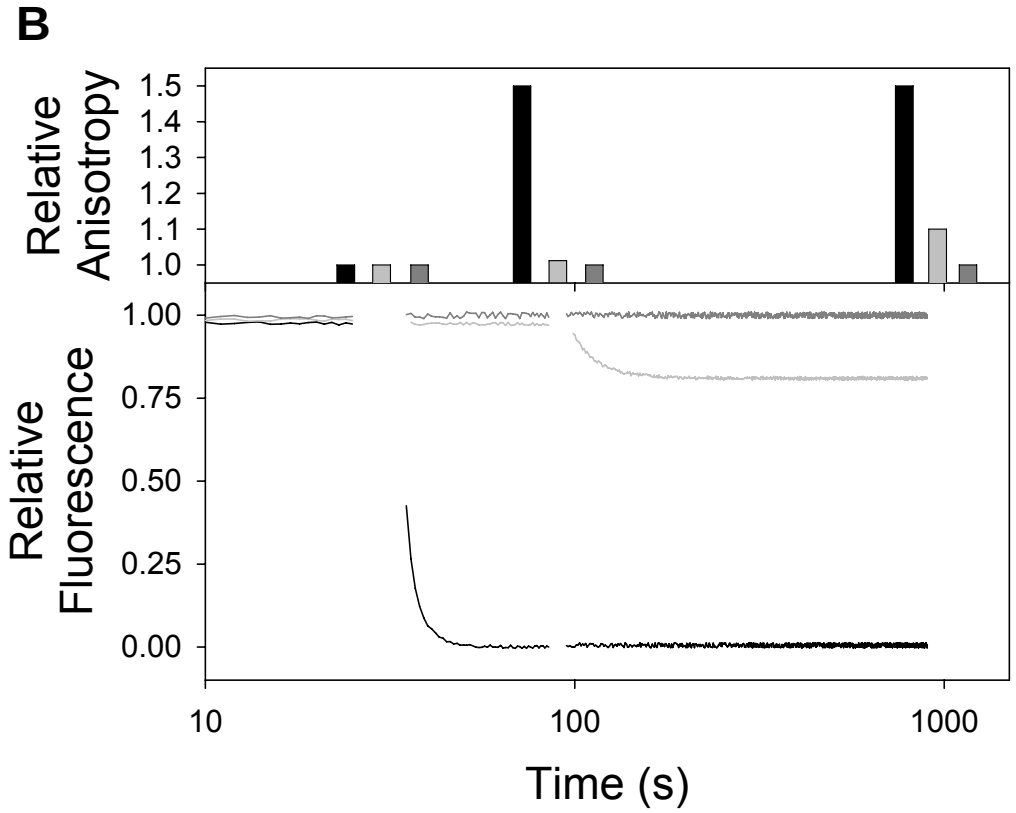

dimerization of K44A/G174W-MJ0796 occurs, albeit at much higher ATP concentrations. This oligomeric transition is in contrast to the behavior of K44A/E171Q-MJ0796 in which the mutant protein exhibits only a dimer as evidenced using HPLC gel filtration and analytical ultracentrifugation (see Figure 3.10).

As with G174W-MJ0796, E171Q/G174W- and K44A/G174W-MJ0796 proteins were assayed for relative fluorescence and anisotropy in the presence of various ATP concentrations and Mg2+ (Figure 4.6). Upon the addition of either 12mM or 120μM ATP to E171Q/G174W-MJ0796, fluorescence stably quenches

while relative anisotropy increases to 1.5 even after the addition of Mg^{2+} after 90 seconds (*black* and *light gray traces* and *bars* respectively in Figure 4.6A). When only 1.2μM ATP is added to E171Q/G174W-MJ0796, the fluorescence is quenched to 25% of original levels while the relative anisotropy increases to 1.4. Addition of Mg^{2+} to this sample results in an increase in fluorescence emission to 75% of original levels and a corresponding decrease in relative anisotropy to 1.1 (*dark gray trace* and *bars* in Figure 4.6A). This effect correlates well with the effect of divalent cations on the dimerization of E171Q-MJ0796 described in Chapter III (Figure 3.5).

While 12mM and 120μM ATP were sufficient to fully quench the fluorescence emission of E171Q/G174W-MJ0796, only 12mM ATP does so for K44A/G174W-MJ0796 (*black trace* in Figure 4.6B). The presence of Mg^{2+} had no effect on the 12mM and 1.2μM ATP samples of K44A/G174W-MJ0796, while addition of the divalent cation to the 120μM ATP sample resulted in a decrease in fluorescence emission to 80% of original levels and an increase in relative anisotropy to 1.1 (*light gray trace* and *bars* in Figure 4.6B). This quench and concomitant anisotropy increase likely represent an increase of nucleotide binding by K44A/G174W-MJ0796 which leads to increased NBD dimerization. These results suggest that the removal of one positive charge from each active site in the K44A/G174W-MJ0796 double mutant favors binding of MgATP, as opposed to

the NaATP preferred for the dimerization of E171Q-MJ0796 (in which a negative charge is removed from each active site).

Protein	Single Species Fit (Da)	K_D μM
WT	34896 ± 1368	285 ± 168
G174W	50813 ± 307	4 ± 5
E171Q	52236 ± 268	3 ± 2
EQ/GW	53203 ± 220	2 ± 1
K44A	31019 ± 577	396 ± 143
KA/GW	33102 ± 140	290 ± 60

Table 4.2 Analytical Ultracentrifugation of Fluorescent MJ0796 Mutants and their Non-fluorescent Backgrounds - 20μM samples spun at 17,000 & 24,000 rpm. Single-species and monomer-dimer K_D fits achieved using SigmaPlot.

Finally, in order to firmly determine that fluorescence emission quenching and anisotropy increases of these single and double mutant proteins factually represents dimerization of the NBDs, analytical ultracentrifugation experiments were conducted at 400μM ATP for these variants. The single species and monomer-dimer K_D fits for the various MJ0796 proteins are summarized in Table 4.2. As expected from the fluorescence and anisotropy results shown in Figure 4.5, E171Q/G174W, E171Q, and G174W mutants exist primarily as dimers at 400μM ATP, whereas wild type, K44A, and K44A/G174W proteins exist primarily as monomers. These results are also replicable using HPLC gel filtration (Figure 4.7).

While the experimental results using the G174W substitution in single and double mutant forms of MJ0796 mentioned above support the inclusion of the dimeric interface witnessed in the E171Q-MJ0796 crystal structure during the hydrolytic cycle of ABC transporter NBDs, further dissection of this proposed reaction cycle is necessary. Ames and colleagues have shown that mixing wild

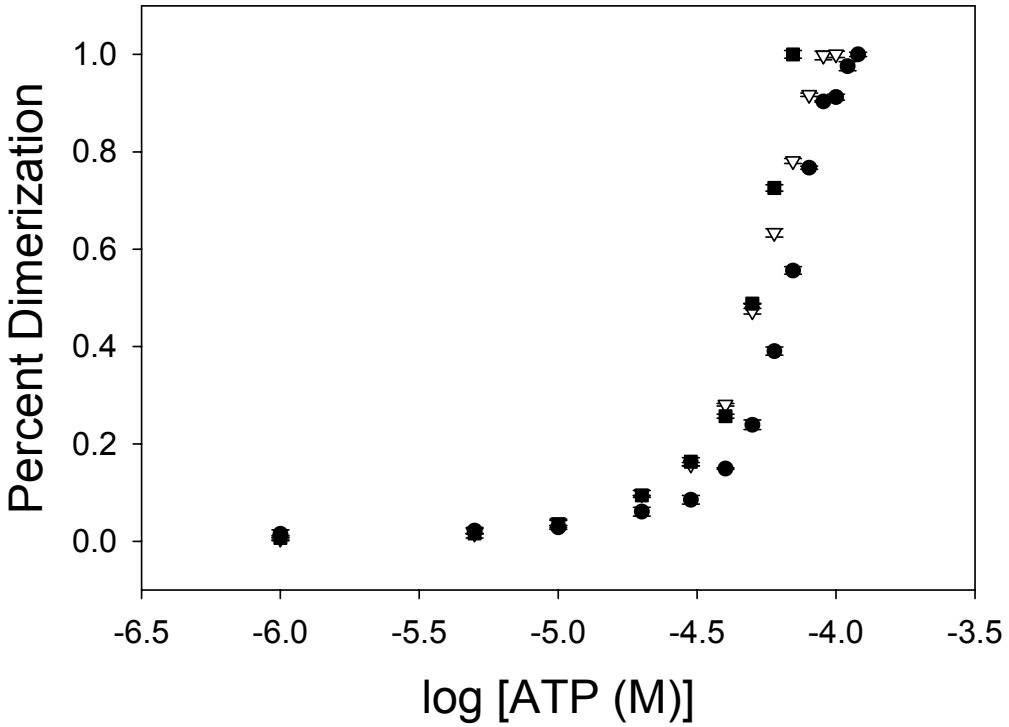

Figure 4.7 Gel Filtration Summary – 30μM protein run at 0.8mL/min. E171Q-MJ0796 shown in *solid circles*. G174W-MJ0796 shown in *open inverted triangles*. E171Q/G174W-MJ0796 shown in *closed squares*.

type and mutant forms of soluble HisP results in heterodimers that possess activity (Nikaido and Ames, 1999) described in Chapter II. This type of mixing experiment can be utilized to address the questions of how many binding and/or hydrolysis events are necessary and sufficient to complete the NBD reaction cycle. By mixing MJ0796 single mutants K44A and S147F (mutation of the highly conserved serine residue of the LSGGQ motif to phenylalanine), one would expect to obtain K44A-K44A and S147F-S147F homodimers, as well as heterodimers with one active site containing both mutations and another active site with all residues necessary for nucleotide binding and hydrolysis. Homodimers of both single mutants lack ATPase activity as measured using a

coupled assay (*open circles* and *squares* respectively in Figure 4.8). At nucleotide concentrations where K44A is not expected to bind nucleotide based upon K44A/G174W fluorescence quench and anisotropy values (*diamonds* in Figure 4.5, i.e., less than 1mM ATP) only the S147F-MJ0796 proteins would stably bind nucleotide. Any heterodimers formed at these unsaturated ATP concentrations should only possess one bound nucleotide at the "wild type" active site. Mixtures of K44A and S147F single mutants lack any detectable ATPase activity (*open triangles* in Figure 4.8) even at nucleotide concentrations up to 60mM (Figure 4.8) and protein concentrations higher than 50μM (data not shown).

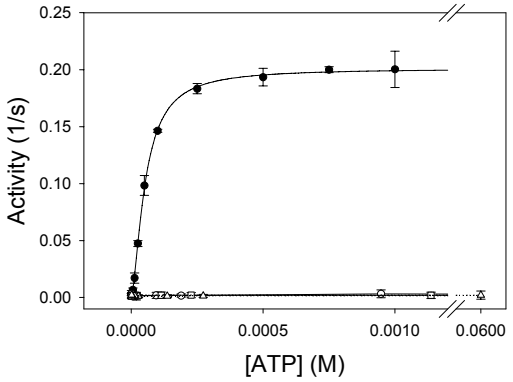

Figure 4.8 Mixture of Walker A and Signature Motif Mutants - ATPase activity of wild type (*filled circles* and *solid line*), K44A- (*open diamonds*), S147F- (*open squares*), and 1:1 mixture of K44A- and S147F- (*open triangles*) MJ0796 proteins at 1μM as a function of molar ATP concentration. Data fit to the Hill equation.

To probe these results using an alternative method, the fluorescent probe of G174W was used. The K44A/G174W-MJ0796 double mutant, hydrolytically deficient like the single mutant K44A-MJ0796 (Figure 4.9), was mixed 1:1 with S147F-MJ0796. In the presence of 12mM ATP, the relative fluorescence of the protein mixture decreases to zero and the relative anisotropy increases to 1.5

(*black trace* and *bars* in Figure 4.9). 120μM or 1.2μM ATP does not affect relative fluorescence emission or anisotropy values of the mixture. Addition of Mg^{2+} after 90 seconds does not change the relative fluorescence emission or the anisotropy values of the 12mM or 1.2μM ATP mixtures (and by extension the amount of stable NBD dimers), while the 120μM ATP mixture undergoes a transition similar to the one exhibited by K44A/G174W-MJ0796 alone (compare the *light gray traces* and *bars* in Figures 4.6B and 4.9). Cumulatively, the presence of Mg^{2+} increases stable NBD dimerization on the K44A-MJ0796 mutant background, while it decreases stable NBD dimerization on the E171Q-MJ0796 mutant background (Figures 4.6, 4.9). Addition of a five-fold excess of S147F-MJ0796 after 300 seconds has no effect on the 12mM and 1.2μM mixtures. In the 120μM ATP mixture, this excess S147F-MJ0796 does slightly decrease fluorescence emission to 72% of original levels, while the relative anisotropy increases from 1.1 to 1.2 (Figure 4.9). This suggests that heterodimers do form between K44A/G174W-MJ0796 and S147F-MJ0796, although no measurable change was detected after this initial quench and anisotropy increase. These fluorescence and anisotropy levels were stable for the maximum time measured, 7200 seconds (data not shown).

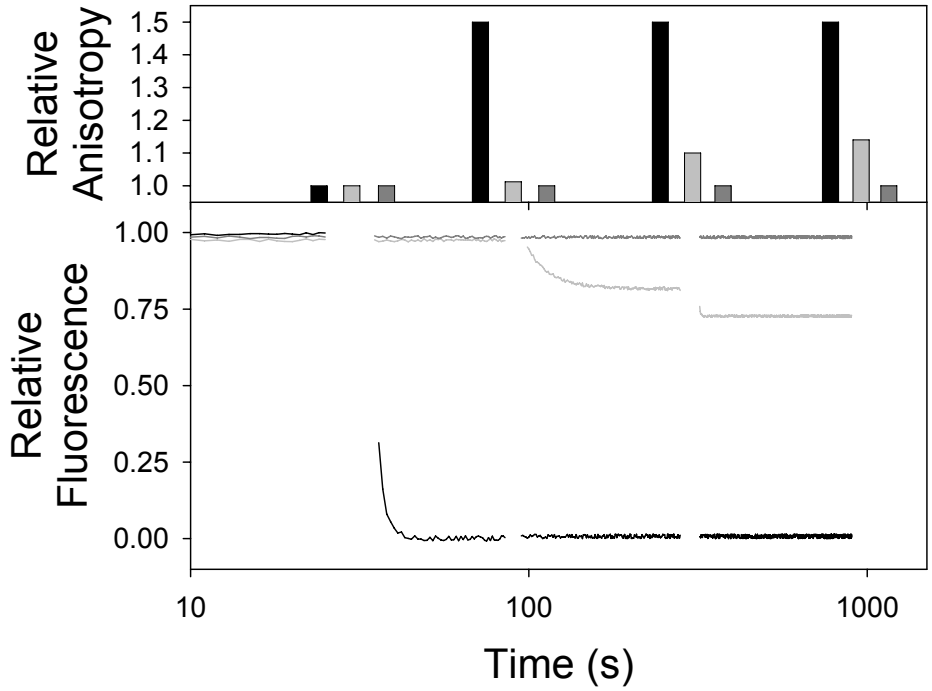

Figure 4.9 Monitoring Fluorescence of a Mixture of Walker A and Signature Motif Mutants - Fluorescence time course and relative anisotropy values of 1:1 mixture of K44A/G174W- and S147F-MJ0796, exciting at 295nm and measuring emission at 343nm. Relative fluorescence trace shown in lower graph by *solid lines*, and anisotropy values in upper graph by *vertical bars*. At time = 0 MJ0796 mixture plus 1mM EDTA was incubated for 30 seconds, upon which ATP was added (*black trace* and *bars* show 12mM ATP, *light gray trace* and *bars* show 120μM ATP, and *dark gray trace* and *bars* show 1.2μM ATP). After 90 seconds, 10mM Mg^{2+} was added. At 300 seconds, a 5-fold excess of S147F-MJ0796 was added to the sample, holding ATP concentration constant. Fluorescence values corrected for dilution at 30, 90 and 300 seconds, background subtracted, and converted along with anisotropy values to relative amounts.

In order to address the number of hydrolysis events necessary and sufficient to complete the NBD reaction cycle, more mixing experiments were employed. A mixture of MJ0796 single mutants S147F and E171Q results in homodimers of both mutants (each is hydrolytically deficient as shown by *open* and *filled triangles* in Figure 4.10) as well as heterodimers containing a doubly-

mutated active site and a composite "wild type" active site as is the case when mixing K44A and S147F single mutants. Since two bound nucleotides appear necessary for efficient dimerization as determined above, heterodimers of S147F and E171Q would possess ATPase activity if and only if one hydrolysis event is sufficient to complete the NBD reaction cycle. This turns out to be the case as shown by open circles in Figure 4.10. A 1:1 mixture of S147F and E171Q produces maximal activity as determined by varying the molar ratio of the two single mutants (data not shown) and the calculated V_{max} of 0.5 sec^{-1} is approximately ¼ the wild type value of 0.2 sec^{-1}. The mixture possesses a K_m of 100μM ATP.

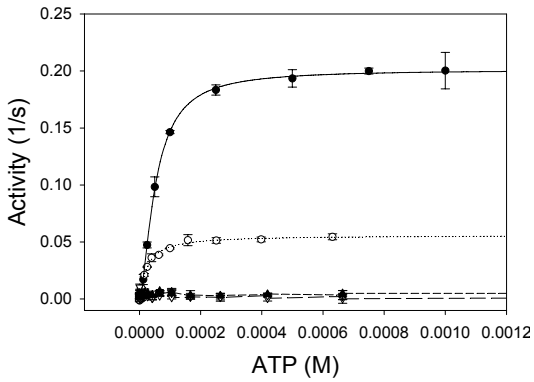

Figure 4.10 Mixture of Walker B and Signature Motif Mutants - ATPase activity of wild type (*filled circles* and *solid line*), S147F- (*filled triangles* and *large dashed line*), E171Q- (*open inverted triangles* and *small dashed line*), and 1:1 mixture of S147F- and E171Q- (*open circles* and *dotted line*) MJ0796 proteins at 1μM as a function of molar ATP concentration. Data fit to the Hill equation using SigmaPlot. 1:1 mixture of S147F- and E171Q-MJ0796 fit results in a V_{max} of 0.05 sec^{-1} and K_m of 100μM.

An explanation for the 75% change in the mutant heterodimer V_{max} is that wild type MJ0796 hydrolysis reflects the catalysis of both ATP molecules bound at the dimeric interface as opposed to a single event per reaction cycle. Assuming that the relative affinities between E171Q- , S147F-MJ0796 and nucleotide are all equal, the 25% activity would result from the "half-active" mutant heterodimers

possessing only one active site and only being present at 50% of the concentration of the doubly-productive wild type homodimers. Also, due to the fact that under our experimental conditions the amount of E171Q- plus S147F-MJ0796 heterodimers present is unknown, the Hill coefficient fit to the ATPase data of the mixture would be meaningless.

Mixing E171Q/G174W-MJ0796 in a 1:1 ratio with S147F-MJ0796 in the presence of 1.2μM ATP results in a fluorescence decrease to roughly 25% of original levels. The relative anisotropy of this mixture increases to 1.4. Addition of Mg^{2+} after 90 seconds to the 1.2μM ATP mixture engenders the return to original fluorescence and anisotropy levels after 30 additional seconds (*dark gray trace* and *bars* in Figure 4.11). In the presence of 120μM ATP, the mixture of E171Q/G174W- and S147F-MJ0796 exhibits a fully quenched fluorescence emission and relative anisotropy of 1.5. After the addition of Mg^{2+} at 90 seconds, the return to original fluorescence and anisotropy values takes almost 3600 seconds (*light gray trace* and *bars* in Figure 4.11). The 12mM ATP mixture, displaying a similar nucleotide-dependent quench and anisotropy increase, does not change after the addition of Mg^{2+} (*black trace* and *bars* in Figure 4.11) during the maximum time measured, 7200 seconds (data not shown).

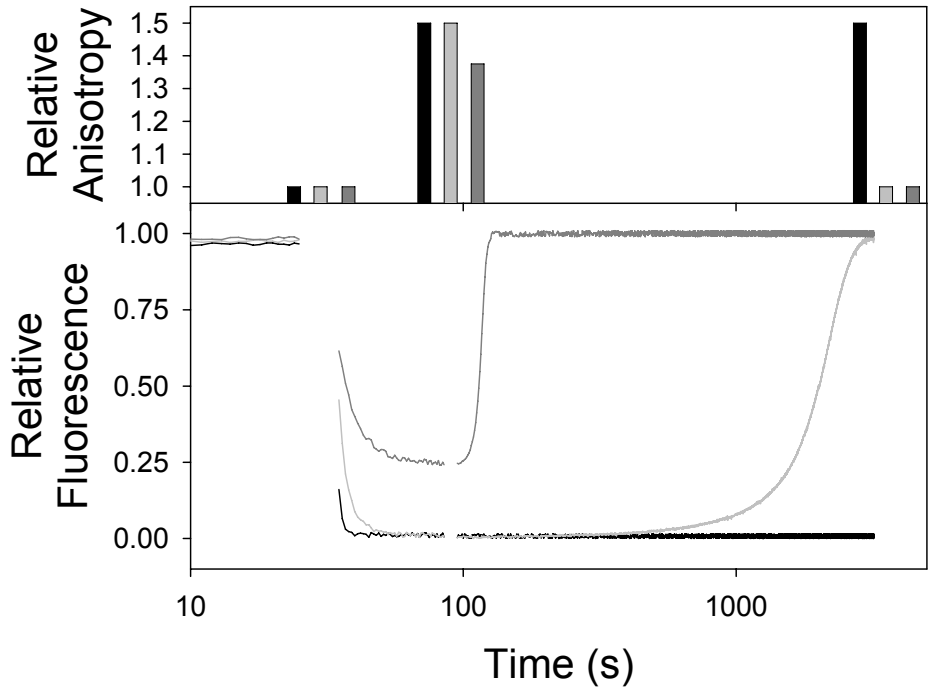

Figure 4.11 Monitoring Fluorescence of a Mixture of Walker B and Signature Sequence Mutants - Fluorescence time course and relative anisotropy values of 1:1 mixture of E171Q/G174W- and S147F-MJ0796, exciting at 295nm and measuring emission at 343nm. Relative fluorescence trace shown in lower graph by *solid lines*, and relative anisotropy values in upper graph by *vertical bars*. At time = 0 MJ0796 mixture plus 1mM EDTA was incubated for 30 seconds, upon which ATP was added (*black trace* and *bars* show 12mM ATP, *light gray trace* and *bars* show 120μM, and *dark gray trace* and *bars* show 1.2μM). After 90 seconds, 10mM Mg^{2+} was added. Fluorescence values corrected for dilution at 30, 90 and 300 seconds, background subtracted, and converted along with anisotropy values to relative amounts.

The aforementioned experimental results suggest that the dimeric interface exhibited by the E171Q-MJ0796 crystal structure is relevant to the NBD reaction cycle, during which two nucleotide binding events and only one hydrolysis event are necessary and sufficient to complete the cycle.

Since these results apply to a system involving only the soluble NBD, the requirements to complete the cycle in a full transport system (two TM domains

plus two NBDs) were probed using the LolCDE system from *Escherichia coli*. This ABC transporter machinery (*lolC* and *lolE* code for the two TM domains, while *lolD* codes for the NBD) is responsible for releasing lipoproteins from the inner membrane that are bound for the outer membrane to the periplasmic chaperone, LolA, which subsequently hands the lipoproteins off to the outer membrane-bound LolB (reviewed in Narita and Tokuda, 2006. A single copy of the NBD, LolD, is located in the operon in *E. coli*, while the functional unit has been shown to be $LolCD_2E$ (Yakushi *et al*., 2000). Significantly, LolD is the closest NBD homologue in *E. coli* to MJ0796, with nearly 50% identity and 70% similarity between the two. Tokuda and colleagues have elegantly characterized the Lol system, and have conclusively shown that at least one copy of wild type *lolD* must be supplied for continued growth. By constructing an *E. coli* strain (CDE4) containing a genomic knockout of the *lolCDE* operon and a temperature-sensitive plasmid supplying the wild type *lolCDE* genes, the authors were able to show that all three gene products (both TM domains and the NBD) are required for growth at non-permissive temperatures (Narita *et al*., 2002). After the kind gift of these strains from Dr. Tokuda's group, we were able to replicate their results and use the LolCDE system to test our hypotheses on the NBD reaction cycle by using LolD mutants.

Single mutants of LolD in the Walker A and extended Walker B motifs in addition to the ABC signature sequence (K48A-, E171Q-, and S147F-LolD,

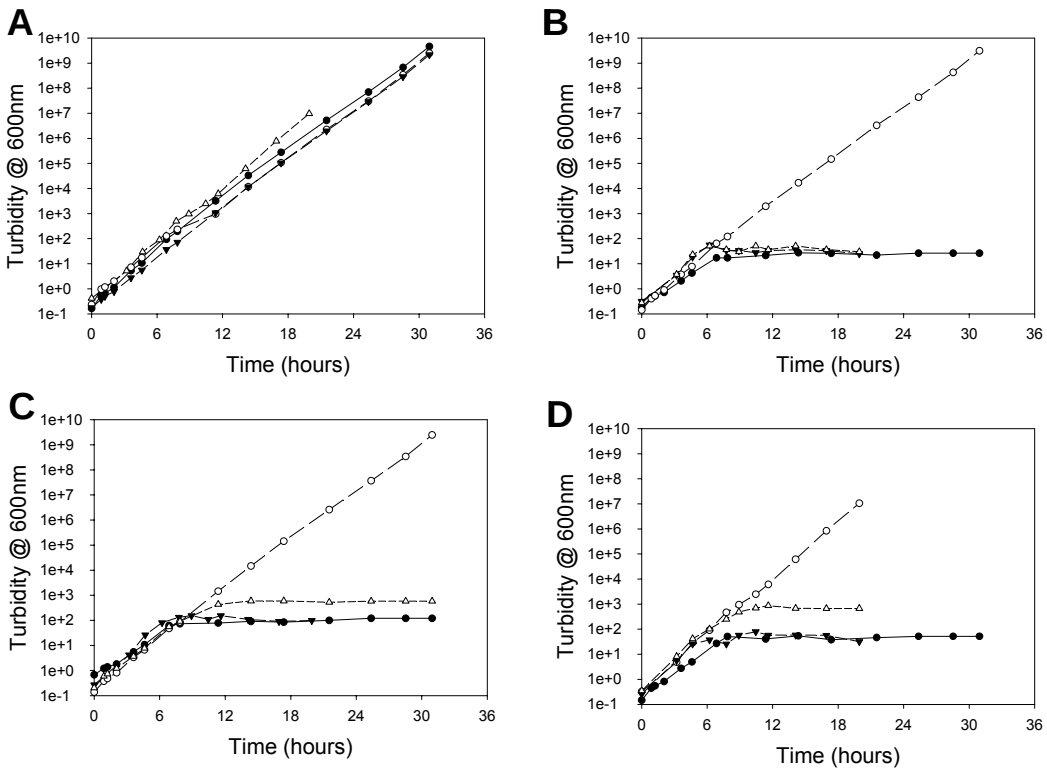

Figure 4.12 Growth Assays - Growth assays plotting turbidity at 600nm versus time in hours. (A) *Closed circles* denote wild type LolD alone, *open circles* show wild type LolD plus K48A-LolD, *filled inverted triangles* represent wild type LolD plus E171Q-LolD, and *open triangles* illustrate wild type LolD plus S147F-LolD. (B) C*losed circles* denote K48A-LolD alone, *open circles* show K48A-LolD plus wild type LolD, *filled inverted triangles* represent K48A-LolD plus E171Q-LolD, and *open triangles* illustrate K48A-LolD plus S147F-LolD. (C) *Closed circles* denote E171Q-LolD alone, *open circles* show E171Q-LolD plus wild type LolD, *filled inverted triangles* represent E171Q-LolD plus K48A-LolD, and *open triangles* illustrate E171Q-LolD plus S147F-LolD. (D) *Closed circles* denote S147F-LolD alone, *open circles* show S147F-LolD plus wild type LolD, *filled inverted triangles* represent S147F-LolD plus K48A-LolD, and *open triangles* illustrate S147F-LolD plus E171Q-LolD.

analogous to K44A-, E171Q-, and S147F-MJ0796) were constructed using pNASCDE (Narita *et al*., 2002) as a template and introducing zeocin resistance as a selectable marker. Positive transformants for all three single mutations were unable to support growth at non-permissive temperatures (*filled circles* in Figures

4.12B-D respectively), while strains possessing a single copy of wild type *lolD* continued to grow logarithmically at non-permissive temperatures (*filled circles* in Figure 4.12A). In order to conduct mixing experiments as summarized in Figures 4.8 and 4.10, we introduced a second copy of *lolD* immediately downstream of *lolE*. Not surprisingly, addition of any of the three single mutants (K48A-, E171Q-, or S147F-LolD) to wild type LolD did not affect growth at non-permissive temperatures (*open circles*, *filled inverted triangles*, and *open triangles* in Figure 4.12A respectively). Illustrating that the inserted second copy of *lolD* is transcribed and translated at sufficient levels in our experiments, addition of wild type *lolD* at the second position rescues growth at non-permissive temperatures for all three single mutants (*open circles* in Figures 4.12B-D). Addition of either E171Q- (*filled inverted triangles*) or S147F-LolD (*open triangles*) to K48A-LolD did not result in growth at non-permissive temperatures as shown in Figure 4.12B. These results coincide with those obtained with MJ0796 ATPase and fluorescence experiments. On the other hand, providing S147F- in addition to E171Q-LolD (*open triangles* in Figure 4.12C) or vice versa (*open triangles* in Figure 4.12D) did not rescue growth at non-permissive temperatures as expected from the MJ0796 experiments. This discrepancy could result from insufficient expression levels of the second copy of *lolD* we have introduced into the operon, but this possibility seems unlikely due to the fact that wild type *lolD* inserted at this position rescues growth at the non-permissive

temperature (*open circles* in Figures 4.12B-D). Alternatively, the lol machinery and other full transport systems may require two hydrolysis events to complete the lipoprotein release during each reaction cycle as suggested by studies of MalK and OpuA (Mimmack *et al*., 1989; Patzlaff *et al*., 2003). As the mutant-wild type HisP heterodimers described in Chapter II from Ames and colleagues' work (Nikaido and Ames, 1999), with only one functional active site transport activity is only 50% of the normal wild type levels. If the mutant heterodimers in the Lol system behave similarly, it is also possible that 50% transport activity is insufficient for logarithmic growth at the non-permissive temperature, and the mixture of E171Q- and S147F-LolD would be unable to support growth.

Based upon the MJ0796 ATPase and fluorescence experimental results, in addition to the growth assays utilizing the *E. coli* Lol system, we have proposed a modified reaction cycle in Figure 4.13. Beginning with two nucleotide-free NBDs, *Step 1* illustrates binding of a single molecule of ATP and the resulting rigid body rotation of the α-helical subdomain (illustrated by the change from *cyan* to *dark blue*), followed by the second nucleotide binding event and conformational change shown by *Step 2*. Dimerization of the ATP-bound NBDs (*Step 3*) occurs quickly, and the only way in which we have been able to witness this event in solution is to increase the sample viscosity significantly (as in our fluorescence time-course experiments). It is this ATP sandwich dimer that Smith *et al* trapped in the E171Q-MJ0796 crystal structure (Figure 3.6). Provided that

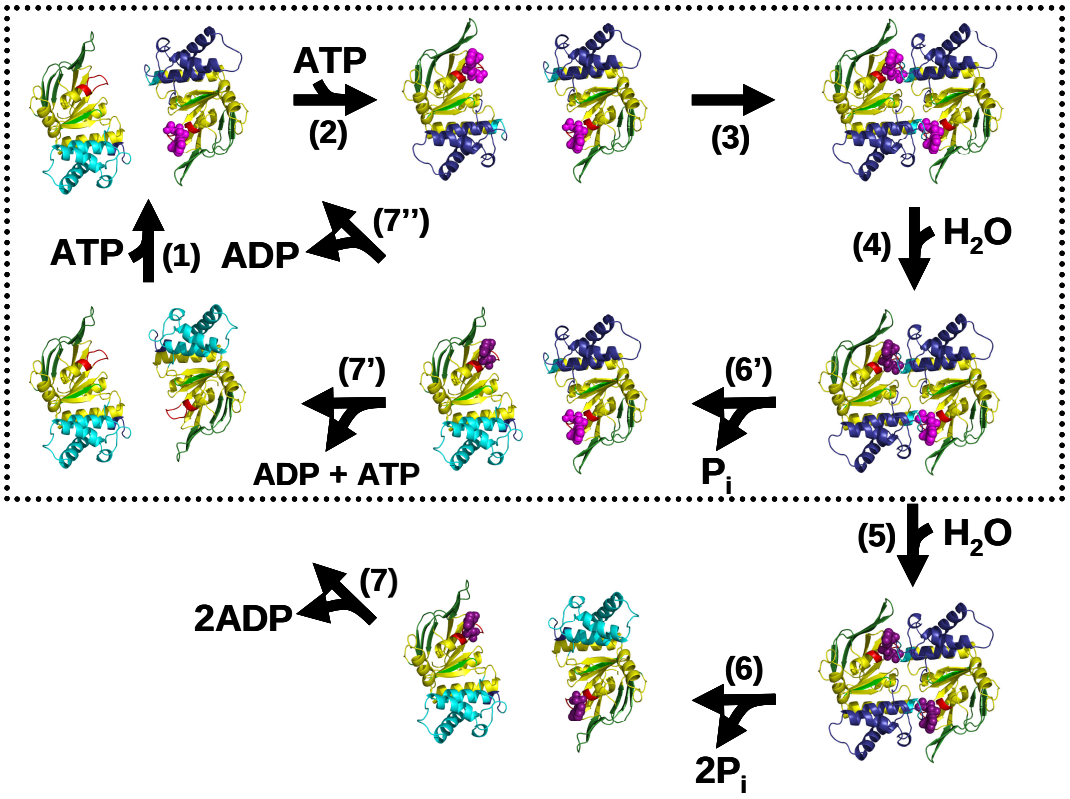

Figure 4.13 Revised Mechanochemical Reaction Cycle of ABC Transporter NBDs - The F_1-type core and anti-parallel β-sheet subdomains combined are shown in *yellow*, while the α-helical subdomain is shown in either *cyan* (nucleotide free and ADP-bound states) or *dark blue* (ADP•P_i- and ATP-bound states). ATP is shown in *magenta*, while ADP and ADP•P_i are shown in *purple*. ATP binds to one of the nucleotide-free monomers (*step 1*) resulting in the α-helical subdomain rotation (signified by the change from *cyan* to *dark blue*). This process is repeated for the second nucleotide-free monomer (*step 2*) followed immediately by dimerization of the cassettes (*step 3*). Hydrolysis of one of the ATP molecules (*step 4*) can either lead to hydrolysis of the second ATP (*step 5*) and release of the inorganic phosphates (*step 6*) or simply to the release of a single inorganic phosphate (*step 6'*). In both cases the release of inorganic phosphate is coupled to dimer dissociation and rotation of the α-helical subdomain in the ADP-bound monomers (signified by the change back to *cyan* from *dark blue*). Finally, release of all bound nucleotides (*step 7 & 7'*) occurs, completing the cycle. Alternatively, following a single hydrolysis event (*steps 4 & 6'*) the ADP alone can dissociate (*step 7"*) to shorten the cycle. The dotted box outlines the cycle (*steps 1-4, 6'-7' / 7"*) which takes place when S147F and E171Q MJ0796 single mutants are mixed together, while the outermost cycle (*steps 1-7*) likely takes place in the full tranporter as suggested using the *lolCDE* system.

divalent cations and all necessary "wild type" residues are present, the cycle proceeds with *Step 4*, hydrolysis of one of the ATP molecules. In a wild type homodimer, the determination of which ATP gets hydrolyzed initially is presumably stochastic. In the case of the MJ0796 mixing experiments involving S147F + E171Q single mutants (cycle denoted by *dotted box* in Figure 4.13), only one of the active sites is capable of hydrolysis. This directed catalytic event is followed quickly by *Step 6'*, release of inorganic phosphate and monomerization of the NBDs into ADP- and ATP-bound forms. The cycle can then be completed by release of ADP and ATP in *Step 7'*, or alternatively, simply release of ADP while ATP remains bound to one monomer (E171Q in the case of the MJ0796 mixing experiments) as shown in *Step 7''*. This shortened cycle is likely applicable to human ABCC subfamily transporters, such as CFTR and SUR, in which one active site contains all of the residues thought to be necessary for nucleotide hydrolysis, while the other active site is degenerate and appears to serve a regulatory role by binding but not hydrolyzing nucleotide (Gadbsy and Nairn, 1999; Vergani *et al*., 2005).

While the cycle enclosed in the *dotted box* of Figure 3.12 (*Steps 1-4, 6'-7'/7''*) is sufficient to produce activity in the soluble NBDs alone as shown in the MJ0796 mixing ATPase and fluorescence experiments described above, the analogous mixtures using the *E. coli* growth assays suggest that for efficient transport the cycle might require *Steps 5-7*, in which the second molecule of ATP

is hydrolyzed, both inorganic phosphates are released during monomerization, and both ADP molecules are released, thus completing the cycle. This involement of the second nucleotide hydrolysis step in the full transport system may be necessary to reset the transport machinery (Lu *et al*., 2005). This possibility is strengthened by the fact that maltose transport systems that have been vanadate-trapped following ATP hydrolysis retain tight binding of the maltose binding protein, MalE, to the TMDs, MalQ and MalM (Chen *et al*., 2001). This suggests that a second ATP molecule must be hydrolyzed to return the transporter to the ground state and allow a second maltose-bound MalE molecule to begin the transport cycle. Experiments in a variety of full transport systems, including those studied herein, have been inconclusive at best in their attempts at determining the stoichiometry of ATP hydrolysis to transport events (Ames *et al*., 1989; Bishop *et al*., 1989; Davidson and Nikaido, 1990). Further study of both homodimeric bacterial NBDs and heterodimeric (with respect to their NBDs) prokaryotic and eukaryotic transporters will be necessary to test this hypothetical reaction cycle.

Chapter V

Future Directions of the Study of ATP-Binding Cassette Transporter Functional Mechanism

In the eight years since the structure of HisP (Hung *et* al., 1998) was solved, 22 additional non-redundant ABC transporter NBDs have had their crystal structures published. In total, 47 different pdb files of NBDs are available (see summary in Table 5.1). Even with all of this structural information, there are still aspects of the reaction cycle that remain speculative. Below are just a few of the recent intriguing developments and important questions remaining to be answered.

Recent work by Senior and colleagues on mouse Mdr3 suggests the existence of an "occluded nucleotide conformation" of ABC transporter NBDs (Tombline *et al*., 2004b; Tombline *et al*., 2005). By mutating the equivalent of E171-MJ0796 to alanine in both Mdr3 NBDs (E552A/E1197A), they are able to illustrate vanadate-independent nucleotide trapping at the active sites with a stoichiometry of 1 mol/mol. The authors take this to represent formation of the "occluded nucleotide conformation" in which the other nucleotide, presumably required to dimerize, has dissociated leaving a single molecule bound (Tombline *et al*., 2004b). This conformation may be related to the *trans*-acting negative

Protein	Source	PDB	Deposit	Publication
HisP	*S. typhimurium*	1B0U	11/12/1998	Hung *et al*., 1998
MJ0796	*M. jannaschii*	1F3O	6/5/2000	Yuan *et al*., 2001
MalK	*T. litoralis*	1G29	10/18/2000	Diederichs *et al*., 2000
MJ1267	*M. jannaschii*	1G6H	11/6/2000	Karpowich *et al*., 2001
MJ1267	*M. jannaschii*	1G9X	11/28/2000	Yuan *et al*., 2003
MJ1267	*M. jannaschii*	1GAJ	11/30/2000	Karpowich *et al*., 2001
Tm1139	*T. maritima*	1JIO	6/28/2001	
TAP1	*H. sapiens*	1JJ7	7/3/2001	Gaudet and Wiley, 2001
MsbA	*E. coli*	1JSQ	8/17/2001	Chang and Roth, 2001
MJ0796	*M. jannaschii*	1L2T	2/24/2002	Smith *et al*., 2002
BtuCD	*E. coli*	1L7V	3/18/2002	Locher *et al*., 2002
HlyB	*E. coli*	1MTO	9/20/2002	Schmitt *et al*, 2003
LmrA	*L. lactis*	1MV5	9/24/2002	
GlcV	*S. solfataricus*	1OXS	4/3/2003	Verdon *et al*., 2003
GlcV	*S. solfataricus*	1OXT	4/3/2003	Verdon *et al*., 2003
GlcV	*S. solfataricus*	1OXU	4/3/2003	Verdon *et al*., 2003
GlcV	*S. solfataricus*	1OXV	4/3/2003	Verdon *et al*., 2003
GlcV	*S. solfataricus*	1OXX	4/3/2003	Verdon *et al*., 2003
MsbA	*V. cholera*	1PF4	5/23/2003	Chang, 2003
MalK	*E. coli*	1Q12	7/18/2003	Chen *et al*., 2003
MalK	*E. coli*	1Q1B	7/18/2003	Chen *et al*., 2003
MalK	*E. coli*	1Q1E	7/19/2003	Chen *et al*., 2003
mNBD1	*M. musculus*	1Q3H	7/29/2003	Lewis *et al*., 2004
mNBD1	*M. musculus*	1R0W	9/23/2003	Lewis *et al*., 2004
mNBD1	*M. musculus*	1R0X	9/23/2003	Lewis *et al*., 2004
mNBD1	*M. musculus*	1R0Y	9/23/2003	Lewis *et al*., 2004
mNBD1	*M. musculus*	1R0Z	9/23/2003	Lewis *et al*., 2004
mNBD1	*M. musculus*	1R10	9/23/2003	Lewis *et al*., 2004
Ph0022	*P. horikoshii OT3*	1V43	11/8/2003	Ose *et al*., 2004
Pf0895	*P. furiosus*	1SGW	2/24/2004	
Ph0022	*P. horikoshii OT3*	1VCI	3/8/2004	Ose *et al*., 2004
HlyB	*E. coli*	1XEF	9/10/2004	Zaitseva *et al*., 2005b
mNBD1	*M. musculus*	1XF9	9/14/2004	Thibodeau *et al*., 2005
mNBD1	*M. musculus*	1XFA	9/14/2004	Thibodeau *et al*., 2005
hNBD1	*H. sapiens*	1XMI	10/2/2004	Lewis *et al*., 2005
hNBD1	*H. sapiens*	1XMJ	10/2/2004	Lewis *et al*., 2005
Tm0544	*T. maritima*	1VPL	11/10/2004	
MsbA	*S. typhimurium*	1Z2R	3/9/2005	Reyes and Chang, 2005
CysA	*A. acidocaldarius*	1Z47	3/15/2005	Scheffel *et al*., 2005
MalK	*E. coli*	2AWN	9/1/2005	Lu *et al*., 2005
SufC	*T. thermophilus HB8*	2D2F	9/5/2005	Watanabe *et al*., 2006
SufC	*T. thermophilus HB8*	2D3W	10/3/2005	Kitaoka *et al*., 2006
hNBD1	*H. sapiens*	2BBO	10/17/2005	
hNBD1	*H. sapiens*	2BBS	10/17/2005	
hNBD1	*H. sapiens*	2BBT	10/17/2005	
MRP1	*H. sapiens*	2CBZ	1/10/2006	Ramaen *et al*., 2006
Py06054	*P. yoelii*	2GHI	3/27/2006	

Table 5.1 ABC Transporter NBD PDB File Summary – All 47 individual ABC transporter NBD .pdb files available as of the writing of this dissertation. Protein, species of origin, PDB code, date of structure deposition, and reference, where applicable, listed. Unpublished structures in *red*.

effect of the Walker A lysine mutation (K44A) studied herein. Structural characterization of this conformation, distinct from the symmetrical sandwich dimer exhibited by the E171Q-MJ0796 structure (Smith *et al*., 2002) would be of great interest to the ABC transporter research community, as most eukaryotic ABC transporters have been postulated to operate asymmetrically with respect to their NBDs (Chen *et al*., 2004; Tombline *et al*., 2004a; Berger *et al*., 2005; Zhang *et al*., 2006). The co-crystallization of NBD1 and NBD2 from any of the eukaryotic ABC transporters, as of yet elusive, would be a landmark step in the determination of the finer details of NBD asymmetric behavior and crosstalk during the transport cycle. Hydrolysis-deficient mutants such as the E171Q mutant championed herein will serve as excellent tools in these future studies. As an example, recent work on E1371Q-CFTR, in which the Walker B glutamate in NBD2 has been mutated, has shown that the open state of the channel is greatly stabilized (Vergani *et al*., 2005). This result suggests that the CFTR NBD1-NBD2 heterodimer is stably formed under these experimental conditions, and any structural characterization (hopefully underway in a number of labs) of this species promises a wealth of information.

Since it is such an easily purified model NBD, MJ0796 itself warrants continued structural examination. Determination of the orientation of G174W at the dimeric interface of an ATP sandwich would be of value. As presented in Figure 4.1, the aromatic side chains do not interact, as PyMol simply found the

lowest energy rotamer to accommodate the mutation. It would be interesting to see if the rings actually stack in the hypothetical sandwich dimer. Limited crystallization screens with G174W-MJ0796 produced small clusters of needles, and consequently was not pursued. In addition to G174W-, K44A/G174W-MJ0796 would be of academic interest to crystallize in the presence of ATP. As dimerization of this double mutant is possible, albeit at extremely high nucleotide concentrations (Figure 4.5), activity is nonetheless undetectable in the presence of up to 60mM ATP (Figure 4.8). The number and orientation of nucleotide(s) at the dimeric interface of K44A/G174W-MJ0796 would be illuminating to the experimental results presented in Chapter IV. Finally, the odd nucleotide-independent dimerization of the double mutant, K44A/E171Q-MJ0796 (Figure 3.10), could potentially be addressed by its crystallization. In limited crystallization screens with K44A/E171Q-MJ0796, two large irregular crystals (Figure 5.1) were obtained. In addition to further crystallization of MJ0796 mutants and conformations, the fluorescent probe of G174W serves as an excellent monitor of protein behavior. This background could continue to serve well as a

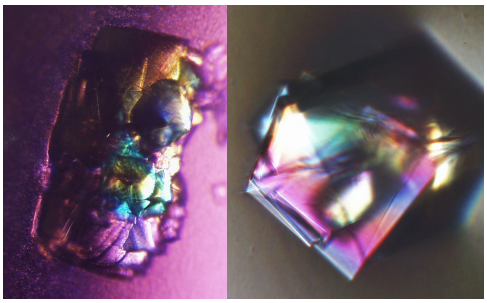

Figure 5.1 K44A/E171Q Crystals – Two large crystals, measuring 10X10X100μm, from drops containing 18% PEG-4000 (w/v), 10% isopropanol, 100mM Na-HEPES pH 7.0 were frozen in liquid propane.

research tool in future experiments, and work is ongoing in the Thomas lab in this endeavor.

Recent work on HlyB suggests that the highly conserved histidine in the H-Loop (Figure 2.2) serves as the catalytic residue in which ATP undergoes substrate-assisted catalysis (SAC) (Dall'Acqua and Carter, 2000), rather than the general base mechanism commonly thought to occur during nucleotide hydrolysis (Zaitseva *et al*., 2005b). By increasing the viscosity of their ATPase assay buffer and showing that activity did not appreciably change, the authors state that a chemical reaction rather than an association/dissociation reaction is rate-limiting under their experimental conditions. They then go on to use solvent isotope effects to measure catalytic efficiency, k_{cat}/K_m, in H_2O versus D_2O. Finally, E631Q-HlyB (the equivalent mutant to E171Q-MJ0796) possesses 10% wild type ATPase activity as opposed to the hydrolytic deficiency of E171Q-MJ0796 and E179Q-MJ1267 (Figure 3.1). The authors show that the pH dependence of E631Q-HlyB is the same as that of wild type HlyB, suggesting that a general base mechanism is unlikely (Zaitseva *et al*., 2005b). Although this hypothesis remains to be tested in a number of other ABC transporter NBDs, it has served to renew interest in the amino acids necessary for catalysis, classically presumed to be the highly recognized Walker A & B motifs.

While the experimental evidence presented in Chapters III & IV is focused on the nucleotide binding domains (NBDs) of ABC transporters and the reaction

cycle they undergo during ATP binding and hydrolysis, there are several additional aspects of ABC transporter functional mechanism that are worthy of further research. One of the aspects of ABC transporter mechanism that is sorely lacking in terms of research findings is the interaction between TMDs and NBDs during the reaction cycle. Presumably the conformational signal to proceed with ATP hydrolysis is transmitted through the TMDs to the NBDs once substrate is bound to the intracellular loops of the TMDs (in the case of eukaryotic exporters.) In the case of bacterial periplasmic permeases, it has been shown that a single nucleotide hydrolysis event results in the tight association of substrate binding proteins to the periplasmic face of the TMDs (Chen *et al*., 2001; Lu *et al*., 2005). In addition, the presence of loaded substrate binding proteins greatly increases ATPase activity of reconstituted ABC transporters (Davidson and Nikaido, 1990), suggesting the following functional scenario using the maltose importer as an example. Maltose-bound MalE associates with the periplasmic face(s) of MalF and/or MalG, the TMDs of the maltose transporter. A signal is transmitted to the MalK dimer associated with MalF and MalG inside the cytoplasm to hydrolyze a molecule of ATP. Transport occurs across the lipid bilayer, and a second nucleotide hydrolysis event is required to release the MalE binding protein allowing the transport to return to the original state. Aside from the dimerization of NBDs studied in Chapters III and IV, every other step in the above

hypothesized reaction cycle has eluded characterization beyond a simple understanding.

By mapping binding protein independent mutations isolated in HisP (Petronilli and Ames, 1991), in which the ABC transporter machinery hydrolyzes nucleotide and allows transport in the absence of its binding protein, HisJ, onto the E171Q-MJ0796 structure, they are seen to cluster in the α-helical subdomains (Figure 5.2). This is not entirely surprising as this region of the protein, between the Q-Loop and LSGGQ signature motif, is the least conserved if one aligns several NBDs (Figure 2.2). This lack of conservation could easily be explained if this region of the NBDs is responsible for interacting with the widely varying

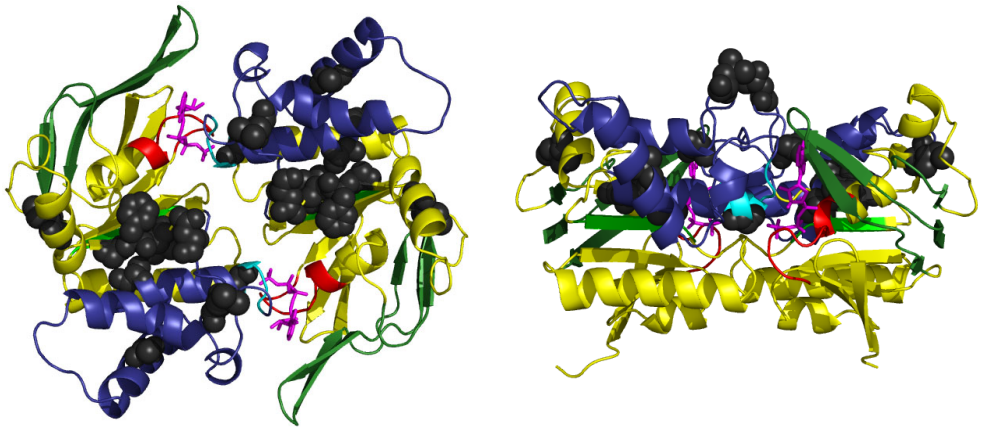

Figure 5.2 Protein Interaction Mutants – Top view shown on left, looking down into the cytoplasm from presumed location of TMDs. Side view along plane of lipid bilayer shown on the right. F_1-Type α/β subdomain colored in *yellow*, α-helical subdomain shown in *dark blue*, and anti-parallel β subdomain shown in *forest green*. Walker A motif highlighted in *red,* Walker B motif highlighted in *bright green,* and LSGGQ signature sequence highlighted in *cyan*. ATP shown in *magenta*. Mutations from HisP and MalK (Petronilli and Ames, 1991; Lipponcott and Traxler, 1997) shown in *spacefilling dark gray*.

TMDs. A number of different ABC transporters studied point towards this subdomain as a protein-protein interaction site (Sheps *et al*., 1995; Boehm *et al*., 1996; Wilken *et al*., 1996). Studies on the maltose transporter have identified a conserved region in the intracellular loops of both TMDs, MalF and MalG, coined the EAA loop. Mutations in this loop abolished transport, and suppressing mutations of EAA loop mutants were isolated in the α-helical subdomain of MalK (Mourez *et al*., 1997). These EAA-suppressing mutations, in addition to mutations isolated that inhibit proper assembly of the $MalFGK_2$ complex (Lippincott and Traxler, 1997), also mostly map to the α-helical subdomain (Figure 5.2). Although the functional equivalent of the EAA loop studied by Dassa and colleagues is not always readily apparent in eukaryotic transporters, as the TMDs from various systems do not align well using primary sequence information, presumably such motifs exist in the intracellular loops of all TMDs. Indeed, intracellular loops from CFTR and Mdr1 have been suggested to interact with the nucleotide binding domains (Currier *et al*., 1992; Xie *et al*., 1995; Cotton *et al*., 1996). Mutational screens and directed mutagenic studies to help elucidate the mechanisms of information coupling between membrane-bound and cytoplasmic domains during the reaction cycle promise to further our understanding of how ABC transporters accomplish the transport of such a wide variety of solutes.

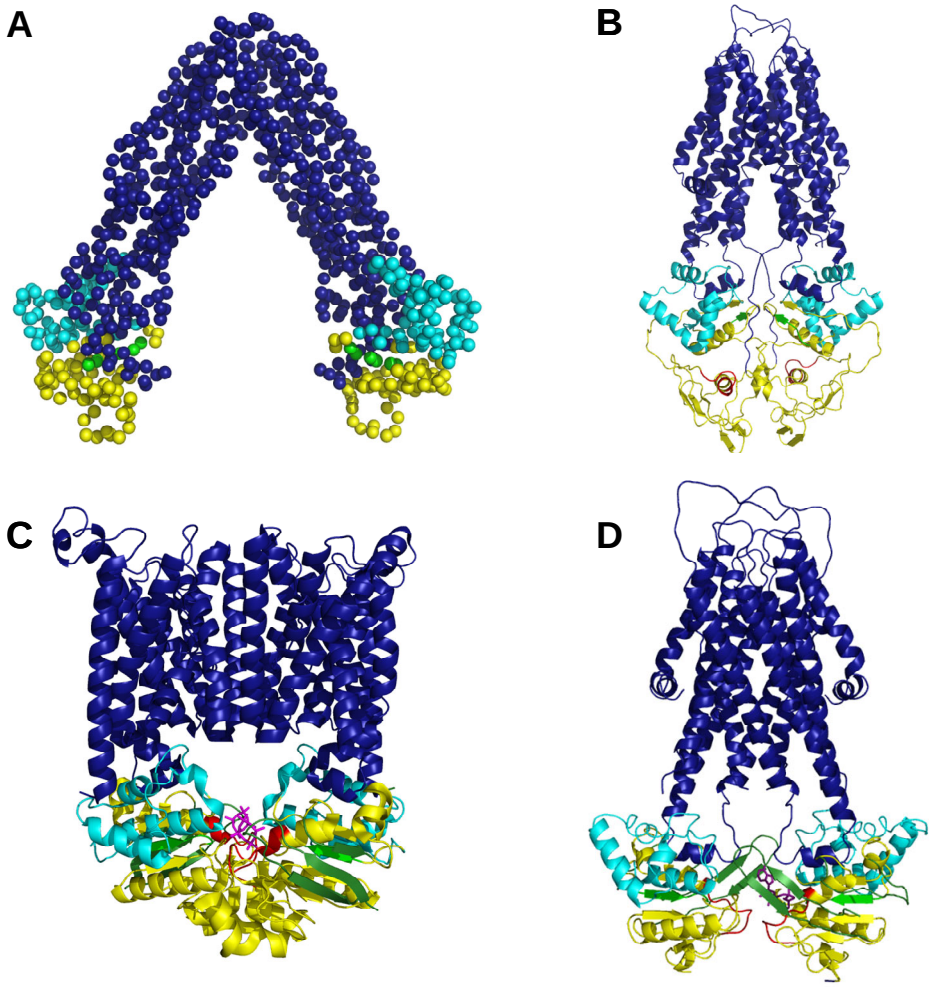

Figure 5.3 Full ABC Transporter Structures –Side view along plane of lipid bilayer shown for all four structures. TMDs colored *dark blue*. F_1-Type α/β subdomain colored in *yellow*, a-helical subdomain shown in *cyan*, and anti-parallel β subdomain shown in *forest green*. Walker A motif highlighted in *red* and Walker B motif highlighted in *bright green*. Vanadate shown in *magenta*. (A) *Escherichia coli* MsbA (B) *Vibrio cholera* MsbA (C) *E. coli* BtuCD (D) *Salmonella thyphimurium* MsbA

Despite the wealth of structural information on the NBDs (summarized in Table 5.1), there are still only four full transporter crystal structures available (Figure 5.3). Two of these, *Escherichia coli* BtuCD (Locher *et al*., 2002) and *Salmonella typhimurium* MsbA (Reyes and Chang, 2005), exhibit a dimer

interface similar to that seen in the E171Q-MJ0796 sandwich dimer (Figure 3.6; Smith *et al*., 2002), while the other two display the NBDs in an orientation that cannot be reconciled with any of the prior structures or experimental data (Chang and Roth, 2001; Chang, 2003). Although much more can be learned by further crystallization of TMDs and NBDs together in transport cycle intermediate conformations, the information provided by the BtuCD and *S. typhimurium* MsbA structures is a good start. Although the BtuCD structure contains 10 transmembrane spanning helices per TMD as opposed to the typical 6 transmembrane spans usually assumed to be contained in canonical ABC transporter TMDs (see Figure 5.3C versus 5.3A-B, -D), several interesting observations can be made from the structure (Locher *et al*., 2002). The intracellular loops of BtuC that contact the α-helical subdomain of BtuD (Figure 5.3) are akin to the EAA loop of Malk mentioned above. The footprint of the TMD, BtuC, on the NBD, BtuD, overlaps well with the mutations mapped onto E171Q-MJ0796 in Figure 5.2.

Looking at the arrangement of BtuCD from above and below the plane of the lipid bilayer (Figure 5.4), it is easy to imagine how the dimerization and monomerization of the NBDs could help reorient the TMDs during a transport cycle. Recent work on LmrA has studied the analogous reorientation of the TMD transmembrane helices using IR spectroscopy (Grimard *et al*., 2001; Vigano *et al*., 2002). Techniques such as these will be instrumental in the dissection of

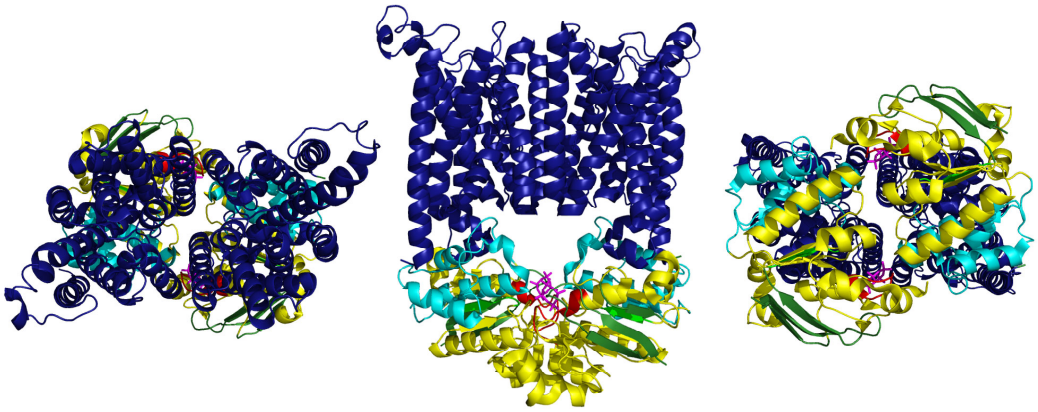

Figure 5.4 Alternate Views of BtuCD – Top view shown on left, looking down into the cytoplasm from extracellular space. Side view along plane of lipid bilayer shown in the middle. Bottom view looking out from the cytoplasm in the extracellular space shown on right. TMDs colored *dark blue*. F_1-Type α/β subdomain colored in *yellow*, a-helical subdomain shown in *cyan*, and anti-parallel β subdomain shown in *forest green*. Walker A motif highlighted in *red* and Walker B motif highlighted in *bright green*. Vanadate shown in *magenta*.

conformational changes that take place in the TMDs as a result of the information transmitted between TMDS and NBDs during each transport cycle.

In conclusion, investigations into the mechanochemical reaction cycle of a model archaeal ATP-binding cassette (ABC) transporter nucleotide binding domain (NBD), MJ0796, has provided insight into the nucleotide-dependent dimerization of these domains thought to supply the power stroke to these protein machines. Continued work as detailed above on this and numerous other ABC transporter systems will be necessary to further out understanding of the many facets of their functional mechanism. With knowledge comes the hope for improved treatment of the large number of genetic disorders and drug-resistant infectious agents and cancerous cells associated with ABC transporters.

References

Abrahams, J. P., Leslie, A. G., Lutter, R., and Walker, J. E. (1994) Structure at 2.8Å Resolution of F_1-ATPase from Bovine Heart Mitochondria. *Nature* **370**, 621-628.

Ahn, J., Beharry, S., Molday, L. L. and Molday, R. S. (2003) Functional Interaction between the Two Halves of the Photoreceptor-specific ATP Binding Cassette Protein ABCR (ABCA4) *J. Biol. Chem.* **278**, 39600-39608.

Allikmets, R., Singh, N., Sun, H., Shroyer, N. F., Hutchinson, A., Chidambaram, A., Gerrard, B., Baird, L., Stauffer, D., Peiffer, A., Rattner, A., Smallwood, P., Li, Y., Anderson, K. L., Lewis, R. A., Nathans, J., Leppert, M., Dean, M. and Lupski, J. R. (1997) A Photoreceptor Cell-Specific ATP-Binding Transporter Gene (*ABCR*) is Mutated in Recessive Stargardt Macular Dystrophy. *Nature Genetics* **15**, 236-246.

Ambudkar, S. V., Cardarelli, C. O., Pashinsky, I. and Stein, W. D. (1997) Relation Between the Turnover Number for Vinblastine Transport and for Vinblastine-Stimulated ATP Hydrolysis by Human P-Glycoprotein. *J. Biol. Chem.* **272**, 21160-21166.

Ames, G. F. and Lever, J. (1970) Components of Histidine Transport: Histidine-Binding Proteins and *hisP* Protein. *Proc. Natl. Acad. Sci.* **66**, 1096-1103.

Ames, G. F. ad Lver, J. E. (1972) The Histidine-Binding Protein J is a Component of Histidine Transport: Identification of its Structural Gene, *hisJ*. *J. Biol. Chem.* **247**, 4309-4316.

Ames, G. F. and Spudich, E. N. (1976) Protein-Protein Interaction in Transport: Periplasmic Histidine-Binding Protein J Interacts with P Protein. *Proc. Natl. Acad. Sci.* **73**, 1877-1881.

Ames, G. F. and Nikaido, K. (1978) Identification of a Membrane Protein as a Histidine Transport Component in *Salmonella typhimurium Proc. Natl. Acad. Sci.* **75**, 5447-5451.

Ames, G. F. and Higgins, C. F. (1983) The Organization, Mechanism of Action and Evolution of Periplasmic Transport Systems. *Trends Biochem. Sci.* **8**, 97-100.

Ames, G. F. (1986) Bacterial Periplasmic Transport Systems: Structure, Mechanism and Evolution. *Annu. Rev. Biochem.* **55**, 397-425.

Ames, G. F., Nikaido, K., Groarke, J. and Petithory, J. (1989) Reconstitution of Periplasmic Transport in Inside-Out Membrane Vesicles: Energization by ATP. *J. Biol. Chem.* **264**, 3998-4002.

Ames, G. F., Mimura, C. S. and Shyamala, V. (1990) Bacterial Periplasmic Permeases Belong to a Family of Transport Proteins Operating from *Escherichia coli* to human: Traffic ATPases. *FEMS Microbiol. Rev.* **75**, 429-446.

Ames, G. F. and Joshi, A. (1991) Energy Coupling in Bacterial Periplasmic Permeases. *J. Bacteriol.* **172**, 4122-4137.

Ames, G. F. and Lecar, H. (1992) ATP-Dependent Bacterial Transporters and Cystic Fibrosis: Analog Between Channels and Transporters. *FASEB J.* **6**, 2660-2666.

Anderson, M. P., Gregory, R. J., Thompson, S., Souza, D. W., Paul, S., Mulligan, R. C., Smith, A. E. and Welsh, M. J. (1991a) Demonstration that CFTR is a Chloride Channel by Alteration of its Anion Selectivity. *Science* **253**, 202-205.

Anderson, M. P., Berger, H. A., Rich, D. P., Gregory, R. J., Smith, A. E. (1991b) Nucleotide Triphosphates are Required to Open the CFTR Chloride Channel. *Cell* **67**, 775-784.

Aparicio, G., Buche, A., Mendez, C. and Salas, J. A. (1996) Characterization of the ATPase Activity of the N-Terminal Nucleotide Binding Domain of an ABC Transporter Involved in Oleandomycin Secretion by *Streptomyces antibioticus*. *FEMS Microbiol. Lett.* **141**, 157-162.

Azzaria, M., Schurr, E. and Gros, P. (1989) Discrete Mutations Introduced in the Predicted Nucleotide-Binding Sites of the *mdr1* Gene Abolish it Ability to Confer Multidrug Resistance. *Mol. Cell Biol.* **9**, 5289-5297.

Bakos, E., Klein, I., Welker, E., Szabo, K., Muë ller, M., Sakardi, B. and Varadi, A. (1997) Characterization of the Human Multidrug Resistance Protein Containing Mutations in the ATP-Binding Cassette Signature Region. *Biochem. J*. **323**, 777-783.

Bavoil, P., Hofnung, M. and Nikaido, H. (1980) Identification of a Cytoplasmic Membrane-Associated Component of the Maltose Transport System of *Escherichia coli*. *J. Biol. Chem.* **255**, 8366-8369.

Bell, A. W., Buckel, S. D., Groarke, J. M., Hope, J. N., Kingsley, D. H. (1986) The Nucleotide Sequence of the *rbsD, rsbA* and *rbsC* genes of *Escherichia coli*. *J. Biol. Chem.* **261**, 7652-7658.

Benabdelhak, H., Schmitt, L., Horn, C., Jumel, K., Blight, M. A. and Holland, I. B. (2005) Positive Co-operative Activity and Dimerization of the Isolated ABC ATPase Domain of HlyB from *Escherichia coli*. *Biochem. J.* **386**, 489-495.

Berger, A. L., Ikuma, M. and Welsh, M. J. (2005) Normal Gating of CFTR Requires ATP Binding to Both Nucleotide-binding Domains and Hydrolysis at the Second Nucleotide-binding Domain. *Proc. Natl. Acad. Sci.* **102**, 455-460.

Berkower, C. and Michaelis, S. (1991) Mutational Analysis of the Yeast a-Factor Transporter STE6, a Member of the ATP Binding Cassette (ABC) Protein Superfamily. *EMBO J.* **10**, 3777-3785.

Bisbal, C., Martinand, C., Silhol, M., Lebleu, B. and Salehzada, T. (1995) Cloning and Characterization of a RNase L Inhibitor: A New Component of the Interferon-Regulated 2-5A Pathway. *J. Biol. Chem.* **270**, 13308-13317.

Bishop, L., Agbayani, R., Ambudkar, S. V., Maloney, P. C. and Ames, G. F. (1989) Reconstitution of a Bacterial Periplasmic Permease in Proteoliposomes and Demonstration of ATP Hydrolysis Concomitant with Transport. *Proc. Natl. Acad. Sci.* **86**, 6953-6957.

Biswas-Fiss, E. E. (2006) Interaction of the Nucleotide Binding Domains and Regulation of the ATPase Activity of the Human Retina Specific ABC Transporter, ABCR. *Biochemistry* **45**, 3813-3823.

Blight, M. A. and Holland, I. B. (1990) Structure and Function of Haemolysin B, P-glycoprotein and other Members of a Novel Family of Membrane Translocators. *Mol. Microbiol.* **4**, 873-880.

Bliss, J. M., Garon, C. F. and Silver, R. P. (1996) Polysialic Acid Export in *Escherichia coli* K1; The Role of KpsT, the ATP-Binding Component of an ABC Transporter, in Chain Translocation. *Glycobiology* **6**, 445-452.

Boëhm, B., Boschert, H. and Koëster, W. (1996) Conserved Amino Acids in the N- and C-terminal Domains of Integral Membrane Transporter FhuB Define Sites Important for Intra- and Intermolecular Interactions. *Mol. Microbiol.* **20**, 223-232.

Browne, B.L., McClendon, V. and Bedwell, D.M. (1996) Mutations Within the First LSGGQ Motif of Ste6p Cause Defects in a-Factor Transport and Mating in *Saccharomyces cerevisiae*. *J. Bacteriol*. **178**, 1712-1719.

Campbell, J. D. and Sansom, M. S. (2005) Nucleotide Binding to the Homodimeric MJ0796 Protein: A Computational Study of a Prokaryotic ABC Transporter NBD Dimer. *FEBS lett.* **579**, 4193-4199.

Carson, M. R., Travis, S. M. and Welsh, M. J. (1995) The Two Nucleotide-Binding Domains of Cystic Fibrosis Transmembrane Conductance Regulator (CFTR) Have Distinct Functions in Controlling Channel Activity. *J. Biol. Chem.* **270**, 1711-1717.

Chang, G. and Roth, C. B. (2001) Structure of MsbA from *E. coli*: A Homolog of the Multidrug Resistance ATP Binding Cassette (ABC) Transporters. *Science* **293**, 1793-1800.

Chang, G. (2003) Structure of MsbA from *Vibrio cholera*: A Multidrug Resistance ABC Transporter Homolog in a Closed Conformation. *J. Mol. Biol.* **330**, 419-430.

Chen, J., Sharma, S., Quiocho, F. A. and Davidson, A. L. (2001) Trapping the Transition State of an ATP-Binding Cassette Transporter: Evidence for a Concerted Mechanism of Maltose Transport. *Proc. Natl. Acad. Sci.* **98**, 1525-1530.

Chen, J., Lu, G., Lin, J., Davidson, A. L. and Quiocho, F. A. (2003) A Tweezers-like Motion of the ATP-Binding Cassette Dimer in an ABC Transport Cycle. *Mol. Cell* **12**, 651-661.

Chen, M., Abele, R. and Tampe, R. (2004) Functional Non-equivalence of ATP-Binding Cassette Signature Motifs in the Transporter Associated with Antigen Processing (TAP). *J. Biol. Chem.* **279**, 46073-46081.

Chloupkova, M., Reaves, S. K., LeBard, L. M. and Koeller, D. M. (2004) The Mitochondrial ABC Transporter Atm1p Functions as a Homodimer. *FEBS lett.* **569**, 65-69.

Cole,S.P., Bhardwaj,G., Gerlach,J.H., Mackie,J.E., Grant,C.E., Almquist,K.C., Stewart,A.J., Kurz,E.U., Duncan,A.M. and Deeley,R.G. (1992) Overexpression of a Transporter Gene in a Multidrug-Resistant Human Lung Cancer Cell Line *Science* **258**, 1650-1654.

Cotton, J. F., Ostedgaard, L. S., Carson, M. R. and Welsh, M. J. (1996) Effect of Cystic Fibrosis-associated Mutations in the Fourth Intracellular Loop of Cystic Fibrosis Transmembrane Conductance Regulator *J. Biol. Chem.* **271**, 21279-21284.

Currier, S. J., Kane, S. E., Willingham, M. C., Cardarelli, C. O., Pastan, I. and Gottesman, M. M. (1992) Identification of Residues in the First Cytoplasmic Loop of P-glycoprotein Involved in the Function of Chimeric Human MDRI-MDR2 Transporters *J. Biol. Chem.* **267**, 25153-25159.

Dall'Acqua W. and Carter P. (2000) Substrate-Assisted catalysis: Molecular Basis and Biological Significance. *Protein Sci.* **9**, 1–9.

Davidson, A. L. and Nikaido, H. (1990) Overproduction, Solubilization and Reconstitution of the Maltose Transport System from *Escherichia coli*. *J. Biol. Chem.* **265**, 4254-4260.

Davidson, A. L. and Nikaido, H. (1991) Purification and Characterization of the Membrane-Associated Components of the Maltose Transport System from *Escherichia coli*. *J. Biol. Chem.* **266**, 8946-8951.

Davidson, A. L., Laghaeian, S. S. and Mannering, D. E. (1996) The Maltose Transport System of *Escherichia coli* Displays Positive Cooperativity in ATP Hydrolysis. *J. Biol. Chem.* **271**, 4858-4863.

Davidson, A. L. and Sharma, S. (1997) Mutation of a Single MalK Subunit Severely Impairs Maltose Transport Activity in *Escherichia coli*. *J. Bacteriol.* **179**, 5458-5464.

Davidson, A. L. (2002) Mechanism of Coupling of Transport to Hydrolysis in Bacterial ATP-Binding Cassette Transporters. *J. Bacteriol.* **184**, 1225-1233.

Davidson, A. L. and Chen, J. (2004) ATP-Binding Cassette Transporters in Bacteria. *Annu. Rev. Biochem.* **73**, 241-268.

Dean, M. (2005) The Genetics of ATP-Binding Cassette Transporters. *Methods Enzymol.* **400**, 409-429.

Delepelaire, P. and Wandersman, C. (1991) Characterization, Localization and Transmembrane Organization of the Three Proteins PrtD, PrtE and PrtF Necessary for Protease Secretion by the Gram-Negative Bacterium *Erwinia chrysanthemi*. *Mol. Microbiol.* **6**, 2427-2434.

Delepelaire, P. (1994) PrtD, the Integral Membrane ATP-Binding Cassette Component of the *Erwinia chrysanthemi* Metalloprotease Secretion System, Exhibits a Secretion Signal-Regulated ATPase Activity. *J. Biol. Chem.* **269**, 27952-27957.

Diederichs, K., Diez, J., Greller, G., Muller, C., Breed, J., Schnell, C., Vonrhein, C., Boos, W. and Welte, W. (2000) Crystal Structure of MalK, the ATPase Subunit of the Trehalose/Maltose ABC Transporter of the Archaeon *Thermococcus litoralis*. *EMBO J.* **19**, 5951-5961.

Eytan, G. D., Regev, R. and Assaraf, Y. G. (1996) Functional Reconstitution of P-Glycoprotein Reveals an Apparent Near Stoichiometric Drug Transport to ATP Hydrolysis. *J. Biol. Chem.* **271**, 3172-3178.

Fetsch, E. E. and Davidson, A. L. (2002) Vanadate-Catalyzed Photocleavage of the Signature Motif of an ATP-Binding Cassette (ABC) Transporter. *Proc. Natl. Acad. Sci.* **99**, 9685-9690.

Gadsby, D. C. and Nairn, A. C. (1999) Control of CFT Channel Gating by Phosphorylation and Nucleotide Hydrolysis. *Physiol. Rev.* **79**, S77-S107.

Gaudet, R. and Wiley, D. C. (2001) Structure of the ABC ATPase Domain of Human TAP1, the Transporter Associated with Antigen Processing. *EMBO J.* **20**, 4964-4972.

Geourjon, C., Orelle, C., Steinfels, E., Blanchet, C., Deleage, G., Di Pietro, A. and Jault, J. (2001) A Common Mechanism for ATP Hydrolysis in ABC Transporter and Helicase Superfamilies. *TRENDS Biochem. Sci.* **26**, 539-544.

Gilson, E., Nikaido, K. and Hofnung, M. (1982a) Sequence of the *malK* Gene in *E. coli*. *Nucleic Acids Res.* **10**, 7449-7458.

Gilson, E., Higgins, C. F., Hofnung, M., Ames, G. F. and Nikaido, H. (1982b) Extensive Homology Between Membrane-Associated Components of Histidine and Maltose Transport Systems of *Salmonella typhimurium* and *Escherichia coli*. *J. Biol. Chem.* **257**, 9915-9918.

Goebel, W. and Hedgpeth, J. (1982) Cloning and Functional Characterization of the Plasmid-Encoded Hemolysin Determinant of *Escherichia coli*. *J. Bacteriol.* **151**, 1290-1298.

Goldsmith, E. J. (1996) Allosteric Enzymes as Models for Chemomechanical Energy Transducing Assemblies. *FASEB J.* **10**, 702-708.

Grimard, V., Vigano, C., Margolles, A., Wattiez, R., van Veen, H. W., Konings, W. N., Ruysschaert, J. and Goormaghtigh, E. (2001) Structure and Dynamics of the Membrane-Embedded Domain of LmrA Investigated by Coupling Polarized ATR-FTIR Spectroscopy and $^{1}H/^{2}H$ Exchange. *Biochemistry* **40**, 11876-11886.

Guo, X., Harrison, R. W. and Tai, P. C. (2006) Nucleotide-Dependent Dimerization of the C-Terminal Domain of the ABC Transporter CvaB in Colicin V Secretion. *J. Bacteriol.* **188**, 2383-2391.

Higgins, C. F. and Ames, G. F. (1981) Two Periplasmic Proteins Which Interact with a Common Membrane Receptor Show Extensive Homology: Complete Nucleotide Sequences. *Proc Natl. Acad. Sci.* **78**, 6038-6042.

Higgins, C. F., Haag, P. D., Nikaido, K., Ardeshir, F., Garcia, G. (1982) Complete Nucleotide Sequence and Identification of Membrane Components of the Histidine Transport Operon of *S. typhimurium*. *Nature* **298**, 723-727.

Higgins, C. F., Hiles, I. D., Whalley, K. and Jamieson, D. J. (1985) Nucleotide Binding by Membrane Components of Bacterial Periplasmic Binding-Protein Dependent Transport Systems. *EMBO J.* **4**, 1033-1040.

Higgins, C. F., Hiles, I. D., Salmond, G. P., Gill, D. R., Downie, J. A. (1986) A Family of Related ATP Binding Subunits Coupled to Many Distinct Biological Processes in Bacteria. *Nature* **323**, 448-450.

Higgins, C. F., Gallagher, M. P., Mimmack, M. L., and Pearce, S. P. (1988) A Family of Closely Related ATP-Binding Subunits from Prokaryotic and Eukaryotic Cells. *Bioessays* **8**, 111-116.

Higgins, C. F. (1990) The Role of ATP in Binding Protein-Dependent Transport System. *Res. Microbiol.* **141**, 353-360.

Higgins, C. F. and Hyde, S. C. (1991) Channeling Our Thoughts. *Nature* **352**, 194-195.

Higgins, C. F. (1992) ABC Transporters: From Microorganisms to Man. *Annu. Rev. Cell Biol.* **8**, 67-113.

Higgins, C. F. and Linton, K. J. (2004) The ATP Switch Model for ABC Transporters. *Nat. Struct. Mol. Biol.* **11**, 918-926.

Hiles, I. D., Gallagher, M. P., Jamieson, D. J. and Higgins, C. F. (1987) Molecular Characterization of the Oligopeptide Permease of *Salmonella typhimurium*. *J. Mol. Biol.* **195**, 125-142.

Hinsa, S. M., Espinosa-Urgel, M., Ramos, J. L. and O'Toole, G. A. (2003) Transition from Reversible to Irreversible Attachment During Biofilm

Formation by *Pseudomonas fluorescens* WCS365 Requires and ABC Transporter and a Large Secreted Protein. *Mol. Microbiol.* **49**, 905-918.

Hobson, A. C., Weatherwax, R. and Ames, G. F. (1984) ATP-Binding Sites in the Membrane Components of Histidine Permease, a Periplasmic Transport System. *Proc. Natl. Acad. Sci.* **81**, 7333-7337.

Hoof, T., Demmer, A., Hadam, M.R., Riordan, J.R. and Tuëmmler, B. (1994) Cystic Fibrosis-type Mutational Analysis in the ATP-Binding Cassette Transporter Signature of Human P-Glycoprotein MDR1. *J. Biol. Chem*. **269**, 20575-20583.

Hopfner, K., Karcher, A., Shin, D. S., Craig, L., Arthur, L. M., Carney, J. P. and Tainer, J. A. (2000) Structural Biology of Rad50 ATPase: ATP-Driven Conformational Control in DNA Double-Strand Break Repair and the ABC-ATPase Superfamily. *Cell* **101**, 789-800.

Horn, C., Bremer, E. and Schmitt, L. (2003) Nucleotide Dependent Monomer/Dimer Equilibrium of OpuAA, the Nucleotide-Binding Protein of the Osmotically Regulated ABC Transporter OpuA from *Bacillus subtilis*. *J. Mol. Biol.* **334**, 403-419.

Hung, L., Wang, I. X., Nikaido, K., Liu, P., Ames, G. F. and Kim, S. (1998) Crystal Structure of the ATP-Binding Subunit of an ABC Transporter. *Nature* **396**, 703-707.

Hunke, S., Mourez, M., Jehano, M., Dassa, E. and Schneider, E. (2000) ATP Modulates Subunit-Subunit Interactions in an ATP-Binding Cassette Transporter ($MalFGK_2$) Determined by Site-directed Chemical Cross-Linking. *J. Biol. Chem.* **275**, 15526-15534.

Hyde, S. C., Emsley, P, Hartshorn, M., Mimmack, M. M., Gileadi, U., Pearce, S. R., Gallagher, M. P., Gill, D. R., Hubbard, R. E. and Higgins, C. F. (1990) Structural Model of ATP-Binding Proteins Associated with Cystic Fibrosis, Multidrug Resistance and Bacterial Transport. *Nature* **346**, 362-365.

Janas, E., Hofacker, M., Chen, M., Gompf, S., van der Does, C. and Tampe, R. (2003) The ATP Hydrolysis Cycle of the Nucleotide-Binding Domain of the Mitochondrial ATP-Binding Cassette Transporter Mdl1p. *J. Biol. Chem.* **278**, 26862-26869.

Jones, P. M. and George, A. M. (1999) Subunit Interactions in ABC Transporters: Towards a Functional Architecture. *FEMS Microbiol. Letters* **179**, 187-202.

Jones, P. M. and George, A. M. (2004) The ABC Transporter Structure and Mechanism: Perspectives on Recent Research. *Cell. Mol. Life Sci.* **61**, 682-699.

Joshi, A. K., Ahmed, S. and Ames, G. F. (1989) Energy Coupling to Bacterial Periplasmic Transport System. *J. Biol. Chem.* **264**, 2126-2133.

Juliano R. L. and Ling V. (1976) A Surface Glycoprotein Modulating Drug Permeability in Chinese Hamster Ovary Cell Mutants. *Biochim Biophys Acta.* **455**, 152-62.

Karpowich, N., Martsinkevich, O., Millen, L., Yuan, Y., Dai, P. L., MacVey, K., Thomas, P. J. and Hunt, J. F. (2001) Crystal Structures of the MJ1267 ATP Binding Cassette Reveal an Induced-Fit Effect at the ATPase Active Site of an ABC Transporter. *Structure* **9**, 571-586.

Kashiwagi, K., Endo, H., Kobayashi, H., Takio, K. and Igarashi, K. (1995) Spermidine-Preferential Uptake System in *Escherichia coli*. ATP Hydrolysis by PotA Protein and its Association with Membranes. *J. Biol. Chem.* **270**, 25377-25382.

Kennedy, K. A. and Traxler, B. (1999) MalK Forms a Dimer Independent of its Assembly into the $MalFGK_2$ ATP-Binding Cassette Transporter of *Escherichia coli*. *J. Biol. Chem.* **274**, 6259-6264.

Kerppola, R. E., Shyamala, U. K., Klebba, P. and Ames, G. F. (1991) The Membrane-Bound Proteins of Periplasmic Permeases Form a Complex. *J. Biol. Chem.* **266**, 9857-9865.

Kerr, I. D. (2002) Structure and Association of ATP-Binding Cassette Transporter Nucleotide-Binding Domains. *Biochim. Biophys. Acta*

Kitaoka, S., Wada, K., Hasegawa, Y., Minami, Y., Fukuyama, K. and Takahashi, Y. (2006) Crystal Structure of *Escherichia coli* SufC, an ABC-type ATPase Component of the SUF Iron-Sulfur Cluster Assembly Machinery. *FEBS lett.* **580**, 137-143.

Koronakis, E., Hughes, C., Milisav, I. and Koronakis, V. (1995) Protein Exporter Function and In Vitro ATPase Activity are Correlated in ABC-Domain Mutants of HlyB. *Mol. Microbiol.* **16**, 87-96.

Leighton, J. and Schatz, G. (1995) An ABC Transporter in the Mitochondrial Inner Membrane is Required for Normal Growth of Yeast. *EMBO J.* **14**, 188-195.

Letoffe, S., Delepelaire, P. and Wandersman, C. (1990) Protease Secretion by *Erwinia chrysanthemi*: The Specific Secretion Functions are Analogous to those if *Escherichia coli* α-Haemolysin. *EMBO J.* **9**, 1375-1382.

Lewis, H. A., Buchanan, S. G., Burley, S. K., Conners, K., Dickey, M., Dorwart, M., Fowler, R., Gao, X., Guggino, W. B., Hendrickson, W. A., Hunt, J. F., Kearins, M. C., Lorimer, D., Maloney, P. C., Post, K. W., Rajashankar, K. R., Rutter, M. E., Sauder, J. M., Shriver, S., Thibodeau, P. H., Thomas, P. J., Zhang, M., Zhao, X., and Emtage, S. (2004) Structure of Nucleotide-Binding Domain 1 of the Cystic Fibrosis Transmembrane Conductance Regulator. *EMBO J.* **23**, 282-293.

Lewis, H. A., Zhao, X., Wang, C., Sauder, J. M., Rooney, I., Noland, B. W., Lorimer, D., Kearins, M. C., Conners, K., Condon, B., Maloney, P. C., Guggino, W. B., Hunt, J. F., and Emtage, S. (2005) Impact of the ΔF508 Mutation in First Nucleotide-Binding Domain of Human Cystic Fibrosis Transmembrane Conductance Regulator on Domain Folding and Structure. *J. Biol. Chem.* **280**, 1346-1353.

Li, C., Ramjeesingh, M., Wang, W., Garami, E., Hewryk, M., Lee, D., Rommens, J. M., Galley, K. and Bear, C. (1996) ATPase Activity of Cystic Fibrosis Transmembrane Conductance Regulator. *J. Biol. Chem.* **271**, 28463-28468.

Linton, K. J. and Higgins, C. F. (1998) The *Escherichia coli* ATP-Binding Cassette (ABC) Proteins. *Mol. Microbiol.* **28**, 5-13.

Lippincott, J., and Traxler, B. (1997) MalFGK Complex Assembly and Transport and Regulatory Characteristics of MalK Insertion Mutants. *J. Bacteriol.* **179**, 1337–1343.

Liu, C. E., Liu, P. and Ames, G. F. (1997) Characterization of the Adenosine Triphosphatase Activity of the Periplasmic Histidine Permease, a Traffic ATPase (ABC Transporter). *J. Biol. Chem.* **272**, 21883-21891.

Locher, K. P., Lee, A. T. and Rees, D. C. (2002) The *E. coli* BtuCD Structure: A Framework for ABC Transporter Architecture and Mechanism. *Science* **296**, 1091-1098.

Loo, T. W. and Clarke, D. M. (1996) Rapid Purification of Human P-Glycoprotein Mutants Expressed Transiently in HEK 293 Cells by Nickel-Chelate Chromotography and Characterization of Their Drug-Stimulated ATPase Activities. *J. Biol. Chem.* **270**, 21449-21452.

Loo, T. W., Bartlett, M. C. and Clarke, D. M. (2002) The "LSGGQ" Motif in Each Nucleotide-Binding Domain of Human P-glycoprotein is Adjacent to the Opposing Walker A Sequence. *J. Biol. Chem.* **277**, 41303-41306.

Lu, G. Westbrooks, J. M., Davidson, A. L. and Chen, J. (2005) ATP Hydrolysis is Required to Reset the ATP-Binding Cassette Dimer into the Resting-State Conformation. *Proc. Natl. Acad. Sci.* **102**, 17969-17974.

Manavalan, P. Dearborn, D. G., McPherson, J. M. and Smith, A. E. (1995) Sequence Homologies Between Nucleotide Binding Regions of CFTR and G-Proteins Suggest Structural and Functional Similarities. *FEBS lett.* **366**, 87-91.

Mimmack, M. L., Gallagher, M. P., Pearce, S. R., Hyde, S. C., Booth, I. R. and Higgins, C. F. (1989) Energy Coupling to Periplasmic Binding Protein-Dependent Transport Systems: Stoichiometry of ATP Hydrolysis During Transport *in vivo*. *Proc. Natl. Acad. Sci.* **86**, 8257-8261.

Mimura, C. S., Admon, A., Hurt, K. A. and Ames, G. F. (1990) The Nucleotide-Binding Site of HisP, a Membrane Protein of the Histidine Permease: Identification of Amino Acid Residues Photoaffinity Labeled by 8-azido ATP. *J. Biol. Chem.* **265**, 19535-19542.

Mimura, C. S., Holbrook, S. R. and Ames, G. F. (1991) Structural Model of the Nucleotide Binding Conserved Component of Periplasmic Permeases. *Proc. Natl. Acad. Sci.* **88**, 84-88.

Moody, J. E., Millen, L., Binns, D., Hunt, J. F. and Thomas, P. J. (2002) Cooperative, ATP-Dependent Association of the Nucleotide Binding Cassettes During the Catalytic Cycle of ATP-Binding Cassette Transporters. *J. Biol. Chem.* **277**, 21111-21114.

Moody, J. E. and Thomas, P. J. (2005) Nucleotide Binding Domain Interactions During the Mechanochemical Reaction Cycle of ATP-Binding Cassette Transporters. *J. Bioenerg. Biomem.* **37**, 475-479.

Mourez, M., Hofnung, M. and Dassa, E. (1997) Subunit Interaction in ABC Transporters. A Conserved Sequence in Hydrophobic Membrane Proteins of Periplasmic Permeases Define Sites of Interaction with the Helical Domain of ABC subunits. *EMBO J*. **16**, 3066-3077.

Narita, S., Tanaka, K., Matsuyama, S. and Tokuda, H. (2002) Disruption of *lolCDE,* Encoding an ATP-Binding Cassette Transporter, is Lethal for *Escherichia coli* and Prevents Release of Lipoproteins from the Inner Membrane. *J. Bacteriol.* **184**, 1417-1422.

Narita, S. and Tokuda, H. (2006) An ABC Transporter Mediating the Membrane Detachment of Bacterial Lipoproteins Depending on Their Sorting Signals. *FEBS lett.* **580**, 1164-1170.

Nikaido, K., Liu, P. and Ames, G. F. (1997) Purification and Characterization of HisP, the ATP-Binding Subunit of a Traffic ATPase (ABC Transporter), the Histidine Permease of *Salmonella typhimurium*. *J. Biol. Chem.* **272**, 27745-27752.

Nikaido, K. and Ames, G. F. (1999) One Intact ATP-Binding Subunit is Sufficient to Support ATP Hydrolysis and Translocation in an ABC Transporter, the Histidine Permease. *J. Biol. Chem.* **274**, 26727-26735.

Orelle, C., Dalmas, O., Gros, P., Di Pietro, A. and Jault, J. (2003) The Conserved Glutamate Residue Adjacent to the Walker-B Motif is the Catalytic Base for ATP Hydrolysis in the ATP-Binding Cassette Transporter BmrA. *J. Biol. Chem.* **278**, 47002-47008.

Ose, T., Fujie, T., Yao, M., Watanabe, N. and Tanaka, I. (2004) Crystal Structure of the ATP-Binding Cassette of Multisugar Transporter from *Pyrococcus horikoshii* OT3. *Proteins: Struct Func. Bioinformatics* **57**, 635-638.

Oswald, C., Holland, I. B. and Schmitt, L. (2006) The Motor Domains of ABC Transporters: What Can Structures Tell Us? *Naunyn-Schmiedeberg's Arch Pharmacol* **372**, 385-399.

Oxender, D. L., Anderson, J. J., Daniels, C. J., Landick, R., Gunsalus, R. P., Zurawski, G., Selker, E. and Yanofsky, C. (1980) Structural and Functional Analysis of Cloned DNA Containing Genes Responsible for Branched-Chain Amino Acid Transport in *Escherichia coli*. *Proc. Natl. Acad. Sci.* **77**, 1412-1416.

Panagiotidis, C. H., Reyes, M., Sievertsen, A., Boos, W. and Shuman, H. A. (1993) Characterization of the Structural Requirements for Reassembly and Nucleotide Binding of an ATP-Binding Cassette Transporter. The Maltose Transport System of *Escherichia coli*. *J. Biol. Chem.* **268**, 23685-23696.

Patzlaff, J. S., Van der Heide, T. and Poolman, B. (2003) The ATP/Substrate Stoichiometry of the ATP-Binding Cassette (ABC) Transporter OpuA. *J. Biol. Chem.* **278**, 29546-29551.

Pavelka, M. S., Wright, L. F. and Silver, R. P. (1991) Identification of Two Genes, *kpsM* and *kpsT*, in Region 3 of the Polysialic Acid Gene Cluster of *Escherichia coli* K1. *J. Bacteriol.* **173**, 4603-4610.

Pavelka, M. S., Hayes, S. F. and Silver, R. P. (1994) Characterization of KpsT, the ATP-Binding Component of the ABC-Transporter Involved with the Export of Capsular Polysialic Acid in *Escherichia col* K1. *J. Biol. Chem.* **269**, 20149-20158.

Petronilli, V. and Ames, G. F. (1991) Binding Protein-Independent Histidine Permease Mutants. *J. Biol. Chem.* **266**, 16293-16296.

Phillips, G. N., Mahajan, V. K., Siu, A. K. and Quiocho, F. A. (1976) Structure of L-Arabinose-Binding Protein from *Escherichia coli* at 5Å Resolution and Preliminary Results at 3.5Å. *Proc. Natl. Acad. Sci.* **73**, 2186-2190.

Quiocho, F. A., Gilliland, G. L. and Phillips, G. N. (1977) The 2.8-Å Resolution Structure of the L-Arabinose-Binding Protein from *Escherichia coli*. *J. Biol. Chem.* **252**, 5142-5149.

Qu, Q. and Sharom, F. J. (2001) FRET Analysis Indicates That the Two ATPase Active Sites of the P-Glycoprotein Multidrug Transporter are Closely Associated. *Biochemistry* **40**, 1413-1422.

Rahamanian, M., Claus, D. R. and Oxender, D. L. (1973) Multiplicity of Leucine Transport Systems in *Escherichia coli* K-12. *J. Bacteriol.* **116**, 1258-1266.

Rai, V., Shukla, S., Jha, S., Komath, S. S. and Prasad, R. (2005) Functional Characterization of N-Terminal Nucleotide Binding Domain (NBD1) of a Major ABC Drug Transporter Cdr1p of *Candida albicans*: Uncommon but Conserved Trp326 of Walker B is Important for ATP Binding. *Biochemistry* **44**, 6650-6661.

Ramaen, O., Leulliot, N., Sizun, C., Ulryk, N., Pamlard, O., Lallemand, J., van Tilbeurgh, H. and Jacquet, E. (2006) Structure of the Human Multidrug Resistance Protein 1 Nucleotide Binding Domain 1 bound to Mg^{2+}/ATP Reveals a Non-productive Catalytic Site. *J. Mol. Biol. In press.*

Reyes, C. L. and Chang, G. (2005) Structure of the ABC Transporter MsbA in Complex with ADP•Vanadate and Lipopolysaccharide. *Science* **308**, 1028-1031.

Richard, M., Drouin, R. and Beaulieu, A. D. (1998) ABC50, a Novel Human ATP-Binding Cassette Protein Found in Tumor Necrosis Factor-α-Stimulated Synoviocytes. *Genomics* **53**, 137-145.

Riordan, J. A., Rommens, J. M., Kerem, B., Alon, N., Rozmahel, R. (1989) Identification of the Cystic Fibrosis Gene: Cloning and Characterization of Complementary DNA. *Science* **245**, 1066-1073.

Rosing, J., Harris, D. A., Kemp, A. and Slater, E. C. (1975) Nucleotide-Binding Properties of Native and Cold-Treated Mitochondrial ATPase. *Biochim. Biophys. Acta* **376**, 13–26.

Saraste, M., Sibbald, P. R. and Wittinghofer, A. (1990) The P-Loop, a Common Motif in ATP- and GTP-Binding Proteins. *Trends Biochem. Sci* **15**, 430-434.

Sauna, Z. E. and Ambudkar, S. V. (2000) Evidence for a Requirement for ATP Hydrolysis at Two Distinct Steps During a Single Turnover of the Catalytic Cycle of Human P-glycoprotein. *Proc. Natl. Acad. Sci.* **97**, 2515-2520.

Sauna, Z. E. and Ambudkar, S. V. (2001) Characterization of the Catalytic Cycle of ATP Hydrolysis by Human P-glycoprotein. *J. Biol. Chem.* **276**, 11653-11661.

Sauna, Z. E., Muller, M., Peng, X. and Ambudkar, S. V. (2002) Importance of the Conserved Walker B Glutamate Residues, 556 and 1201, for the Completion of the Catalytic Cycle of ATP Hydrolysis by Human P-glycoprotein (ABCB1). *Biochemistry* **41**, 13989-14000.

Scheffel, F., Demmer, U., Warkentin, E., Hulsmann, A., Schneider, E. and Ermler, U. (2005) Structure of the ATPase Subunit CysA of the Putative Sulfate ATP-Binding Cassette (ABC) Transporter from *Alicyclobacillus acidocaldarius*. *FEBS lett.* **579**, 2953-2958.

Schmees, G., Stein, A., Hunke, S., Landmesser, H. and Schneider, E. (1999) Functional Consequences of Mutations in the Conserved 'Signature Sequence' of the ATP-Binding Cassette Protein MalK. *Eur. J. Biochem.* **266**, 420-430.

Schmitt, L. and Tampe, R. (2002) Structure and Mechanism of ABC Transporters. *Curr. Opin. Struct. Biol.* **12**, 754-760.

Schmitt, L., Benabdelhak, H., Blight, M. A., Holland, I. B. and Stubbs, M. T. (2003) Crystal Structure of the Nucleotide-Binding Domain of the ABC Transporter Haemolysin B: Identification of a Variable Region Within ABC Helical Domains. *J. Mol. Biol.* **330**, 333-342.

Schneider, E. and Walter, C. (1991) A Chimeric Nucleotide-Binding Protein, Encoded by a HisP-MalK Hybrid Gene, is Functional in Maltose Transport in *Salmonella typhimurium*. *Mol. Microbiol.* **5**, 1375-1383.

Schneider, E., Wilken, S. and Schmid, R. (1994) Nucleotide-Induced Conformational Changes of MalK, a Bacterial ATP Binding Cassette Transporter Protein. *J. Biol. Chem.* **269**, 20456-20461.

Senior, A. E., Al-Shawi, M. K. and Urbatsch, I. L. (1995) The Catalytic Cycle of P-glycoprotein. *FEBS lett.* **377**, 285-289.

Shapiro, A. B. and Ling, V. (1998) Stoichiometry of Coupling Rhodamine 123 Transport to ATP Hydrolysis by P-Glycoprotein. *Eur. J. Biochem.* **254**, 189-193.

Sharma, S. and Davidson, A. L. (2000) Vanadate-Induced Trapping of Nucleotides by Purified Maltose Transport Complex Requires ATP Hydrolysis. *J. Bacteriol.* **182**, 6570-6576.

Sheps, J.A., Cheung, I. and Ling, V. (1995) Hemolysin Transport in *Escherichia coli*. Point Mutants in HlyB Compensate for a Deletion in the Predicted Amphiphilic Helix Region of the HlyA signal. *J. Biol. Chem.* **270**, 14829-14834.

Shuman, H. A., Silhavy, T. J. and Beckwith, J. R. (1980) Labeling of Proteins with β-Galactosidase by Gene Fusion: Identification of a Cytoplasmic Membrane Component of the *Escherichia coli* Maltose Transport System. *J. Biol. Chem.* **255**, 168-174.

Shuman, H. A. and Silhavy, T. J. (1981) Identification of the *malK* Gene Product. *J. Biol. Chem.* **256**, 560-562.

Shuman, H. A. (1982) Active Transport of Maltose in *Escherichia coli* K12. *J. Biol. Chem.* **257**, 5455-5461.

Shyamala, V., Baichwal, V., Beall, E. and Ames, G. F. (1991) Structure-Function Analysis of the Histidine Permease and Comparison with Cystic Fibrosis Mutations. *J. Biol. Chem.* **266**, 18714-18719.

Smith, P. C., Karpowich, N., Millen, L., Moody, J. E., Rosen, J., Thomas, P. J., and Hunt, J. F. (2002) ATP Binding to the Motor Domain from an ABC Transporter Drives Formation of a Nucleotide Sandwich Dimer. *Mol. Cell* **10**, 139-149.

Story, R. M. and Steitz, T. A. (1992) Structure of the recA Protein-ADP Complex. *Nature* **355**, 374-376.

Thibodeau, P. H., Brautigam, C. A., Machius, M. and Thomas, P. J. (2005) Side Chain and Backbone Contributions of Phe508 to CFTR Folding. *Nature Struc. Mol. Biol.* **12**, 10-16.

Tombline, G., Bartholemew, L., Gimi, K., Tyndall, G. A. and Senior, A. E. (2004a) Synergy Between Conserved ABC Signature Ser Residues in P-glycoprotein Catalysis. *J. Biol Chem.* **279**, 5363-5373.

Tombline, G., Bartholemew, L. A., Urbatsch, I. L. and Senior, A. E. (2004b) Combined Mutation of Catalytic Glutamate Residues in the Two Nucleotide Binding Domains of P-glycoprotein Generates a Conformation That Binds ATP and ADP Tightly. *J. Biol. Chem.* **279**, 31212-31220.

Tombline, G., Muharemagic, A., White, L. B. and Senior, A. E. (2005) Involvement of the "Occluded Nucleotide Conformation" of P-glycoprotein in the Catalytic Pathway. *Biochemistry* **44**, 12879-12886.

Trowsdale, J., Hanson, I., Mockridge, I., Beck, S., Townsend, A. and Kelly, A. (1990) Sequences Encoded in the Class II Region of the MHC Related to the 'ABC' Superfamily of Transporters. *Nature* **348**, 741-744.

Urbatsch, I. L., Julien, M., Carrier, I., Rousseau, M., Cayrol, R. and Gros, P. (2000) Mutational Analysis of Conserved Carboxylate Residues in the Nucleotide Binding Sites of P-glycoprotein. *Biochemistry* **39**, 14138-14149.

Urbatsch, I. L., Tyndall, G. A., Tombline, G. and Senior, A. E. (2003) P-glycoprotein Catalytic Mechanism: Studies of the ADP-Vanadate Inhibited State. *J. Biol. Chem.* **278**, 23171-23179.

van der Does, C., Presenti, C., Schulze, K., Dinkelaker, S. and Tampe, R. (2006) Kinetics of the ATP Hydrolysis Cycle of the Nucleotide-Binding Domain of Mdl1 Studied by a Novel Site-specific Labeling Technique. *J. Biol. Chem.* **281**, 5694-5701.

van Veen, H. W., Venema, K., Bolhuis, H., Oussenko, I., Kok, J., Poolman, B., Driessen, A. J. and Konings, W. N. (1996) Multidrug Resistance Mediated by a Bacterial Homolog of the Human Multidrug Transporter MDR1. *Proc. Natl. Acad. Sci.* **93**, 10668-10672.

van Veen, H. W., Margolles, A., Muller, M., Higgins, C. F., and Konings, W. N. (2000) The Homodimeric ATP-Binding Cassette Transporter LmrA Mediates Multidrug Transport by an Alternating Two-Site (Two-Cylinder Engine) Mechanism. *EMBO J.* **19**, 2503-2514.

Verdon, G., Albers, S. V., Dijkstra, B. W., Driessen, A. J. and Thunnissen, A. W. (2003) Crystal Structures of the ATPase Subunit of the Glucose ABC Transporter from *Sulfolobus solfatarius*: Nucleotide-free and Nucleotide-bound Conformations. *J. Mol. Biol.* **330**, 343-358.

Verdon, G., Albers, S. V., van Oosterwijk, N., Dijkstra, B. W., Driessen, A. J. and Thunnissen, A. W. (2003) Formation of the Productive ATP-Mg^{2+}-bound

Dimer of GlcV, an ABC-ATPase from *Sulfolobus solfatarius*. *J. Mol. Biol.* **334**, 255-267.

Vergani, P., Nairn, A. C. and Gadsby, D. C. (2003) On The Mechanism of MgATP-Dependent Gating of CFTR Cl^- Channels. *J. Gen. Physiol.* **120**, 17-36.

Vergani, P., Lockless, S. W., Nairn, A. C. and Gadsby, D. C. (2005) CFTR Channel Opening by ATP-Driven Tight Dimerization of its Nucleotide-Binding Domains. *Nature* **433**, 876-880.

Vigano, C., Grimard, V., Margolles, A., Goormaghtigh, E., van Veen, H. W., Konings, W. N. and Ruysschaert, J. (2002) A New Experimental Approach to Detect Long-Range Conformational Changes Transmitted Between the Membrane and Cytosolic Domains of LmrA, a Bacterial Multidrug Transporter. *FEBS Lett.* **530**, 197-203.

Walker, J. E., Saraste, M., Runswick, M. J. and Gay, N. J. (1982) Distantly Related Sequences in the a- and b-Subunits of ATP Synthase, Myosin, Kinases and Other ATP-Requiring Enzymes and a Common Nucleotide Binding Fold. *EMBO J.* **1**, 945-951.

Walter, C., Wilken, S. and Schneider, E. (1992) Characterization of Site-Directed Mutations in Conserved Domains of MalK, a Bacterial Member of the ATP-Binding Cassette (ABC) Family. *FEBS Lett.* **413**, 211-214.

Wandersman, C., Delepelaire, P., Letoffe, S. and Schwartz, M. (1987) Characterization of *Erwinia chrysanthemi* Extracellular Proteases: Cloning and Expression of the Protease Genes in *Escherichia coli*. *J. Bacteriol.* **169**, 5046-5053.

Watanabe, S., Kita, A. and Miki, K. (2005) Crystal Structure of Atypical Cytoplasmic ABC-ATPase SufC from *Thermus thermophilus* HB8. *J. Mol. Biol.* **353**, 1043-1054.

Welsh, M. J. and Smith, A. E. (1993) Molecular Mechanism of CFTR Chloride Channel Dysfunction in Cystic Fibrosis. *Cell* **73**, 1251-1254.

Wilken, S., Schmees, G. and Schneider, E. (1996) A Putative Helical Domain in the MalK Subunit of the ATP-Binding-Cassette Transport System for Maltose of *Salmonella typhimurium* ($MalFGK_2$) is Crucial for Interaction with MalF and MalG. A Study Using the LacK protein of *Agrobacterium radiobacter* as a Tool. Mol. Microbiol. **22**, 555-666.

Wilkinson, D.J., Mansoura, M.K., Warson, P.Y., Smit, L.S., Collins, F.S. and Dawson, D.C. (1996) CFTR: The Nucleotide Binding Folds Regulate the Accessibility and Stability of the Activated State. *J. Gen. Physiol.* **107**, 103-119.

Xie, J., Drumm, M.L., Ma, J. and Davis, P.B. (1995) Intracellular Loop Between Transmembrane Segments IV and V of Cystic Fibrosis Transmembrane Conductance Regulator is Involved in Regulation of Chloride Conductance State. *J. Biol. Chem.* **270**, 28084-28091.

Xu, J., Liu, Y., Yang, Y., Bates, S. and Zhang, J. (2004) Characterization of Oligomeric Human Half-ABC Transporter ATP-Binding Cassette G2. *J. Biol. Chem.* **279**, 19781-19789.

Yakushi, T., Masuda, K., Narita, S., Matsuyama, S. and Tokuda, H. (2000) A New ABC Transporter Mediating the Detachment of Lipid-Modified Proteins From Membranes. *Nature Cell Biol.* **2**, 212-218.

Yoshida, M. and Amano, T. (1995) A Common Topology of Proteins Catalyzing ATP-Triggered Reactions. *FEBS lett.* **359**, 1-5.

Yuan, Y., Blecker, S., Martsinkevich, O., Millen, L., Thomas, P. J. and Hunt, J. F. (2001) The Crystal Structure of the MJ0796 ATP-Binding Cassette: Implications for the Structural Consequences of ATP Hydrolysis in the Active Site of an ABC Transporter. *J. Biol. Chem.* **276**, 32313-32321.

Yuan, Y., Martsinkevich, O. and Hunt, J. F. (2003) Structural Characterization of an MJ1267 ATP-Binding Cassette Crystal with a Complex Pattern of Twinning Caused by Promiscuous Fiber Packing. *Acta Biol. Crystallography* **D59**, 225-238.

Zaitseva, J., Jenewein, S., Wiedenmann, A., Benabdelhak, H., Holland, I. B. and Schmitt, L. (2005a) Functional Characterization and ATP-Induced Dimerization of the Isolated ABC-Domain of the Haemolysin B Transporter. *Biochemistry* **44**, 9680-9690.

Zaitseva, J., Jenewein, S., Jumpertz, T., Holland, I. B. and Schmitt, L. (2005b) H662 is the Linchpin of ATP Hydrolysis in the Nucleotide-Binding Domain of the ABC Transporter HlyB. *EMBO J.* **24**, 1901-1910.

Zhang, D., Graf, G. A., Gerard, R. D., Cohen, J. C. and Hobbs, H. H. (2006) Functional Asymmetry of Nucleotide-Binding Domains in ABCG5 and ABCG8. *J. Biol. Chem.* **281**, 4507-4516.

Vitae

Jonathan Edward Moody was born on April 13, 1979, in Indianapolis, Indiana to Dean and Martha Moody of Brownsburg, Indiana. Jonathan graduated from Allen High School in Allen, Texas in 1997 ranked second in his class. He attended Texas A&M University in College Station, Texas, as a President's Endowed Scholar where he graduated summa cum laude with a B.S. in biochemistry in August, 2000. Jonathan worked as a research technician II under the supervision of Drs. Wojciech Kedzierski, Jian Wang and Roxana Radu in the laboratory of Dr. Gabriel Travis at the University of Texas Southwestern Medical Center in the Center for Basic Neuroscience. He began work on his Ph. D. in the fall of 2001, joining the laboratory of Dr. Philip J. Thomas soon thereafter. Jonathan completed his doctoral work in August, 2006. He was awarded the degree of Doctorate of Philosophy in Molecular Biophysics in December, 2006. Jonathan currently teaches honors chemistry and coaches cross country and track at Ursuline Academy of Dallas.

Dr. Jonathan Edward Moody

1018 San Jacinto Dr. Apt #1521

Irving, TX 75063